Technische Universität München
TUM School of Life Sciences

Targeting the intestinal circadian clock by meal timing ameliorates gastrointestinal inflammation

Yunhui Niu

Vollständiger Abdruck der von der TUM School of Life Sciences der Technischen Universität München zur Erlangung eines

Doktors der Naturwissenschaften (Dr. rer. nat.)

genehmigten Dissertation.

Vorsitz: Prof. Dr. Martin Klingenspor

Prüfer*innen der Dissertation:

1. Prof. Dr. Dirk Haller
2. Prof. Dr. Henriette Uhlenhaut

Die Dissertation wurde am 30.05.2023 bei der Technischen Universität München eingereicht und durch die TUM School of Life Sciences am 01.09.2023 angenommen.

Abstract

Circadian rhythm disruption, which occurs in shift work, has been linked to an increased risk of inflammatory bowel disease (IBD). Although regulators of intestine homeostasis are controlled by the circadian system, it remains unclear whether intestinal clocks have a functional impact on local immune defence. Since we found disrupted clock gene expression restricted to inflamed colonic regions in *Il-10*$^{-/-}$ mice, a genetic model for colitis, we aim to investigate the cause and effect relationship between colon clock disruption and colon inflammation.

RNA-seq analysis of intestinal epithelial cells (IEC) specific Bmal1 deficient mice (*Bmal1*$^{IEC-/-}$) identified altered colon genes involved in immune/inflammatory responses and bacteria defence. This led us to hypothesize that a dysfunctional intestinal clock might impact the development or progression of gut inflammation. Indeed, DSS administration in *Bmal1*$_{IEC}^{-/-}$ mice induced severe acute intestinal inflammation. Compared to controls, we observed increased colitis severity according to reduced body weight, significantly shortened colon and severely enhanced macrophage and neutrophil infiltration in the lamina propria measured by flow cytometry. To genetically assess the impact of IEC clocks on IBD development, we crossed *Il-10*$^{-/-}$ and *Bmal1*$^{IEC-/-}$ mice. These mice demonstrated reduced survival, enhanced inflammation, determined by histological scoring, qPCR of inflammatory markers and increased immune cell recruitment to the lamina propria, demonstrating that lack of IEC clocks promotes the sensitivity to acute and chronic colon inflammation. Transferring disease-associated microbiota into germ free (GF) *Bmal1*$^{IEC-/-}$ recipients resulted in enhanced colon inflammatory response, whereas colonization with rhythmic/arrhythmic microbiota into GF *Il-10*$^{-/-}$ recipients led to similar tissue pathological changes. These results indicated that the host intestinal clock might play a more important role in IBD development.

Moreover, restoring the colon clock of *Il-10*$^{-/-}$ mice by night restricted feeding (RF) significantly enhanced survival and reduced gut inflammation. Importantly, we provide evidence that IEC clocks gate the inflammatory response and influences the severity and progression of IBD symptoms, because RF failed to ameliorate the colitis symptoms and survival in *Bmal1*$^{IEC-/-}$x *Il-10*$^{-/-}$ mice. These results demonstrate that functional IEC clocks are essential to maintain gastrointestinal homeostasis and represents a major player in IBD.

Taken together, our findings indicate that enhancing intestinal clock function by meal-timing could become a novel strategy to ameliorate the symptoms in IBD patients.

Zusammenfassung

Eine Störung des zirkadianen Rhythmus, wie sie bei Schichtarbeit auftritt, wird mit einem erhöhten Risiko für entzündliche Darmerkrankungen in Verbindung gebracht (IBD). Obwohl die Homöostase des Darms durch das zirkadiane System gesteuert wird, bleibt unklar, ob die intestinalen Uhren einen funktionellen Einfluss auf die lokale Immunabwehr haben. Da wir in *Il-10*$^{-/-}$ Mäusen, einem genetischen Modell für Kolitis, eine gestörte Genexpression der Darmuhr gefunden haben, die auf entzündete Kolonregionen beschränkt ist, wollen wir die Ursache-Wirkungs-Beziehung zwischen der Störung der Darmuhr und der Kolonentzündung untersuchen.

RNA-seq-Analysen von Darmepithelzellen (IEC) spezifischer Bmal1-defizienter Mäuse (*Bmal1*$^{IEC-/-}$) ergaben veränderte Gene im Dickdarm, die an Immun-/Entzündungsreaktionen und der Bakterienabwehr beteiligt sind. Dies veranlasste uns zu der Hypothese, dass eine gestörte intestinale Uhr die Entwicklung oder das Fortschreiten von Darmentzündungen beeinflussen könnte. In der Tat führte die Verabreichung von DSS bei *Bmal1*$^{IEC-/-}$ Mäusen zu einer schweren akuten Darmentzündung. Im Vergleich zu den Kontrollen beobachteten wir einen erhöhten Schweregrad der Kolitis, der sich in einem verringerten Körpergewicht, einem deutlich verkürzten Dickdarm und einer stark erhöhten Makrophagen- und Neutrophileninfiltration in der Lamina propria, gemessen mittels Durchflusszytometrie, zeigte. Um den Einfluss der IEC-Uhren auf die IBD-Entwicklung genetisch zu bewerten, kreuzten wir *Il-10*$^{-/-}$ und *Bmal1*$^{IEC-/-}$ Mäuse. Diese Mäuse zeigten eine reduzierte Überlebensrate, eine verstärkte Entzündung, die durch histologische Untersuchungen und qPCR von Entzündungsmarkern bestimmt wurde, sowie eine erhöhte Rekrutierung von Immunzellen in die Lamina propria, was zeigt, dass das Fehlen von IEC-Taktgebern die Empfindlichkeit für akute und chronische Dickdarmentzündungen fördert. Der Transfer von krankheitsassoziierter Mikrobiota in keimfreie (GF) *Bmal1*$^{IEC-/-}$-Empfänger führte zu einer verstärkten

Entzündungsreaktion im Dickdarm, während die Besiedlung von GF *Il-10*$^{-/-}$-Empfängern mit rhythmischer/arrhythmischer Mikrobiota zu ähnlichen pathologischen Veränderungen im Gewebe führte. Diese Ergebnisse deuten darauf hin, dass die intestinale Uhr des Wirtes eine wichtigere Rolle bei der Entwicklung von IBD spielen könnte.

Die Wiederherstellung der Dickdarmuhr von *Il-10*$^{-/-}$ Mäusen durch nächtliche Fütterungsbeschränkung (RF) verbesserte das Überleben signifikant und reduzierte die Darmentzündung. Wichtig ist, dass wir Beweise dafür liefern, dass IEC-Uhren die Entzündungsreaktion steuern und die Schwere und das Fortschreiten von IBD-Symptomen beeinflussen, da RF die Colitis-Symptome und das Überleben in *Bmal1*$^{IEC-/-}$x*Il-10*$^{-/-}$ Mäusen nicht verbessern konnte. Diese Ergebnisse zeigen, dass funktionelle IEC-Uhren für die Aufrechterhaltung der gastrointestinalen Homöostase unerlässlich sind und eine wichtige Rolle bei IBD spielen.

Insgesamt deuten unsere Ergebnisse darauf hin, dass die Verbesserung der intestinalen Uhrfunktion durch das Timing der Mahlzeiten eine neue Strategie zur Verbesserung der Symptome bei IBD-Patienten sein könnte.

Table of contents

1 Introduction

1.1 Circadian system

The circadian system is a hierarchical organization that consists of the central pacemaker in the suprachiasmatic nucleus (SCN), which drives behavioral rhythms[1] and peripheral clocks that rhythmically regulate tissue-specific functions. The core SCN clock regulates and synchronizes peripheral clocks through multiple endogenous regulatory factors such as neural signals and hormones reviewed by [2].

Free-running rhythm is only identifiable under constant environmental conditions such as constant light conditions (constant darkness, DD or constant light, LL) and constant temperature. The intrinsic cycles measured under these conditions exhibit a period close to but slightly deviated from 24h[3]. Various free-running rhythms have been demonstrated in mice and humans at the organism level, such as sleep-wakefulness and behaviour and are often temperature compensated. Moreover, diurnal and circadian variation of considerable amount of gene and protein expression are observed as well at the cellular level[3]. Indeed, the complex circadian system consists oscillating proteins that compose transcription–translation feedback loops (TTFLs)[4]. In details, CLOCK and BMAL1, the two transcriptional activator proteins form the heteromeric complexes and bind to the promoters through E-box, which activate the transcription of three *Per* and two *Cryptochrome* (*Cry*) genes[5]. The accumulation of PER/CRY protein complexes in the nucleus in turn suppress the previous E-box activation which regulated by CLOCK and BMAL1. Subsequently, the reactivation of this loop will only occur as long as CLOCK and BMAL1 have been degraded. In addition to this core negative feedback loop, several others accessory loops work in parallel. For example, the orphan nuclear receptors RORs and REV-ERBα are the most characterized ones. The transcription factors

RORs (positively) and REV-ERBα (negatively) regulates the expression of BMAL1 through REV-ERBα/RORs response elements (RORE) in the *Bmal1* promoter. Indeed, the oscillation and peak of *Bmal1* expression are anti-phase to the negative factors PER and CRY[6]. These accessory loops not only help support and maintain the cycle, but also provide additional path to the transcriptional regulation of other output genes containing RORE sequences[6], and thereby expanding the abundance of the circadian transcriptome.

The master clock in the SCN is reset and entrained by photic signals, and this process is implemented by the photosensitive retinal ganglion cells in the retina (projecting photic signals to the SCN)[7] and the retinohypothalamic tract (transmission of photic signals) [8]. In brief, glutamate, the neurotransmitter of the retinohypothalamic tract, induces Ca^{2+}-Camp response element-binding protein and thus activate the transcription of key clock genes such as *Per1* and *Per2*[9, 10] after the photic signals. Consequently, the initiation of the TTFLs involved in the circadian system starts. Subsequently, the SCN core clock synchronizes other peripheral clocks through humoral factors and peripheral autonomic nervous system[11, 12].

However, lots of evidence have been found over the last decades that external cues, such as food availability, is one of the major factor to entrain peripheral clocks[13, 14]. For example, feeding patterns and caloric content are both capable to synchronize or reset peripheral clocks through pathways that are involved in nutrient sensing and absorption, such as insulin/IGF-1, AMPK and mTOR reviewed by [15]. Therefore, it becomes necessary to dissect peripheral clocks from the central clock when investigating tissue-specific functions. Indeed, methodologies such as RNA sequencing and DNA microarrays have been widely applied to characterize circadian oscillations in transcript expression in different murine organs. It has been predicted in mice that more than half of the protein-coding genome is rhythmic somewhere

in the body since 43% of the protein coding genes oscillates in at least one organ among the 12 organs which were tested[16]. Importantly, the majority of these transcriptional rhythms are organ-specific, which further confirms the dominant role of organ-specific clock in regulating biological processes in each organ[17, 18].

1.2 Circadian disruption and gastrointestinal health

The circadian clock evolved to adjust the host's physiology to recurring the environmental diurnal changes. For example, light-dark cycles or temperature changes over the course of the 24 hour day can act as *Zeitgebers* for the circadian systems[19]. The misalignment of behavioural cycles with environmental changes or disruption on molecular, cellular, tissue levels of the circadian system is called "circadian disruption".

Disruption of the circadian system, for example as experienced during jet lag and shift work[20], relates to immune deficits and pathologies, such as cancer, infection[21, 22], metabolic alterations[23, 24], and has been associated to a wide range of diseases including inflammatory bowel disease (IBD) (reviewed by[25].

The GI tracts respond to various intrinsic or external stimulus in the first place, such as food intake, nutrient availability and bacterial presentation. These stimulus, together with environmental timing cues such as light, in turn impact the circadian regulation of the GI tracts[26]. Indeed, the peripheral intestinal clock has been identified under constant darkness and starvation[27]. Circadian rhythms have been identified along the intestine to regulate the regeneration of intestinal stem cells, gut motility, nutrient absorption and mucosal immunity[28-32], as well as in the microbiome[27], to maintain intestinal homeostasis.

Consequently, disruption of the intestinal clock might result in impairment of mucosal immune rhythms, as well as microbiome rhythms and thus alters GI physiology which likely contributes to the development and progression of GI diseases. Indeed, epidemiological studies report suppressed clock genes expression in biopsies from IBD patients [33-35], supporting an involvement of intestine-specific clocks in the disease occurrence. However, the importance of the intestinal clock in GI diseases remains to be addressed.

1.3 Anatomy of the intestine

The intestinal tract in humans consists of the small intestine (duodenum, jejunum and ileum) and large intestine. The large intestine, so called colon, starts from the cecum and consists of three compartments of the proximal, transverse and distal colon[36]. The epithelial structure of each part of the intestine is organized in a specific pattern to meet its physiological requirements. For example, one of the major differences between these two tracts is that colon don't harbour villi, which is an important region to absorb nutrients, as well as the nutrient exchange between the host and the lumen. Colon plays the major role in water reabsorption from faeces and act as a barrier to the commensal microbiota. Indeed, a large number of goblet cells are located in colon and produce an extensive and thick layer of protective mucus to protect the host from microbial invasion[37]. Taken together, as the front line of host's immune system, the intestinal tracts are routinely challenged by various food derived antigens, allergens and nutrients, as well as commensal/pathogenic microbiota. To maintain intestinal homeostasis, immune activation

and quiescence are regulated bidirectional in the gut, which requires certain types of immune cells and organs.

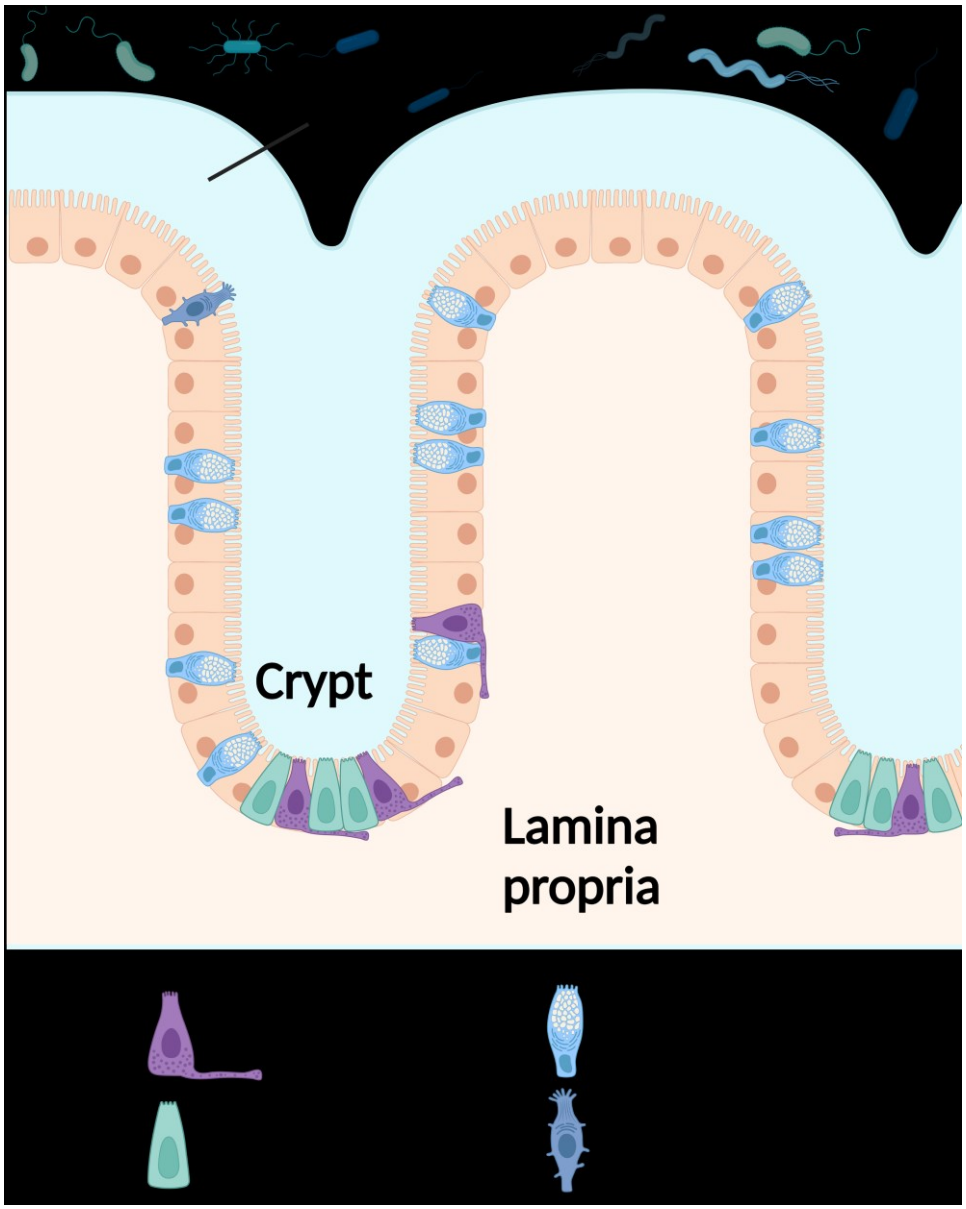

Figure 1 Structure of colon and major epithelial cell types

Intestinal stem cells mainly reside at the crypt base and are dominantly involved in the remarkable ability of renewing and repairing the intestinal epithelium. Enteroendocrine cells are a rare subset of epithelial cells that mainly responsible for intestinal motility and secretion of hormones. Tuft cells constitute a small proportion of IECs (~0.5%). Goblet cells are responsible for the production and maintenance of the protective mucus blanket by synthesizing and secreting mucins.

1.4 The intestinal lamina propria and its mucosal immune system

The intestinal immune response is typically subdivided into two parts: The intestinal inductive sites including the Peyer's patches (PP) and mesenteric lymph nodes (MLN) and the effector sites which consist the lamina propria (LP) and intraepithelial lymphocyte (IEL) compartment[38]. The increase of T-lymphocytes, as well as plasma cells and neutrophils in the lamina propria are normally considered as the sign of inflammation[39].Importantly, the largest population (70%-80%) of immune cells such as T cells, plasma cells and macrophages in the body are located in the intestinal lamina propria and epithelium[40]. The lamina propria contains B cells, T cells and numerous innate immune cell populations — including DCs, macrophages, eosinophils and mast cells — whereas the epithelium primarily contains T cells[37]. Thus focusing on the alteration of immune cell population especially in the lamina propria becomes critical in characterizing IBD development and progression.

Mucosal lymphocytes originate from the bone marrow and subsequently reach the circulation. These lymphocytes are primed after entering lymph nodes or additionally primed locally in the lamina propria via dendritic cells in the subepithelial dome region[41]. Moreover, specific surface receptors such as $\alpha 4\beta 7$ integrin heterodimer that binds to the addressin MAdCAM-1 on intestinal endothelial cells regulates the homing of these lymphocytes. Thus targeting the homing of lymphocytes, including the population alteration in the lamina propria becomes critical in IBD research and therapy.

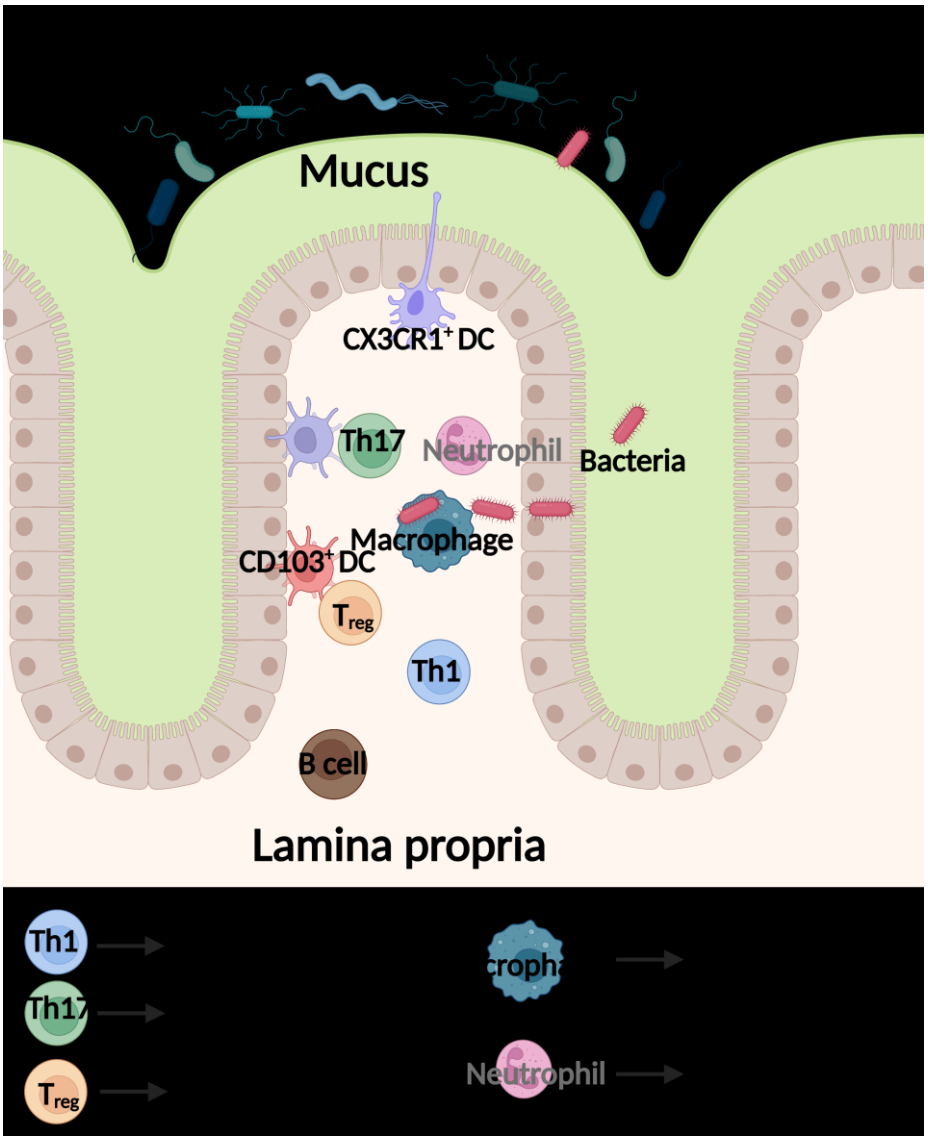

Figure 2 Major immune cell population in the colon lamina propria

Activation of immune cells, as well as the derived cytokines and mediators contribute to the IBD development and progression.

1.4.1 $CD4^+$ and $CD8^+$ T cells

Lamina propria is a mucosal region that located beneath the epithelial cell layer's basement membrane and lamina propria lymphocytes (LPL) are derived from conventional T cells and display an effector memory phenotype in both rodents and humans[42]. The origin of LPL is thymus, where CD4-CD8- progenitors developed into CD4+T cells (MHC I) or CD8+ T cells

(MHC II) through conventional T cells as intermediate stage[43]. To fulfil their task of encountering antigens, they migrate to peripheral lymphoid organs, such as the lymph nodes and subsequently acquire an activated effector phenotype that drives their migration to the gut associated lymphoid tissues (GALTs)[44]. For example, chemokines such as CCL25 (ligand of CCR9) secreted by the IECs guide the migration of T cells[45] and the integrins α4β7 which expressed on the T-cell surface interact with adhesion molecules such as mucosal vascular addressin cell adhesion molecule 1 (MAdCAM-1) to initiate the attachment and distribution into the intestine[46].

Importantly, unlike the CD8+ enriched compartment IEL, the LP is dominated by T cells expressing the CD4 glycoprotein [47]. Among all CD4+ T cells, helper CD4 T cells (Th) including IL-2+, IL-2+IFNγ+, IFNγ+ and IL-17+ cells, are the major subsets that execute immune functions such as activation and growth of cytotoxic T cells, B cell differentiation and antibody production. [48, 49]. In details, interferon-γ secreted T helper type 1 (Th1) cells participate in host defense against intracellular pathogens; T helper type 2 (Th2) cells produce IL-10, IL-13, IL-5, and IL-4 to protect host against helminths; and T helper 17 (Th17) cells are involved in defense response of extracellular bacteria and parasites through producing IL-17, IL-21, and IL-22 and activating the production of anti-microbial peptides reviewed by[50]. Moreover, interactions between LP CD4 T cells and the gut microbiota are critical for shaping the adaptive immune response in the gut. For instance, the cytokines such as IL17A and IL22 secreted by Th17 cells show protective effects in extracellular pathogenic infection such as Citrobacter rodentium (C. rod)[51, 52]. Similarly, Th17 cells also exert beneficial effects on enteric rodent pathogen infection including intestinal segmented filamentous bacterial (SFB) colonization[53].

1.4.2 Regulatory T cells

Foxp3 expressing regulatory T cells (Treg) also play an important role in intestinal immune homeostasis, especially in regulating responses against bacteria reviewed by[54]. Subtype of Treg, the induced Treg (iTreg) are generated from naïve conventional T cells and are mainly found in the lamina propria and GALT reviewed by[55]. This generation is antigen-driven, particularly the dietary antigens and microbiota at mucosal surfaces.

1.4.3 Dendritic cells

Dendritic cells (DCs) have been characterized to localize in the LP facing the lumen along the intestine[56], as well as GALTs including PP and MLN[57]. The subtype of DCs reside in the LP are diverse. For example, $CD103^+$ DCs induct the proliferation of $CD4^+$ and $CD8^+$ T cells and facilitate the differentiation of $Foxp3^+$ regulatory T cells through inducing the expression of intestinal homing molecules reviewed by[58]. Constitutively migrating to the MLN and delivering antigens from both commensal bacteria [59] and apoptotic IECs[60] are the classic roles of $CD103^+$ DCs in the intestine. Another major subtype of DCs in the LP is $CX3CR1^+$ DCs which regulate the sampling of luminal antigens by extending dendrites through the epithelial cell layer into the lumen[61]. This subtype has been demonstrated to harbour a nonmigratory gut-resident behaviour and considered to regulate intestinal immune response directly in the mucosa[58].

1.4.4 Macrophages

Under steady state, intestinal macrophages are non-inflammatory and act as the major population to phagocytose and kill invading microorganisms[58]. In addition, they do not response actively to cytokines or pathogens which typically induce the production of pro-

inflammatory mediators. This is likely due to the presence of suppressive cytokines, such as IL-10 and TGF-b in the mucosal microenvironment[62]. Indeed, intestinal macrophages produce IL-10 constitutively, and the intestinal macrophages from *Il-10*$^{-/-}$ mice do response to TLP ligand stimulation through elevated cytokine production[63]. In contrast, during intestinal inflammation, as occurs in IBD patients, macrophages are recruited from the blood to the inflamed regions where they release different types of pro-inflammatory cytokines, such as TNF, macrophage infiltrating factor (MIF) and IL-18[64], which have been addressed to be involved in the development of intestinal diseases.

1.4.5 Neutrophils

Neutrophils comprise 50%-60% blood circulating leukocytes and are recruited to the infected/inflamed sites within minutes[65]. Therefore neutrophils are normally the first immune cells which reach the sites and perform a variety of antimicrobial functions including degranulation and phagocytosis in the gut [66] to kill luminal microbes that translocate across the epithelium and invade the mucosa. To fulfil that, neutrophils must first exit the circulation, migrate through the lamina propria and cross the epithelial barrier finally reach the intestinal lumen[65]. Moreover, neutrophils also produce massive amount of pro-inflammatory cytokines such as CXCL8 and anti-inflammatory cytokines including IL-10, and thus are significantly involved in intestinal inflammatory diseases reviewed by[67].

1.5 IBD

Inflammatory bowel disease (IBD) is a chronic inflammatory disease in the GI tracts which is typically classified with Crohn's disease (CD)[68] and ulcerative colitis (UC) [69] with unknown etiology. Clinical characterization of IBD symptoms normally contains abdominal

pain, diarrhea, bloody stools, weight loss and abnormal immune cells infiltration in the intestine [68, 69]. In most patients with CD, the phenotypes (histologically thickened submucosa, transmural inflammation, fissuring ulceration, and granulomas) occurs in a patchy pattern along the GI tracts, dominantly in the terminal ileum and ileocaecal junction[70], whereas UC mainly occurs in the colonic mucosa and submucosa. IBD is a lifelong disease and the incidence and prevalence remarkably increased over the last decades. Importantly, IBD has been considered as one of the most prevalent gastrointestinal diseases with accelerating incidence in newly industrialized countries and developed countries, especially in Europe (ulcerative colitis 505 per 100,000 persons in the southeast of Norway; Crohn's disease 322 per 100,000 persons in Hesse, Germany) and USA[71].

1.5.1 Pathogenesis of IBD

Considerable progress has been made regarding the pathogenesis of IBD and evidence has been found that IBD occurrence is most associated with the host genetic risk, intestinal microbiota, environmental factors and immunological alterations reviewed by[71].

1.5.1.1 Genetic risk

Genome-wide association studies (GWAS) have been notably successful at implicating IBD risk loci, especially under the state that the power has increased due to the increasing amount of the IBD cases in GWAS. Trans-ancestry association studies of IBD have identified differential risk associations for NOD2 and TNFSF15 in European populations and East Asian populations, respectively[72]. In addition, studies have revealed more than 200 genetic variants statistically associated with risk of developing IBD, including ones with unclear functions.[73].

Nevertheless, new associations at common variants contribute to the identification and prioritization of potential genes as therapeutic target.

1.5.1.2 Intestinal microbiota

The presence of symbiotic microorganisms is a key element involved in both forms of IBD pathogenesis, although the association with specific susceptibility loci and the type of immune response, as well as pathology differs between CD and UC reviewed by[74]. The considerable amount of microorganisms in the intestine is separated from host tissues by epithelium to minimize the contact between microorganisms and the epithelial surface. This is largely aimed to restrict the access of potentially harmful microorganisms to the mucosal surface, which is achieved by mucus secretion, release of antimicrobial proteins and immunoglobulins into the intestinal lumen reviewed by [75]. In addition, IgA also contributed to the separation of intestinal bacteria from the epithelial surface by coating bacteria and binding to microbial antigens through T cell-independent and T cell-dependent processes reviewed by[76]. Breakdown of the separation and the abnormal mucus layer promote the close contact between microbiota and the intestinal epithelial surface and thus likely increase the susceptibility to IBD development reviewed by[75]. Indeed, enteric pathogens, such as *Salmonella enterica*, produce mucin-degrading enzymes and have evolved mechanisms to counter antimicrobial proteins[77].

Although no pathogen or pathobiont has been consistently identified as the causal for IBD, human and rodent studies have provided solid evidence to support the role of microbiota in the pathogenesis of IBD. For example, antibiotic treatment can induce remission as well as prevent relapse in IBD patients[78]. In animal models, oral transfer of the faecal microbiota from mice

with colitis into healthy animals is sufficient to induce disease[79] and germ free mice are free of immune-mediated colitis[80].

1.5.1.3 Immunological alterations in IBD

Innate and adaptive immune system are both involved in the immunological regulations in IBD development and progression.

The innate arm of the mucosal immune system contains innate lymphoid cells (ILCs), which are grouped based on their expression of transcription factors and cytokines with lineages, namely IFN-γ-expressing group 1 ILCs (ILC1) depend on the transcriptional factor T-bet, IL-5-expressing group 2 ILCs (ILC2) depend on RORa and GATA3 and IL-17A-producing group 3 ILCs (ILC3) reviewed by[81]. ILCs are not capable to be differentiated by antigen-specific receptors and markers but bridge the innate and adaptive immune system. Moreover, ILC1 are found to elevated in CD patients[82] and ILC3 are involved in the development of UC-like colitis[83], indicating the link between ILCs and IBD.

Antigen-presenting cells such as dendritic cells, macrophages and B cells are important in initiating T-cell-mediated responses and highly involved in intestinal homeostasis. For example, DCs have been found to enriched in inflamed intestinal regions in IBD patients[84] and increased in the lamina propria in mice with colitis [85]. Similarly, in CD patients, amount of macrophages in the mucosa are also elevated, following massive amount of proinflammatory cytokine TNF-a[86]. B cells modulate the effector response but not the primary T-cell responses while acting as APCs reviewed by[87] and increased amount of B cells have been identified in UC patients[88], although the functional implications remain to be addressed.

In addition, IBD is a strongly T-cell mediated disease through specific responses to antigens, which is in contrast to the innate immune system. In CD patients, mucosal T cells secreted significantly higher levels of Th1-response cytokines such as IFN-y, which result in the release of TNF-a[89]. Th-17 cells and its cytokines also plays important roles in regulating inflammatory responses in IBD. Genome-wide association scan characterized several IBD susceptibility genes related to Th17[73] and IBD patients have high amount of Th17 cell, as well as related cytokines such as IL-23 and IL-17A in the mucosa and lamina propria[90]. Nevertheless, evidence have been found to demonstrate the protective role of IL-17A in intestinal inflammation. For example, IL-17A deficiency exacerbates the experimental colitis in mice[91] and ameliorates inflammation through inhibiting Th1 cells[92].

Treg cells suppress innate and adaptive immune responses through cytokines or interaction with immune cells. In details, Treg produces TGF-β which negatively regulates T-cell function, and IL-10 which is identified to perform anti-inflammatory effects. Both cytokines have been found to be expressed abnormally in the intestinal mucosa of IBD patients reviewed by[55]. Moreover, direct evidence which highlight the critical role of Treg in intestinal inflammation has been shown in both mouse models (Treg deficiency results in colitis)[93] and IBD patients (Treg are enriched in the intestinal mucosa).

1.6 Circadian control of the pathogenic factors

1.6.1 Circadian control of intestinal microbiota

Microbial dysbiosis has been considered to play a major role in the development of metabolic diseases, colorectal cancer and gastrointestinal inflammation[94-96]. Moreover, circadian

disruption is also associated with similar physiological consequences [97] including microbial dysbiosis[98]. Nevertheless, little is known regarding the rhythmicity of microbiota in regulating host intestinal homeostasis.

In mice, gut microbiota composition and abundance is highly dependent on meal timing, diet and other environmental cues, roughly 10–15% of gut bacteria undergo diurnal oscillations[98, 99]. Recent research from our group provided evidence that the intestinal clock is indeed the main driver of microbial rhythmicity and arrhythmic microbiota can indeed alter gastrointestinal immune homeostasis, such as altering the expression of inflammatory genes and supressing the recruitment of immune cells to the colon lamina propria[27]. Similar to mice, in a large scale cohort human study, arrhythmic microbiota is capable to be used to classify and predict the risk of type-2 diabetes[94]. These findings demonstrated a functional link between microbial rhythmicity and health, although direct evidence proving the cause-effect relationship between disruption of microbial rhythmicity and intestinal diseases remains to be addressed.

1.6.2 Circadian control in host-pathogen interactions

Many studies shed lights on how time of day impact the outcome of infection initiated by bacteria and virus. For example, mice infected by Salmonella enterica subsp. enterica serovar Typhimurium (S. typhimurium) during the day have higher levels of the pathogen compared to the night. And global disruption of CLOCK alters this time-dependent difference[100]. Similarly, by genetically deleting the core clock gene *Bmal1* in mice globally, viral infections of herpes, influenza A, and respiratory viruses of the Paramyxoviridae family are enhanced[101, 102]. In addition to genetic disruption of circadian system, chronic jet lag induced

desynchronization and misalignment of circadian rhythms exacerbates Sendai virus (SeV) or influenza A virus induced acute bronchiolitis in mice[103].

1.6.3 Circadian control in immune cells development and trafficking

Evidence have been found that both innate and adaptive immune system are under circadian control. Innate immune cells such as monocytes, macrophages, neutrophils have been demonstrated to harbour intrinsic clocks reviewed by [104]. Similarly, immune cells involved in adaptive immune system such as T cells[105], B cells[106] and dendritic cells[106] also follow circadian oscillation. Moreover, not only the development of immune cells, but also the trafficking, exhibit circadian patterns. Several pro-migratory factors such as the chemokine receptor CXCR4 has been associated with the rhythmic trafficking of immune cells through the regulation of glucocorticoid[107]. Interleukin-7 receptor (IL-7R) plays a vital role in T cell differentiation and its transcription can be rhythmically activated by glucocorticoid, thereby enhancing CXCR4 expression and supporting T cell recruit to various tissues[108]. Moreover, the rhythmic migration and traffic of immune cells has its physiological outcome. For example, the diurnal recruitment of T cells into immune organs enhances the immune responses to soluble antigens and systemic bacterial infection at night[109]. Previous studies also demonstrated that innate immune cells efficiently respond to bacterial infections at subjective night reviewed by[110]. Taken together, these findings indicate that the recruitment and effectiveness of immune cells involved in immune and infection response relies on circadian cues to optimize their working efficiency.

1.7 The link between IBD and the circadian clock

As discussed in the previous sections, massive amount of evidence have confirmed that various bio-physiological processes along the GI tract are under circadian control, thus disruption of the circadian clock likely contributes to the IBD development and progression. Indeed, environmental circadian disruption in form of shift work as well as system-wide genetic clock dysfunction, e.g. in *Per1/2*$^{-/-}$, *Rev-erbα*$^{-/-}$ and *Bmal1*$^{-/-}$ mice promotes the severity of DSS-induced colitis[111-113].

In addition to the animal research, data from human clinical studies further suggest the importance of functional circadian clock in IBD development. For instance, sleep disturbances reflected by decreased sleeping time and efficiency has been evaluated as a predictive value for IBD histological alteration assessed by colonoscopy[114]. Moreover, a large population longitudinally study which includes 151871 women reported that women with short (<6h/d) sleep or long sleep (>9h/d) were more susceptible to get UC[115]. More interesting interaction were found under molecular level. Severer CD and early diagnosis of IBD were associated with the rs2797685, the allele of clock gene *Per3*[116]. Moreover, not only circadian genes expression were found to be correlated to IBD disease activity, but clock-associated genes expression were identified to be altered under active status[34].

1.8 The impact of food availability on circadian system and diseases

IBD patients are predominantly suffered from multiple periods of relapse and remission. Despite the disease severity might differ among individuals, the majority undergo the alteration between these two stages once diagnosed[117]. Due to the unclear mechanisms of IBD occurrence and relapse, this is still an incurable disease. Although a wide range of medicines

and therapy strategies have been developed in recent years, each of them have their disadvantages and limitations. Thus, additional therapy strategies such as food intervention have been investigated to accomplish the major goal of IBD treatment- maintain the remission stage.

Current major treatment for IBD

Type	Example	Limitations
Aminosalicylates	5-aminosalicylic acid	More effective during early intervention
Corticosteroids	Dexamethasone	Various adverse effects
Immunomodulators	methotrexate	Gastrointestinal intorlerance
Biologics	Adalimumab (Anti-TNF therapy)	Up to 40% of patients do not respond
Small molecules	Tofacitinib (JAK inhibitor)	Further research/clinical data are required
Intestinal microecology	Fecal microbiota transplantation	The long-term efficacy, the safety and the feasibility of universal implementation are unknown

Except social jet lag and sleep debt which are the most common forms of circadian misalignment, inconsistent meal timing were associated with more aggressive phenotypes of IBD and poorer life quality[118]. Peripheral clocks are extremely sensitive to the food availability and pattern since it involves in various biological pathways including energy sensing and nutrients intake. For example, fasting increases AMP/ATP ratio and activates the

AMPK pathway including SIRT1, which binds the CLOCK:BMAL1 complex and supresses the *Per2* transcription[119].

Time restricted feeding/eating (RF) has been considered to be beneficial for the health. Several preclinical and murine studies consistently show the robust effect of RF or other forms of intermittent fasting on improving a wide range of chronic disorders, including obesity[120], cancer[121], and neurodegenerative diseases[122], as well as improving leukocyte responsiveness and inflammation outcomes[123]. Importantly, RF has been additionally applied to entrain peripheral circadian clocks, such as liver and adipose tissue clocks[124] and RF was capable to influence the rhythmicity of major clock genes in intestinal tissues independent of the central clock in mice [125, 126]. These findings indicate that the fasting-feeding cycle is more potent for entraning peripheral clocks and RF might exert its beneficial effects partially through restoring tissue-specific clocks and functions.

2 Study objective

Reduced major clock genes expression in the intestine have been identified to correlate with IBD phenotype in both rodent studies and clinical samples, indicating the involvement of circadian clock in intestinal homeostasis, especially inflammation. Tissue specific peripheral clocks dominantly regulates the rhythm of tissue-specific functions and intestinal functions which involved in IBD development, such as mucosal immunity and the microbiome, are under circadian control. Therefore, specific disrupted intestinal clock might contribute to the development and progression of IBD. Indeed, RNA-seq analysis on colonic tissue from *Bmal1*$^{IEC-/-}$ mice helped us to characterize the biological importance of the intestinal clock on transcription level. Based on the complex cause-effect relationship between intestinal clock dysfunction and the severity of GI-inflammation, microbiota transfer experiments were used to demonstrate whether microbial rhythm or host intestinal clock dominantly drives GI-inflammation. Importantly, night-time restricted feeding (RF) in *Il-10*$^{-/-}$ mice was identified as a treatment to restore colonic clock functions, induce microbial rhythms, ameliorate the colitis phenotype and enhance their overall survival. Due to the systemic-wide effect of RF, RF on *Il-10*$^{-/-}$ mice which additionally lack the intestinal clock (*Bmal1*$^{IEC-/-}$x*Il-10*$^{-/-}$) made it possible to validate the target of the beneficial effect of RF.

3 Materials and Methods

3.1 Animal experiments

3.1.1 Ethics statement

All animal experiments were approved by the Committee of the Upper Bavaria for Animal Health Care and Use (Regierung von Oberbayern; TVA ROB-55.2Vet-2532.Vet_02-18-14), and the EEC recommendations for the care and use of Lab. Anim. (European Communities Council Directive of 24 November 1986 (86/609/EEC)) were also strictly followed.

3.1.2 Mouse models

3.1.2.1 *Bmal1*$^{IEC\ -/-}$ and *Bmal1*$^{flox/flox}$ mouse generation

Mice with *Bmal1* deletion in the intestinal epithelial cells serve as the model for intestinal clock dysfunction. With this in vivo mouse model, the impact of the intestinal circadian clock on GI-functions can be specifically examined since all other clocks outside the intestine, including the SCN clock are still functional. For this purpose the Cre/loxP-System was used. In particular, mice with a floxed allele of the clock gene *Bmal1* will be used to disrupt the circadian clock locally. Mice which express Cre recombinase under the direction of the mouse villin 1 promoter will act as Cre-lox tool for deletion of Bmal1 floxed sequences in intestinal epithelial cells of the villi and crypt cells of the small and large intestines. Intestine conditional Bmal1 knockout mice (*Bmal1*$^{IEC-/-}$) are generated by crossing floxed Bmal1 female mice obtained from Jackson Laboratories (B6.129S4 (Cg)-Arntltm1Weit/J) with hemizygous Vil-Cre male mice.

3.1.2.2 *Bmal1*$^{IEC\ -/-}$x*Il-10*$^{-/-BL6}$ mouse generation and *Il-10*$^{-/-Sv129}$ mouse

As a human IBD-related mouse model, *Il-10*$^{-/-}$mice were also used alone or cross bred with *Bmal1*$^{IEC-/-}$ mice to generate the double knocked out mice. Male intestinal epithelial cell-specific *Bmal1* and interleukin-10 double knock-out mice (*Bmal1*$^{IEC\ -/-}$x*Il-10*$^{-/-BL6}$) were generated by crossing *Bmal1*$^{flox/flox}$x*Il-10*$^{+/-BL6}$ with *Bmal1*$^{IEC-/-}$x*Il-10*$^{+/-BL6}$ under SPF conditions. Interleukin-10 knock-out mice under BL6 and Sv129 background were initially provided by The Jackson Laboratory and bred internally. All mice were bred for several generations in our animal facility to harmonize the intestinal microbiota and were sacrificed at different ages according to various experimental aims. All mice received an ad libitum standard diet (autoclaved V1124-300; Ssniff, Soest, Germany), or proved night restricted feeding diet, and autoclaved water. All mice were single-housed with running wheels under normal light conditions(LD:12-12), or 2 weeks-constant darkness if specified, to examine the activity. Cervical dislocation was performed in the end point of all the experiments.

3.1.3 Behavior analysis

Handling and activity measurements during experiments were performed as described[127]. Wheel-running activity was analyzed using ClockLab software (Actimetrics). The last 10-14 days of each condition were used to determine the period (tau, calculated using a X^2 periodogram and confirmed by fitting a line to the onsets of activity), the duration of the active period (alpha), the amount of activity and the subjective day/night activity ratio (where the subjective day under DD conditions is the inactive period between the offset of activity and the onset of activity and the subjective night is the active period between the onset of activity and the offset of activity). Average daily food intake was measured in the second week of different light conditions under *ad libitum* condition. For restricted feeding condition, average daily food

intake was measured manually over 3 consecutive days in the last week of restricted feeding period.

3.1.4 Light-dark (LD) and constant darkness (DD) conditions

Male *Il-10*$^{-/-Sv129}$ mice and wild type littermates were single-housed at 8 weeks old under LD cycle for 2 weeks (age 8-10 weeks), switched to a DD cycle for 2 more weeks (age 10-12 weeks) and subsequently back to LD.

3.1.5 Tissue collection

All male mice, unless stated otherwise, were sacrificed by cervical dislocation at the age of 18-20 weeks in the second day of darkness at the indicated circadian times (CT), which is considered as the same indicated time points used for normal LD. This was performed independent of external timing cues (Zeitgeber), such as the light-dark cycle to demonstrate rhythms generated by endogenous intestinal clocks. Eyes were removed prior to tissue dissection in dim red light. Tissues were harvested and directly transferred into RNA stabilization solution (NucleoProtect® RNA, MACHEREY-NAGEL) overnight at 4 degrees and then stored in -80 degrees. For fixation, tissues were freshly harvested and then transferred into 4% Formaldehyde.

3.1.6 DSS treatment

At age of 8-9 weeks old, mice were single housed under LD till age of 14w, then got released into DD to exclude extra timing cues and treated with 2% (w/v) DSS (MW = 40,000; AppliChem, Darmstadt, Germany) through their drinking water for 5 days. 2 days of normal drinking water was then applied after the DSS administration. Mice were sacrificed on day 7

circadian time 7 (defined by calculation of running wheel activity). The Disease Activity Index (DAI), ranging from 0 to 12, was determined for each mouse daily by scoring weight loss, stool consistency, and rectal bleeding of mice throughout DSS treatment, as described previously[128].The scores were defined as follows: weight loss (no loss = 0; < 5% = 1; 5%–10% = 2; 10%–20% = 3; > 20% = 4), stool consistency (normal = 0; loose stool = 2; diarrhea = 4), and rectal bleeding (no blood = 0; Hemoccult positive = 1; visual pellet bleeding = 2; gross bleeding or blood around anus = 4). On the day of sacrificing, the spleen, jejunum, mesenteric lymph nodes and colon were harvested. The jejunum and colon were processed according to the method described in 3.1.9. Approximately 2 pieces of 0.5 cm of the jejunum, proximal colon (adjacent to the caecum) and distal colon was removed, one fixed with 4% formaldehyde for subsequent histological analysis. And the other pieces were stored in RNAlater stabilization solution (MACHEREY-NAGEL, Düren, Germany) for subsequent RNA analysis.

3.1.7 Restricted feeding of the mice (night)

As nocturnal animal, the majority of eating behaviour for mice happens during the night[129]. Two different strains of *Il-10*$^{-/-}$ mice have gone through the protocol of night restricted feeding (RF), namely internal bred C57BL/6 and 129/Sv background *Il-10*$^{-/-}$ mice, as well as the corresponding control and double knocked out mice, got single housed at age of 8 weeks, then went through normal light/dark cycle(LD(12:12)) for 2 weeks, constant darkness(DD) for 2 weeks, and back to normal LD for 2 weeks, followed by 3 days of ZT13-ZT21 RF, 3days of ZT13-ZT19, then stable ZT13-ZT17(4hours-night RF) for 4 weeks. The same RF regimen also applied to *Bmal1*$^{flox/flox}$, *Bmal1*$^{IEC-/-}$, *Il-10*$^{-/-BL6}$ and *Il-10*$^{-/-BL6}$ x *Bmal1*$^{IEC-/-}$ mice, with an earlier start point at age of 10 weeks. Tissues were harvested at the end of the 4-week-RF period, on the 2nd day in constant darkness.

The gradual RF protocol described above was aiming to try to introduce the minimum stress and impact to the mice.

3.1.8 Complement 3 (C3) ELISA

As the most important and abundant protein in the complement system and immune response, C3 levels were measured by mouse C3 ELISA kit (BIOZOL, Eching, Germany) in feces of the $Bmal1_{IEC}^{-/-}$ and WT mice at age of 20w old according to the manufacturer's instructions. Briefly, feces were weighed and dissolved in PBS. After centrifugation (5min; 500xg), the supernatant was collected and dissolved in 1x dilution buffer (1:25). Enzyme antibody diluted in 1x wash buffer (1:100) and added to the samples/ standards. After 20 min of incubation with substrate solution in dark, the reaction was stopped and the C3 concentration was measured at 450nm using a Thermo labsystem multiscan spectrometer.

3.1.9 Immune cell isolation from the lamina propria and IEC isolation

Freshly harvest jejunum and colon were flipped, gently washed in PBS and cut into 1 cm pieces. To firstly isolate the epithelial cells, all pieces were incubated in 20ml DMEM (Gibbco, Cincinnati, OH) containing 10% fetal calf serum (FCS superior, Biochrom, Berlin), 1.0% Glutamine and 0.8% antibiotics/antimycotics (all Sigma- Aldrich, Taufkirchen, Germany) with 20 µL of 1M dithiothreitol (DTT, Roth, Karlsruhe, Germany) at 37°C. After 200rpm shaking for 15 min, tissues were transferred into 20ml PBS with 200 µL of 150mM EDTA at 37°C followed by another 10 min shaking. The media were centrifuged at 500g for 5 min, the pellets were combined and washed and stored in lysis buffer at -80°C until further processing. Jejunum tissue was then digested at 37°C for approximately 15 min in Thermoshake with 0.6 mg/ml type VIII collagenase (Sigma-Aldrich). Colonic tissue was digested simultaneously under the

same condition for approximately 25 min but with the mixture of 0.85 mg/ml collagenase V (Sigma-Aldrich), 1.25 mg/ml collagenase D (Sigma-Aldrich), 10µl/ml Amphotericin (100x), 1 mg/mL Dispase II, and 30 U/mL Deoxyribonuclease I (Sigma). Following digestion, intestinal cells were passed through a 40 µm strainer. Consequently, cells were fixed with 2% PFA for 20min, then washed, and stored in RPMI at 4 °C until further processing.

3.1.10 Microbiota transfer experiment

Cecal microbiota (collected at CT13) from either *Bmal1*$^{IEC-/-}$ and their controls, or severely inflamed *Il-10*$^{-/-BL6}$ mice (n=4, mixture) were gavaged into germ-free *Il-10*$^{-/-BL6}$ recipient mice, or germ-free *Bmal1*$^{IEC-/-}$ and their control recipient mice, respectively. 100µl of 7x10^{6} bacteria/µl were used for gavaging each mouse. Mice were weekly monitored for bodyweight changes and feces was sampled and stored in DNA stabilizer at week 5 after gavage. Mice were sacrificed on the second day of constant darkness at CT1 and CT13. All mice were kept in the gnotobiology facility in isolators equipped with HEPA-filters at 22 ± 1 °C with a 12-h light/dark cycle (lights on 5 am till 5 pm). Mice were single housed and had ad libitum access to autoclaved chow (V1124-300, Sniff Diets, Soest, Germany) and autoclaved water.

3.2 Organoid culture

Freshly isolated tissue pieces from small intestine and colon were placed in phosphate-buffered saline (PBS) and 120µl 0.5M EDTA to detach the villi from the tissue. Tissues were changed to new tubes after 30 min incubation at 4 °C with gently shaking. Intestinal crypts were resuspended in Matrigel™ (BD Biosciences) and then seeded in 25 µl drops in 64-well plates after filtering and centrifuging. Plates were incubated at 37ºC for 15min to allow suspension to polymerize before fresh medium was supplied. Organoid medium (IntesticultTM, Stemcell)

was replaced every 3-4 days. Organoids for each time point were plated into a separate plate to limit manipulation or exposure to possible resetting cues, such as temperature. After synchronization with serum shock (50% Fetal Bovine Serum and 50% Intesticult) for 2 hours, medium was replaced with basic organoid medium (IntesticultTM, Stemcell). Every 6 hours over a 24-hour period (starting at 12h after serum shock) medium was removed and organoids were transferred to -80°C until further processing.

3.3 Flow cytometry measurement

Fixed cells were washed and then permeabilized with 0.5% saponin for 10min, followed by several washing steps. Antibody mixture dissolved in staining buffer were added and cells were incubated in dark on ice for 30min. After washing cells were resuspended into Flow buffer and keep on ice until measuring. The detailed antibody strategy is listed below:

Antibody	Dilution	Company
PerCP-Cy5.5 anti CD3	1:50	BioLegend
FITC anti CD4	1:100	BD Biosciences
PE anti CD8	1:100	BD Biosciences
PE-Cy7 anti IL-17A	1:50	BioLegend
APC anti IFN-y	1:50	eBiosicence
PE anti CD11c	1:100	BD Biosciences
APC-Cy7 anti CD11b	1:100	BioLegend
PE-Cy7 anti F4/80	1:100	BioLegend
APC anti Ly6G	1:100	BioLegend

3.4 RNA-seq

Colon tissue were collected through 6 different time points with 4h interval, each time points 4 replicates. RNA quality was verified using an Agilent2100 Bioanalyzer with RNA 6000Nano Reagents. Library preparation and rRNA depletion was performed using the TruSeq Stranded mRNA Library Prep Kit. After the final QC, the libraries were sequenced in a paired-end mode (2x150 bases) in the Novaseq6000 sequencer (Illumina) with a depth of $\geq$ 12 Million paired reads per sample.

3.4.1 Pre-processing

The quality of Next Generation Sequencing data was assessed with FastQC v0.11.5 (RRID:SCR_014583, http://www.bioinformatics.babraham.ac.uk/projects/fastqc/). Adapter content and low quality reads were removed using Trimmomatic v0.39 [130]

Trimmed FASTQ files were then mapped against the mouse mm10 genome with the STAR v2.7.5c aligner[131]. Format conversions were performed using samtools v1.3.1 [132]. The featureCounts program v1.4.6 [133] was used to count reads located within an exon, do not overlap multiple features, with a threshold of MAPQ > = 4 and are not chimeric.

3.4.2 Normalization and differentially expressed genes analysis

DESeq2 version 1.22.0 (RRID:SCR_015687 [134]) was used to normalize the read count matrix and perform differential expression analysis. Bioconductor package ‘‘biomaRt’’ version 2.38(RRID:SCR_002987 [135]) was used to map MGI symbols to Ensembl gene IDs. To identify general DEGs between WT and KO mice, an initial model (Genotype + Time) was used with filtering FC>1.5, Benjamini-Hochberg-Adj.p<0.05 (significantly changed DEGs).

Then a muti-model (Genotype + Period + Genotype::Period) was used to compare day vs night difference.

Gene Ontology biological process enrichment was performed using clusterProfiler (RRID: SCR_016884[136]), GO terms were significantly enriched with the q value<0.05. All genes expressed with minimum 1 count in any of the samples were used as the background universe. Redundant terms were removed manually.

3.4.3 Circadian analysis

The rhythmicity of oscillating transcripts was measured by JTK cycle (Hughes et al., 2010) through the MetaCycle R package[137].With the setting: Period=24h and adj.p < 0.05, filtered genes were then defined as rhythmic. Package compareRhythms[138] was modified and applied to compare rhythmicity differences in transcripts between control and *Bmal1*$^{IEC-/-}$ mice as previously described[27].

3.5 High-Throughput 16S Ribosomal RNA (rRNA) Gene Amplicon Sequencing Analysis

Genomic DNA was isolated from snap-frozen fecal pellets according to a modified protocol of [139] as previously described[94]. DNA NucleoSpin gDNA columns (Machery-Nagel, No. 740230.250) were used for DNA purification. In a two-step PCR the V3-V4 region (using the primers 341F-ovh and 785r-ov) of the 16S rRNA gene was amplified from 24 ng DNA. After pooling, the multiplexed samples were sequenced on an Illumina HiSeq in paired-end mode (2x250 bp) using the Rapid v2 chemistry, in accordance with[94]. Two negative controls, consisting of DNA stabilizer without stool, were used for every 45 samples to control for artifacts and insure reproducibility. High-Quality sequences of read counts > 5000 were used

for 16s rRNA data analysis. Reads FASTQ files were consequently processed using an in-house developed NGSToolkit (Version Toolkit 3.5.2_64) based on USEARCH 11[140]. A trim score of 5 was used on the 5' end and 3'end for the R1 and R2 read followed by chimera removal[141] using the FASTQ mergepair script of USEARCH[140]. Quality filtered reads were merged, deduplicated, clustered and a denoised clustering approach was applied to generate zOTUs[140, 142]. Taxonomic assignment was performed with the EZBiocloud database (Yoon et al., 2017). Data was further analyzed with the R-based pipeline RHEA[143]. Phylogenetic trees are generated by a maximum likelihood approach, which was performed on an alignment generated by MUSCLE with the software MegaX[144]. Trees were visualized and annotated with the use of the online tool EvolView (http://www.evolgenius.info/evolview/)[145]. Spike-in of 12 artificial DNA standards mimicking 16S rRNA genes (a surrogate for bacterial numbers) were used to determine the quantitative copy numbers of rRNA genes per gram of fecal sample between samples. Briefly, the same amount of artificial DNA (6ng) was added to each weighted fecal sample before DNA extraction. After sequencing as described above, FASTQ files were mapped against the spike FASTA sequences (using bowtie2), removing the spike reads and generating a new FASTQ file. By comparing the spike sequencing reads to the fecal bacterial reads; we calculate the quantitative number of 16S rRNA gene copies per gram of sample. The copy number of 16S rRNA gene is proportional to the number of bacteria present in a sample. Thus, this approach enables estimation of microbial abundances relative between samples, suitable for comparative analysis according to[146].

3.6 Untargeted metabolite analyses

Fecal samples were collected from *Il-10*$^{-/-\text{Sv129}}$ mice and their littermates wild types every 3 hours over the course of a 24h day. Samples were directly snap frozen and stored at -80 ◦C upon metabolite extraction. The untargeted analysis was performed using a Nexera UHPLC system

(Shimadzu, Duisburg, Germany) coupled to a Q-TOF mass spectrometer (TripleTOF 6600, AB Sciex, Darmstadt, Germany). Separation of the fecal samples was performed either using a UPLC BEH Amide 2.1 × 100 mm, 1.7 µm analytic column (Waters, Eschborn, Germany) with a 400 µL/min flow rate or with a Kinetex XB18 2.1 x 100 mm, 1.7 µm (Phenomenex, Aschaffenburg, Germany) with a 300 µL/min flow rate. For the HILIC-separation the settings were as follows: The mobile phase was 5 mM ammonium acetate in water (eluent A) and 5 mM ammonium acetate in acetonitrile/water (95/5, v/v) (eluent B). The gradient profile was 100% B from 0 to 1.5 min, 60% B at 8 min and 20% B at 10 min to 11.5 min and 100% B at 12 to 15 min. For the reversed-phase separation eluent A was 0.1% formic acid and eluent B was 0.1% formic acid in acetonitrile. The gradient profile started with 0.2% B which was held for 0.5 min. Afterwards the concentration of eluent B was increased to 100% until 10 min which was held for 3.25 min. Afterward the column was equilibrated at starting conditions. A volume of 5 µL per sample was injected. The autosampler was cooled to 10 °C and the column oven heated to 40 °C. Every tenth run a quality control (QC) sample which was pooled from all samples was injected. The samples were measured in a randomized order and in the Information Dependent Acquisition (IDA) mode. MS settings in the positive mode were as follows: Gas 1 55, Gas 2 65, Curtain gas 35, Temperature 500 °C, Ion Spray Voltage 5500, declustering potential 80. The mass range of the TOF MS and MS/MS scans were 50–2000 m/z and the collision energy was ramped from 15–55 V. MS settings in the negative mode were as follows: Gas 1 55, Gas 2 65, Cur 35, Temperature 500 °C, Ion Spray Voltage –4500, declustering potential –80. The mass range of the TOF MS and MS/MS scans were 50–2000 m/z and the collision energy was ramped from –15–55 V.

The “msconvert” from ProteoWizard[147] were used to convert raw files to mzXML (de-noised by centroid peaks). The bioconductor/R package xcms[148] was used for data processing and feature identification. More specifically, the matched filter algorithm was used to identify peaks

(full width at half maximum set to 7.5 s). Then the peaks were grouped into features using the "peak density" method[148]. The area under the peaks was integrated to represent the abundance of features. The retention time was adjusted based on the peak groups presented in most of the samples. To annotate possible metabolites to identified features, the exact mass and MS2 fragmentation pattern of the measured features were compared to the records in HMDB[149] and the public MS/MS database in MSDIAL[150], referred to as MS1 and MS2 annotation, respectively. The QC samples were used to control and remove the potential batch effect, t-test was used to compare the features' intensity between the groups.

3.7 Targeted metabolite analyses

3.7.1 Sample preparation for targeted metabolite analyses

Approximately 20 mg of mouse cecal content was weighed extracted by bead beating (3 times of 20s 6 m/s with 30s breaks) with FastPrep-24 5G bead beating grinder (MP Biomedicals) supplied with a CoolPrep adapter. To measure BA and SCFAs, we used multiple reaction monitoring method and 3-NPH method respectively, as described previously[151]. Analyst 1.7 software (Sciex, Darmstadt, Germany) were used for data acquisition.

3.7.2 Targeted bile acid measurement

20 µL of isotopically labelled bile acids (ca. 7 µM each) were added to 100 µL of sample extract. Targeted bile acid measurement was performed using a QTRAP 5500 triple quadrupole mass spectrometer (Sciex, Darmstadt, Germany) coupled to an ExionLC AD (Sciex, Darmstadt, Germany) ultrahigh performance liquid chromatography system. A multiple reaction monitoring (MRM) method was used for the detection and quantification of the bile acids. An electrospray ion voltage of −4500 V and the following ion source parameters were used: curtain

gas (35 psi), temperature (450 °C), gas 1 (55 psi), gas 2 (65 psi), and entrance potential (−10 V). The MS parameters and LC conditions were optimized using commercially available standards of endogenous bile acids and deuterated bile acids, for the simultaneous quantification of selected 28 analytes. For separation of the analytes a 100 × 2.1 mm, 100 Å, 1.7 µm, Kinetex C18 column (Phenomenex, Aschaffenburg, Germany) was used. Chromatographic separation was performed with a constant flow rate of 0.4 mL/min using a mobile phase consisted of water (eluent A) and acetonitrile/water (95/5, v/v, eluent B), both containing 5 mM ammonium acetate and 0.1% formic acid. The gradient elution started with 25% B for 2 min, increased at 3.5 min to 27% B, in 2 min to 35% B, which was hold until 10 min, increased in 1 min to 43% B, held for 1 min, increased in 2 min to 58% B; held 3 min isocratically at 58% B, then the concentration was increased to 65% at 17.5 min, with another increase to 80% B at 18 min, following an increase at 19 min to 100% B which was hold for 1 min, at 20.5 min the column was equilibrated for 4.5 min at starting. The injection volume for all samples was 1 µL, the column oven temperature was set to 40 °C, and the auto-sampler was kept at 15 °C. Data acquisition and instrumental control were performed with Analyst 1.7 software (Sciex, Darmstadt, Germany) as previously described 90. Briefly, a standard curve (0.5 nM to 15000 nM, 16 points), linear regression and weighting type of 1/x was used to calculated BA concentrations 90. BAs measured are Cholic acid (CA), chenodeoxycholic acid (CDCA), a-Muricholic acid (aMCA), b-Muricholic acid (bMCA), Taurocholic acid (TCA), Taurochenodeoxycholic acid (TCDCA), Tauroursodeoxycholic acid (TUDCA), Taurohyodeoxycholic acid (THDCA), Taurolithocholic acid (TLCA), Taurodeoxycholic acid (TDCA), Tauro-a-Muricholic acid (TaMCA), Glycochenodeoxycholic acid (GCDCA), Glycocholic acid (GCA), Deoxycholic acid (DCA), Lithocholic acid (LCA), y-Muricholic acid (y-MCA), 12-Dehydrocholic acid (12-DHCA), 12-Ketolithocholic acid (12-keto-LCA), 3-Dehydrocholic acid (3-DHCA), 6-Ketolithocholic acid (6-keto-LCA), 7-Dehydrocholic acid (7-DHCA), 7-Sulfocholic acid (7-sulfo-CA), Allocholic acid (ACA), Cholic acid-7ol-3one

(CA-7ol-3one), Ursocholic acid (UCA), Dehydrolithocholic acid (DHLCA), Hyodeoxycholic acid (HDCA), Murideoxycholic acid (MDCA), Ursodeoxycholic acid (UDCA).

3.7.3 Targeted short-chain fatty acid measurement

For the quantitation of short-chain fatty acids (SCFAs) the 3-NPH method was used 91. Briefly, 40 µL of the fecal extract and 15 µL of isotopically labeled standards (ca 50 µM) were mixed with 20 µL 120 mM EDC HCl-6% pyridine-solution and 20 µL of 200 mM 3-NPH HCL solution. After 30 min at 40°C and shaking at 1000 rpm using an Eppendorf Thermomix (Eppendorf, Hamburg, Germany), 900 µL acetonitrile/water (50/50, v/v) was added. After centrifugation at 13000 U/min for 2 min the clear supernatant was used for analysis. The same system as described above was used. The electrospray voltage was set to -4500 V, curtain gas to 35 psi, ion source gas 1 to 55, ion source gas 2 to 65 and the temperature to 500°C. The MRM-parameters were optimized using commercially available standards for the SCFAs. The chromatographic separation was performed on a 100 × 2.1 mm, 100 Å, 1.7 µm, Kinetex C18 column (Phenomenex, Aschaffenburg, Germany) column with 0.1% formic acid (eluent A) and 0.1% formic acid in acetonitrile (eluent B) as elution solvents. An injection volume of 1 µL and a flow rate of 0.4 mL/min was used. The gradient elution started at 23% B which was held for 3 min, afterward the concentration was increased to 30% B at 4 min, with another increase to 40%B at 6.5 min, at 7 min 100% B was used which was hold for 1 min, at 8.5 min the column was equilibrated at starting conditions. The column oven was set to 40°C and the autosampler to 15°C. Data acquisition and instrumental control were performed with Analyst 1.7 software (Sciex, Darmstadt, Germany). Concentrations of SCFA were calculated with the use of linear regression using a standard curve (ranging 0.0004 mM to 2 mM (12 points), SCFAs measured are Acetate, Propionate, Butyrate, Valeric acid, Desaminotyrosine and the Branched-chain Fatty acids (Isobutyric acid, 2-Methylbutyric acid and Isovaleric acid).

3.8 PICRUST 2.0

Sequence of the zOTUs which gained rhythmicity after restricted feeding in *Il-10*$^{-/-Sv129}$ group were used to construct the metagenome using PICRUST2.0[152] for prediction of functional of metagenomic functionality. Corrected zOTU 16 s rRNA gene copy number is multiplied by the predicted functionality to predicted the metagenome. Resulted enzymatic genes classified according to Enzyme Commission (EC) numbers were mapped to Metacyc pathways. Superclasses were removed and Metacyc pathways abundance was used for statistical analysis using STAMP (2.1.3). Statistical differences were calculated based on White's non-parametric t-test and Benjamini Hochberg dales discovery rate to adjusted for multiple testing.

3.9 Gene expression analysis (qRT-PCR) Quantitative real-time PCR

Fresh taken tissues were directly transferred into RNA-later overnight at 4°C and then stored at -80°C. RNA was extracted using RNA purification kits (NucleoSpin RNAII kit, Macherey-Nagel, Düren, Germany) according to the manufacture's instruction. RNA was eluted in 40-60µl (depending on the tissue(size)) RNase free water (Macherey-Nagel, Düren, Germany). The concentration of isolated RNA was measured with NanoPhotometer N60(IMPLEN). cDNA was synthesized from 1000ng RNA using cDNA synthesis kit Multiscribe RT (Thermofischer Scientific). qPCR was performed in a Light Cylcer 480 system (Roche Diagnostiscs, Mannheim, Germany) using Universal Probe Library system according to manufacturer's instructions. For genes expression the following primers and probes were used: Brain and Muscle ARNT-Like 1 (Bmal1) F 5'-ATTCCAGGGGGAACCAGA-' R 5'-GGCGATGACCCTCTTATCC-3' Probe 15, Period 2 (Per2) F 5'-TCCGAGTATATCGTGAAGAACG-3' R 5'- CAGGATCTTCCCAGAAACCA-3' probe 5, Nuclear receptor subfamily 1 group D member 1 (Reverbα) F 5'-AGGAGCTGGGCCTATTCAC-3' R 5'-CGGTTCTTCAGCACCAGAG-3' probe 1, Toll-like

receptor 2 (Tlr2) F- 5'-GGGGCTTCACTTCTCTGCTT-3' R 5'-AGCA TCCTCTGAGATTTGACG-3' probe 50, Angiogenin 4 (Ang4) F 5'-CCCCAGTTGGAGGAAAGC-3' R 5'-CGTAGGAATTTTTCGTACCTTTCA-3' probe 106, Mucin 2 (Muc2) F 5'- GGCAGTACAAG AACCGGAGt-3' R 5'-GGTCTGGCAGTCCTCGAA-3' probe 66, Histone Deacetylase 3 (Hdac3) F 5'- GAGAGGTC CCGAGGAGAAC-3' R 5'-CGCCATCATAGAACTCATTGG-3' probe 40, Tumor necrosis factor alpha (Tnfa) F 5'- TGCCTATGTCTCAGCCTCTTC-3' R 5'-GAGGCCATTTGGGAACTTCT-3' probe 49, Leucine Rich Repeat Containing G Protein-Coupled Receptor 5 (Lgr5) F 5'- CTTCACTCGGTGCAGTGCT-3' R 5'-CAGCCAGCTACCAAATAGGTG-3' probe 60, Toll like receptor (Tlr4) F 5'-GGACTCTGATCATGGCACTG -3' R 5'-CTGATCCATGCATTGGTAGGT-3' probe 2, Nuclear factor kappa-light-chain-enhancer of activated B cells (Nfkb) F 5'-CCCAGACCGCAGTATCCAT -3' R 5'- GCTCCAGGTCTCGCTTCTT-3' probe 47. RNA abundance was normalized to the housekeeping gene Elongation factor 1-alpha (Ef1a) F 5'-GCCAAT TTCTGGTTGGAATG-3' R 5'-GGTGACTTTCCATCCCTTGA-3' probe 67. For Interleukin33 (Il33) gene was used syber green to run the gene using the following primer F 5'-GAACATGAGTCCCATCAAAG -3' R 5'- CAGCTGGTTATCTTTTACTCC -3' and RNA abundance was normalized to the housekeeping gene Ef1a F 5'- GCCAAT TTCTGGTTGGAATG-3' R 5'-GGTGACTTTCCATCCCTTGA-3'.

3.10 Histology

Fixated and dehydrated tissue sections were cut into 5 µm thick slices and consequently stained according to the following steps: xylene/ 5 min, xylene/ 5 min, Ethanol 100%/ 5 min, Ethanol 100%/ 5 min, Ethanol 96%/ 2 min, Ethanol 96%/ 2 min, Ethanol 70%/ 2 min, Ethanol 70%/ 2 min, Water/ 30 s, hematoxylin/ 2 min, tap water/ 15 s, Scotts Tap Water/ 30 s, Water/ 30 s,

Ethanol 96%/ 30 s, Eosin/ 30 s, Ethanol 96%/ 30s, Ethanol 96%/ 30 s, Ethanol 100%/ 30 s, Ethanol 100%/ 30 s, Xylene/ 90 s, Xylene/ 90s (Leica ST5020 multistainer). DPX new mounting media (Merck) was added to preserve the tissues. Histological scores were assessed blindly based on the degree of immune cell infiltration of all colonic wall layers (mucosa, submucosa and muscularis), crypt hyperplasia, goblet cell depletion and mucosal damage, resulting in a score from 0 (not inflamed) to 12 (severely inflamed) according to Katakura method[153].

For AB/PAS staining, tissue slices were deparaffinized and rehydrated before being stained with Alcian blue solution for acidic mucins (1% volume/volume in 3% acetic acid, pH 2.5, 15 minutes), treated with periodic acid solution (0.5% volume/volume, 5 minutes) and co-stained with Schiff's reagent for neutral mucins (Sigma-Aldrich, 10 minutes). Nuclei were then counterstained with hematoxylin. Consequently, tissue sections were differentiated (0.2% ammonia water), dehydrated, and mounted. The number of goblet cells was calculated as a total number per 100 µm2.

3.11 Genotyping

To determine the presence of the knockout allele in the murine intestine, DNA was extracted using the NucleoSpin RNAII kit (Macherey-Nagel, Düren, Germany) from small intestinal tissue samples of mice according to the manufacturer's instructions. For DNA PCR, 100ng DNA was dissolved in 10µL ddH2O. 1µL DNA was mixed with 10µl 2x Onetaq DNA polymerase (NEB) and the necessary quantity and combination of primers, designed for detection of the WT and the knockout allele. The final volume was adjusted to 20 µl with PCR water. The PCR program and details for primers are listed below.

Primer	Sequence	Product size (bp)	Program	Temperature /Time (s)	Target
2402	ACTGGAAGTAACTTTATCAAACTGCAG	mutant: 431 hetero: 328 + 431 wt: 328	Initial Denaturation	94/60	Bmal1
2403	TCTGACCAACTTGCTAACAATTAATTA		Denaturation	94/15	
			Annealing	55/15	
			Extension	68/20	
			Final extension	68/60	
			Cooling	10	
3129L	GTGAAACAGCATTGCTGTCACTT	cre Band: ~ 100 DNA control band: ~ 300	Initial Denaturation	94/60	Villin cre
3129R	GCGGTCTGGCAGTAAAAACTATC		Denaturation	94/15	
2669	GTAGGTGGAAATTCTAGCATCATC		Annealing	58/15	
2670	TAGGCCACAGAATTGAAAGATCT		Extension	68/20	
			Final extension	68/60	
			Cooling	10	
2762	CTTGCACTACCAAAGCCACA	wt band: 137 hetero band: 137 + 312 homo band: 312	Initial Denaturation	94/120	IL-10
2763	CCACACGCGTCACCTTAATA		Denaturation	94/15	
			Annealing	60/15	
			Extension	72/15	
			Final extension	72/30	
			Cooling	10	
2764	GTTATTGTCTTCCCGGCTGT				

3.12 Statistical Analyses

Statistical analyses were performed using GraphPad Prism, version 9.0.0 (GraphPad Software), JTK_cycle v3.1.R[154] or R. Between-sample microbiota diversity is calculated by generalized UniFrac using GUniFrac v1.1. distances within the Rhea[143] pipeline. Microbiota composition comparison was calculated by PERMANOVA test on generalized Unifrac dissimilarity matrix and illustrated by MDS[143]. Circadian profile graphs, as well as phase calculation were analysed by fitting a cosine-wave equation: $y=\text{baseline} + (\text{amplitude} \cdot \cos(2 \cdot \pi \cdot ((x-[\text{phase shift})/24)))$. Non-parametric algorithm JTK_cycle was used for overall rhythmicity of all zOTUs and transcripts. Connected curves in circadian profile graphs within the figures indicate significant rhythmicity based on cosine analyses whereas connected straight lines indicate non-significant cosine fit. Comparison of rhythms between data sets was performed by adjusted version of compareRhythms as previously described[27]. Amplitude calculations depicted in the manhattan plots are based on the output of JTK_cycle and the phase was calculated by cosine-wave regression. Analysis between two groups was performed using the non-parametric Mann-Whitney test (two-sided). Two-way ANOVA followed with Benjamini-Hochberg correction was used to compare dataset with two categorical variables. Three-way ANOVA following Benjamini, Krieger and Yekutieli correction was used to compare dataset which contains three categorical factors. A p value ≤ 0.05 was assumed as statistically significant.

4 Results

4.1 Night time restricted feeding restores the disrupted colonic clock in *Il-10*$^{-/-Sv129}$ mice and ameliorates the colitis

4.1.1 *Il-10*$^{-/-Sv129}$ mice have normal chronotype under various light and feeding conditions

Il-10$^{-/-}$ mice are prone to get human IBD-like colitis and have been widely studied to simulate the conditions in IBD patients [155]. To further investigate the relationship between circadian clock and development of colitis, *Il-10*$^{-/-}$ mice under Sv129 (*Il-10*$^{-/-Sv129}$) background were used to characterize the chronotype of mice suffering from more severe colonic inflammation comparing to BL6 background [155]. In details, mice were released into 12h:12h light-dark cycle and constant darkness (DD) with free access to food (ad libitum, AD) or restricted feeding (RF) (**Figure 1**).

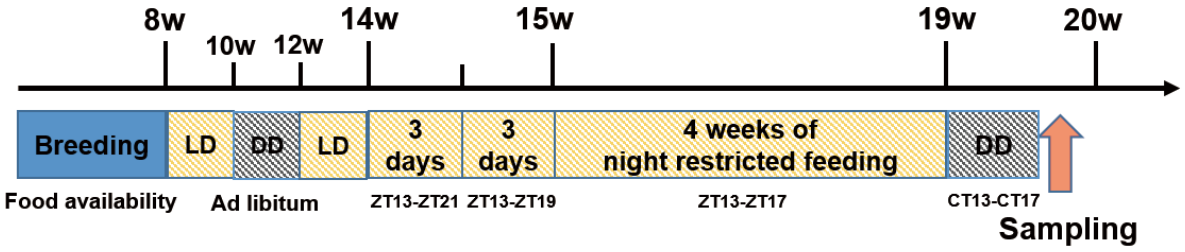

Figure 3 Schematic illustration of the experimental plan for *Il-10*$^{-/-Sv129}$ mice
Running wheel activity were recorded and analysed through the whole experiment.

The development of various GI diseases, including IBD[25] has been linked to circadian disruption, such as occurs during shift work and frequent travel across time zones[20]. In order to characterize whether *Il-10*$^{-/-Sv129}$ mice exhibit a circadian phenotype, 20 weeks old male mice were kept in different light and feeding conditions. Central circadian clock functions, such as rhythmicity of wheel running activity and night time activity during a rhythmic 12-hour

light/12-hour dark (LD) cycle and for at least 14 days in constant darkness (DD) was undistinguishable from controls, although total activity was slightly reduced in *Il-10*$^{-/-\ Sv129}$ mice (**Fig. 2B, C**). No difference in food intake was identified though different light and feeding conditions (**Fig. 2D**).

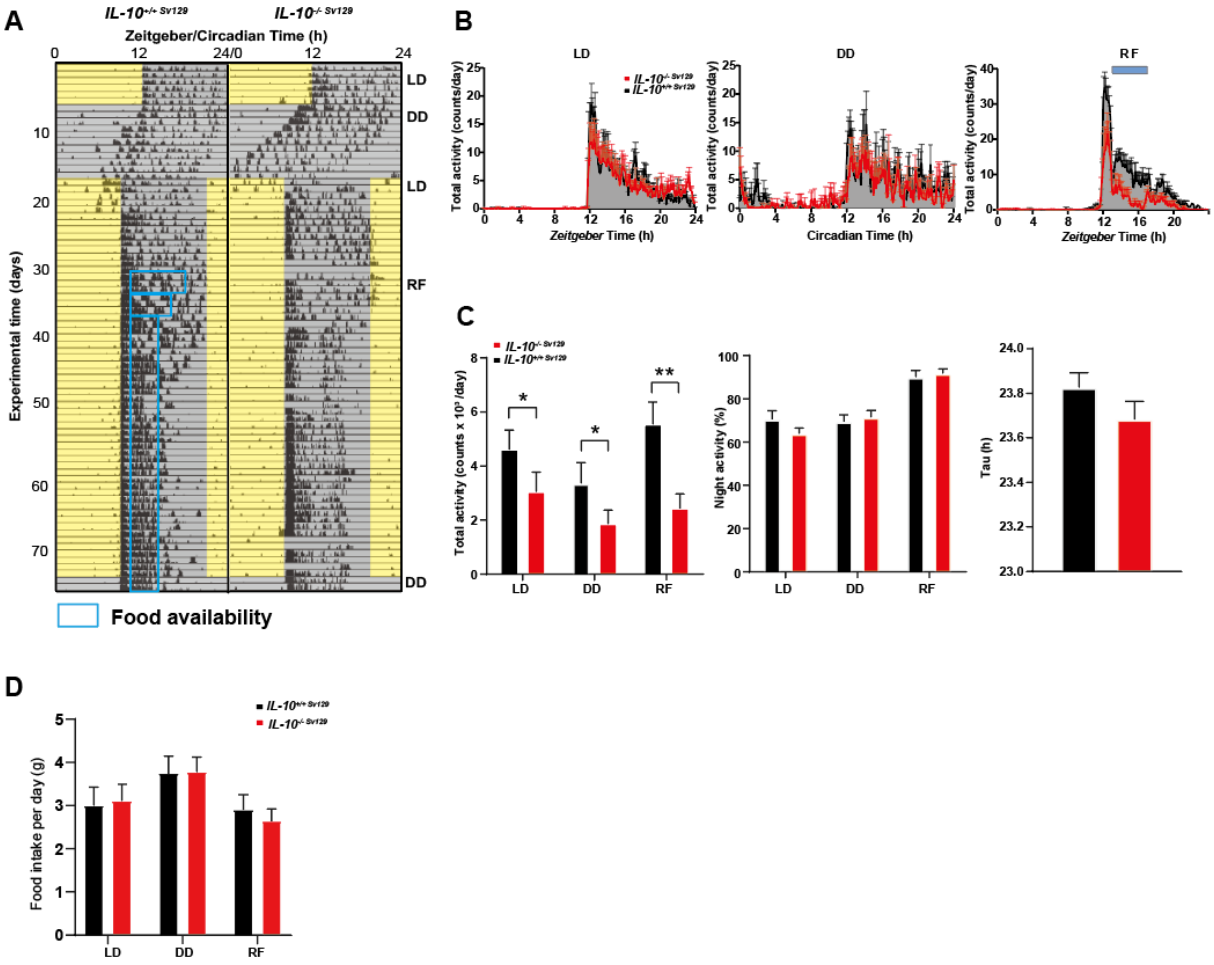

Figure 4 *Il-10*$^{-/-Sv129}$ mice exhibited reduced total activity but normal other chronotype

(**A**) Representative actogram of wild type (*Il-10*$^{+/+Sv129}$) and *Il-10*$^{-/-Sv129}$ mice exposed to light-dark cycle (LD), constant darkness (DD), and night restricted feeding (RF). Tick marks represent running wheel activity; yellow and grey shadings represent light and darkness respectively; blue boxes indicate the time period of food access during RF. (**B**) Representative graph of total activity of control and *Il-10*$^{-/-SV129}$ mice for an individual day and (**C**) Quantification of total activity and Tau. (**D**) Food intake of control and *Il-10*$^{-/-SV129}$ mice in LD, DD and RF. Significance were calculated by two-way ANOVA following Benjamini-Hochberg correction, * $p \leq 0.05$, ** $p \leq 0.01$, *** $p \leq 0.001$, **** $p \leq 0.0001$. Data are represented as mean ± SD.

4.1.2 Altered Major clock genes expression were restored after RF and correlated to pathologic phenotype in *Il-10*$^{-/-Sv129}$ mice

Recently we demonstrated an imbalance of the GI immune homeostasis in a genetic mouse model lacking a functional intestinal clock[27]. This prompted us to characterize the molecular intestinal clock in inflamed *Il-10*$^{-/-Sv129}$ mice. Robust circadian rhythms were found in the expression of the essential clock genes *Bmal1* (*Arntl*), *Rev-erbα* (*NR1D1*) and *Dbp* in cultured jejunal and colonic organoids from wild types (*Il-10*$^{+/+Sv129}$) (**Fig. 3A, B**). Interestingly, clock gene expression was arrhythmic and suppressed in colonic organoids from inflamed *Il-10*$^{-/-\ Sv129}$ mice (**Fig. 3B**), indicating a dysfunctional colonic clock. In contrast, clock gene rhythms in jejunal organoids were comparable between genotypes **(Fig. 3A)**. These data suggest that circadian dysfunction is restricted to inflamed regions of the intestine. Similar to results obtained from organoids, the rhythmicity of clock gene expression was dramatically altered in colonic tissues from 20 weeks old *Il-10*$^{-/-\ Sv129}$ mice. A genotype difference was identified for *Bmal1* ($p=0.0315$), and the amplitude of *Rev-Erbα* ($p<0.0001$) and *Dbp* ($p=0.0003$) expression were strongly reduced in colonic tissue of *Il-10*$^{-/-\ Sv129}$ mice compared to wild type littermates, although low amplitude oscillations persist (**Fig. 3C**). Furthermore, the peak expression of most clock genes was strongly correlated to the colonic histological scores, frequency of immune cells in the lamina propria, including macrophages, neutrophils, $CD4^+$ cells and dendritic cells, as well as the expression of genes involved in intestinal barrier function (**Fig. 3D, E**). These results indicate a potential causal relationship between colon clock dysfunction in *Il-10*$^{-/-}$ mice and their inflammatory phenotype.

Night-time restricted feeding (RF) is a widely-studied approach in mice to influence the rhythmicity of peripheral clocks[156]. This prompted us to test whether RF in *Il-10*$^{-/-\ Sv129}$ mice restores the colonic clock and impacts their Crohn's disease-like phenotype. Indeed, RF

improved the circadian amplitude and baseline of clock gene expression in *Il-10*$^{-/-\ Sv129}$ colonic tissue to similar levels observed in control mice under *ad libitum* (AD) condition (*Rev-erba* p<0.0001, *Dbp* p<0.0001) (**Fig. 3C**). Of note, RF also enhanced the amplitude of clock gene expression in wild types *(Rev-erba* p<0.0001, *Dbp* p=0.0313) (**Fig. 3C**).

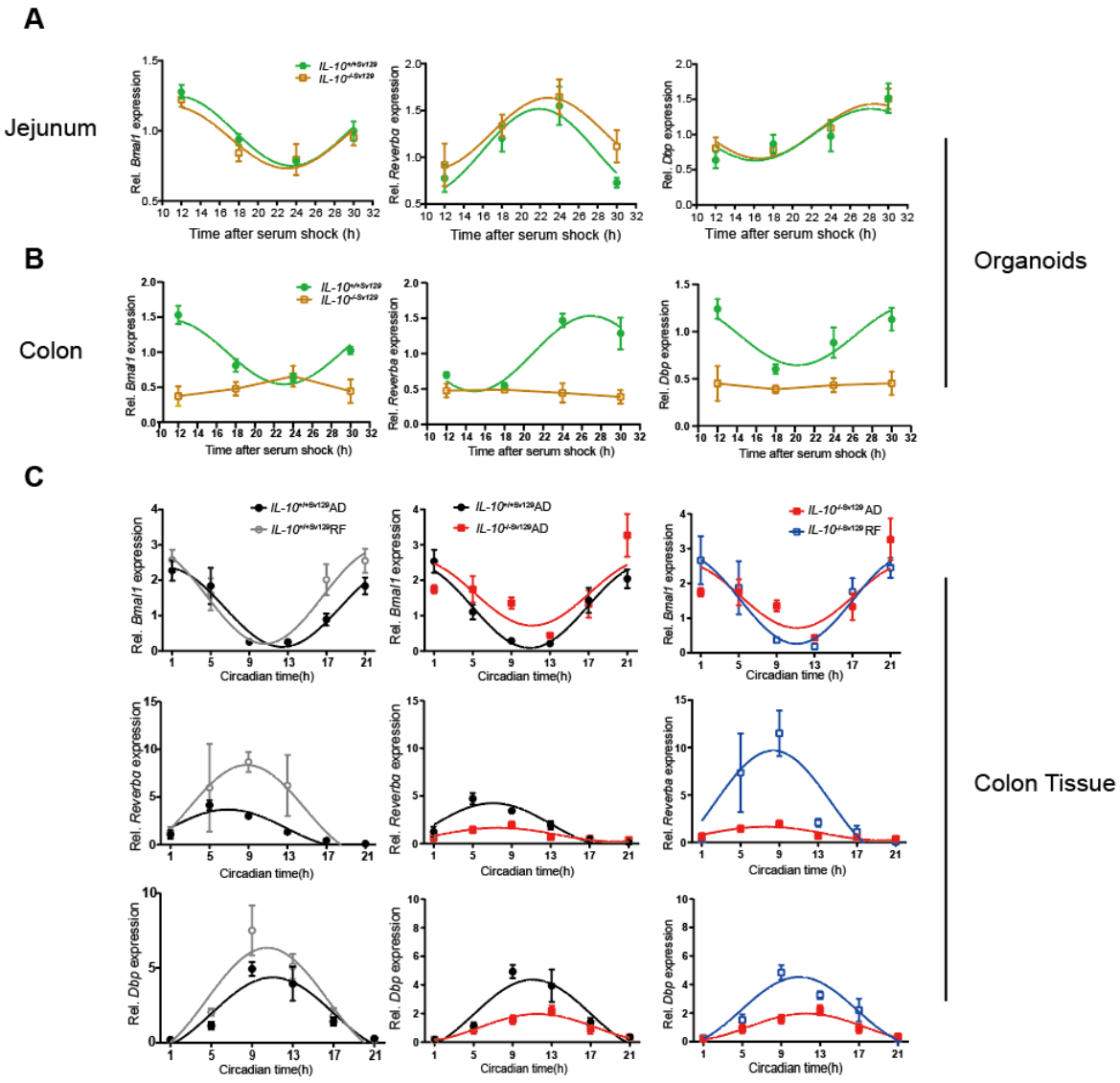

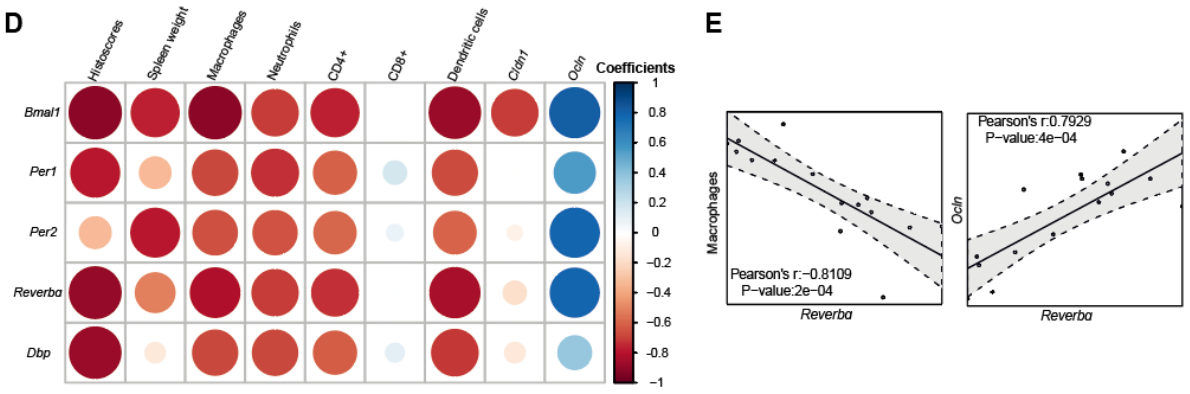

Figure 5 Disrupted clock genes expression in colon tissue from *Il-10*$^{-/-\text{Sv129}}$ mice were restored after RF

(**A**) Clock genes expression in jejunal organoids from control and *Il-10*$^{-/-\text{SV129}}$ mice. (**B**) Clock genes expression in colonic organoids from control and *Il-10*$^{-/-\text{SV129}}$ mice. (**C**) Clock genes expression in colon tissue from control and *Il-10*$^{-/-\text{SV129}}$ mice under AD and RF conditions. Significant rhythms are illustrated with fitted cosine-wave regression using a line (significance: cos-fit p-value ≤ 0.05). Statistics were performed by two-way ANOVA followed with Turkey correction. Data are represented as mean ± SEM. (**D**) Graphical display of all variables combinations in a matrix. Each correlation is depicted as a circle coloured according to the direction of correlation coefficients (negative, red; positive, blue). The size of the circles is dictated by the uncorrected p-value. (**E**) Representative correlation plot from (**H**).

4.1.3 RF ameliorated the IBD-like phenotype in *Il-10*$^{-/-\text{SV129}}$ mice

In addition to the restoration of clock genes expression, RF improved the pathological alteration in *Il-10*$^{-/-\text{ Sv129}}$ mice as well. Importantly, restoration of the colonic clock in *Il-10*$^{-/-\ Sv129}$ mice exposed to RF conditions was reflected by reduced levels of *Tnf* and *Ifn-γ* expression and restored rhythmicity of *Tnf* were observed in *Il-10*$^{-/-\ Sv129}$ mice in contrast to enhanced and arrhythmic expression in AD-fed *Il-10*$^{-/-\ Sv129}$ mice (**Fig. 4A**). In parallel to disruption of the colonic clock in *Il-10*$^{-/-\text{ Sv129}}$ mice, complete loss of rhythmicity of lymphocyte recruitment to the lamina propria. $CD3^+CD4^+$ and $CD3^+CD8^+$ T-cell recruitment was observed, whereas immune cell recruitment underwent circadian oscillation in wild types (**Fig. 4B, C**). Reduced inflammation following RF in *Il-10*$^{-/-\ Sv129}$ mice was additionally reflected by restored rhythmicity in the amount of $CD3^+CD4^+$ cells isolated from colonic lamina propria and an overall reduced amount of CD4 T-lymphocytes (**Fig. 4B**). In contrast, $CD3^+CD8^+$ cells

recruitment remained arrhythmic (**Fig. 4C**). Consistently, the weight of spleen, mesenteric lymph nodes (MLN) and colon density which were severely heavier in AD-fed *Il-10*$^{-/-Sv129}$ mice, were significantly reduced during RF and undistinguishable from controls (**Fig. 4D**). Histological analysis of colon cross sections further revealed more than 58% of *Il-10*$^{-/-Sv129}$ mice under AD condition were identified as highly-inflamed (Histoscore>5), which was dramatically reduced to 5% under RF condition (**Fig. 4E, F**). These data demonstrate that RF restores disruption of colon clock function and completely ameliorates the immune phenotype in *Il-10*$^{-/-Sv129}$ mice.

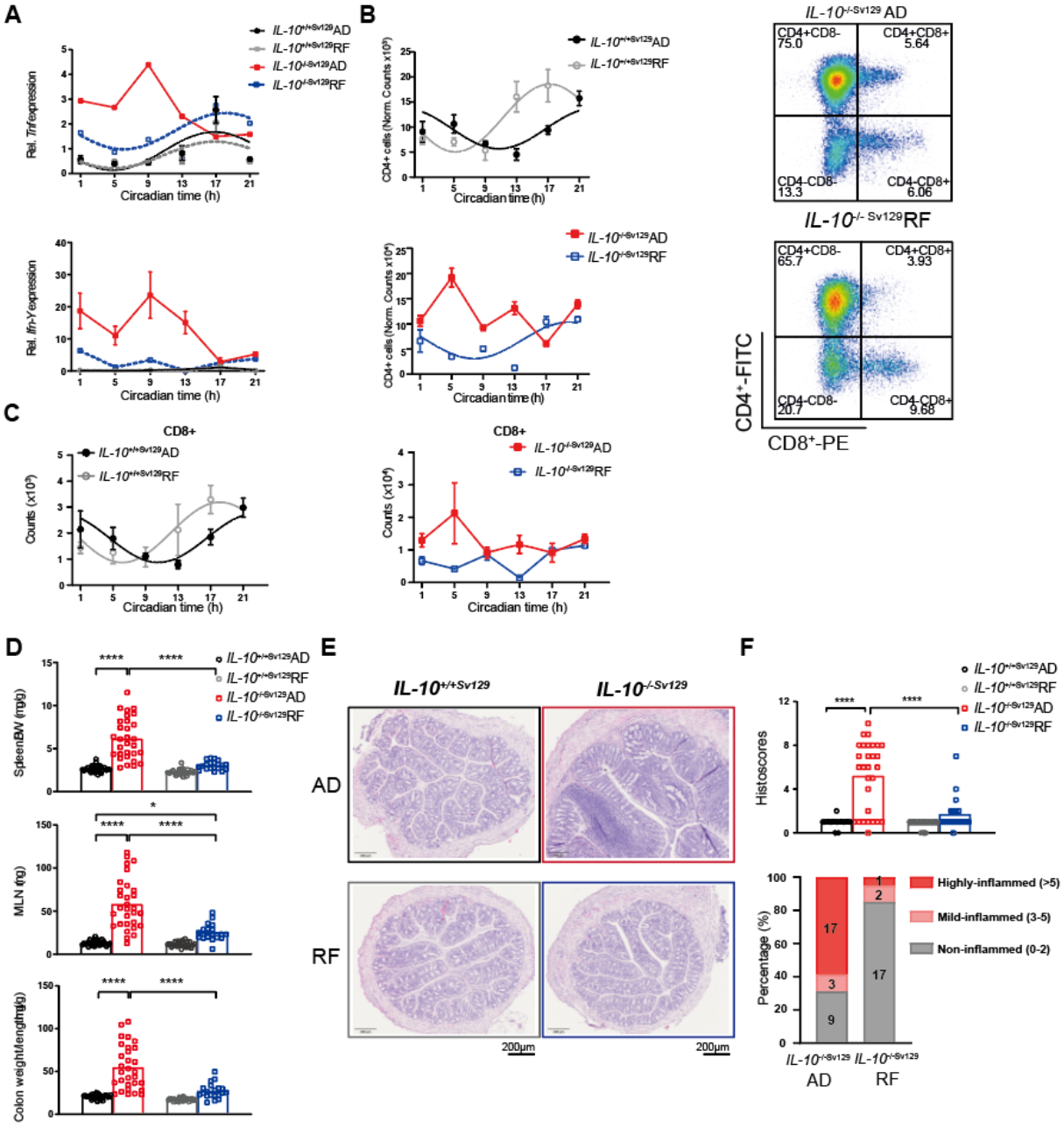

Figure 6 Time-restricted feeding ameliorated the IBD phenotype in *Il-10*$^{-/-Sv129}$ mice

(**A**) Inflammatory genes expression profile of *Tnf* and *Ifn-y* in colonic tissues from wild type and *Il-10*$^{-/-Sv129}$ mice under AD and RF conditions. (**B**) Quantification of the amount of CD4+ T cells in the colon lamina propria from wild type and *Il-10*$^{-/-Sv129}$ mice under AD and RF conditions measured by flow cytometry (left) and representative flow cytometric plots for CD4^{+} and CD8^{+} cells (right). (**C**) Quantification of the amount of CD8+ T cells in the colon lamina propria. (**D**) Organ weights of spleen, mesenteric lymph nodes (MLN) and colon from wild type and *Il-10*$^{-/-Sv129}$ mice in AD and RF conditions. (**E**) Representative colonic cross section stained with Hematoxylin&eosin (H&E) from wild type and *Il-10*$^{-/-Sv129}$ mice in AD and RF conditions. (**F**) Histopathological scores of colonic tissues from wild type and *Il-10*$^{-/-Sv129}$ mice in AD and RF conditions (left) and the quantification of individual mice which characterized with different inflammation degrees (right). Tissues with scores between 0-2 are classified as non-inflamed, 3-5 as mildly inflamed and >5 as highly inflamed. Significant rhythms are illustrated with fitted

cosine-wave regression using a line (significance: cos-fit p-value ≤ 0.05). Statistics were performed by two-way ANOVA followed with Turkey correction. Data are represented as mean ± SEM or individual dot. Asterisks indicate significant differences *p<0.05, **p<0.01, ***p<0.001.

4.2 Loss of microbial rhythmicity during colonic inflammation in *Il-10*$^{-/-Sv129}$ mice is restored by RF

Gut microbiota dysbiosis has been associated with the development of IBD in humans and mouse models[157, 158]. Indeed, microbiota composition differed significantly between genotypes despite the feeding conditions (**Fig. 5A).** In accordance to results obtained from IBD patients[159, 160], reduced abundance of *Lachnospiraceae* and *Oscillospiraceae* and increased level of *Erysipelotrichaceae* were observed in *Il-10*$^{-/-}$ mice under AD conditions (**Fig. 5B**). The genera *Oscillibacter, Eubacterium, Clostridium* and *Pseudoflavonifractor* are among the taxa which significantly differed in their abundance between genotypes (**Fig. 5C, left**). Moreover, we detected significant correlations between disease markers, such as histological score, inflammatory marker gene expression and zOTUs belonging to *Lachnospiraceae* and *Oscillospiraceae* (**Fig. 5D, right**), which is consistent with our recent findings showing a correlation between *Lachnospiraceae* and active disease in IBD patients[161].

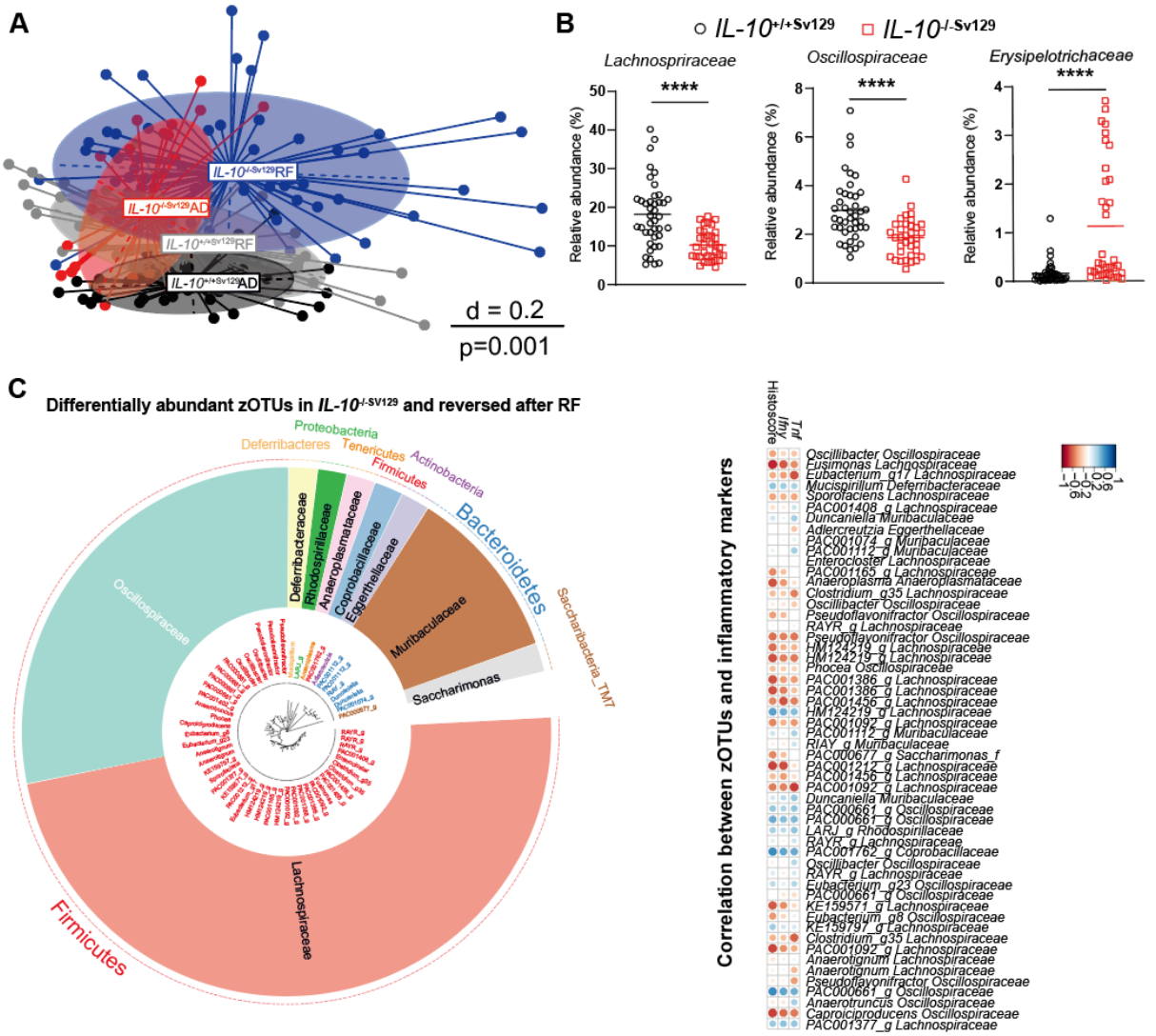

Figure 7 RF altered microbiota composition and most of zOTUs which are relevant for IBD development belongs to family *Lachnospiraceae* and *Oscillospiraceae*

(**A**) Beta-diversity illustrated by MDS plots of fecal microbiota based on generalized UniFrac distances (GUniFrac) in wild type and *Il-10*$^{-/-Sv129}$ mice under AD and RF conditions. Comparison of genotype and feeding effects was performed by PERMANOVA (adj.p=0.001). (**B**) Representative taxa (*Lachnospriraceae, Oscillospiraceae and Erysipelotrichaceae*) which differentially abundant in fecal samples from *Il-10*$^{-/-Sv129}$ mice. (**C**) Taxonomic tree of fecal microbiota which differentially abundant in *Il-10*$^{-/-SV129}$ mice and reversed after RF. Taxonomic ranks are from phylum (outer dashed ring), family (inner ring highlighted) to genera (middle, color coded according to phylum) which are indicated by the individual branches (left) and correlations of zOTUs in (B) with histoscores, *Tnf* and *Ifn-y* gene expression (right). Statistics were performed by Mann–Whitney U test. Asterisks indicate significant differences *p<0.05, **p<0.01, ***p<0.001.

Previously we provided the novel link between the intestinal clock, microbiome rhythms and GI homeostasis[27]. This prompted us to investigate circadian rhythmicity in microbiota composition and function in inflamed *Il-10*$^{-/-}$ mice. Interestingly, circadian rhythmicity in community diversity (normalized species richness) was abolished in AD-fed *Il-10*$^{-/-Sv129}$ mice (**Fig. 6A, left)**. Similarly, the abundance of both major phyla, Bacteroidota and Firmicutes and highly abundant families, including *Lachnospiraceae* and *Oscillospiraceae* as well as zOTUs, followed circadian oscillation in wild types, whereas these rhythms were abolished in AD-fed *Il-10*$^{-/-Sv129}$ mice (**Fig. 6A, right, B**). Importantly, RF not only restored abundance differences between genotypes (**Fig. 5C**), but also restored microbial rhythmicity in *Il-10*$^{-/-Sv129}$ mice, illustrated in community diversity and on the level of major phyla, the two major families *Lachnospiraceae* and *Oscillospiraceae* (**Fig. 6A, B)**. Enhanced microbial rhythmicity was also found among the 237 identified zOTUs visualized by heatmaps and Manhattan plots of the amplitude and adj.p value of zOTUs **(Fig. 6C, D**). More than 50% of the zOTUs which gained rhythmicity during RF in *Il-10*$^{-/-}$ mice belong to the family *Lachnospiraceae*, which includes bacteria taxa important for SCFA production and secondary bile acids (BAs) conversion and thus plays crucial roles in IBD progression[162].

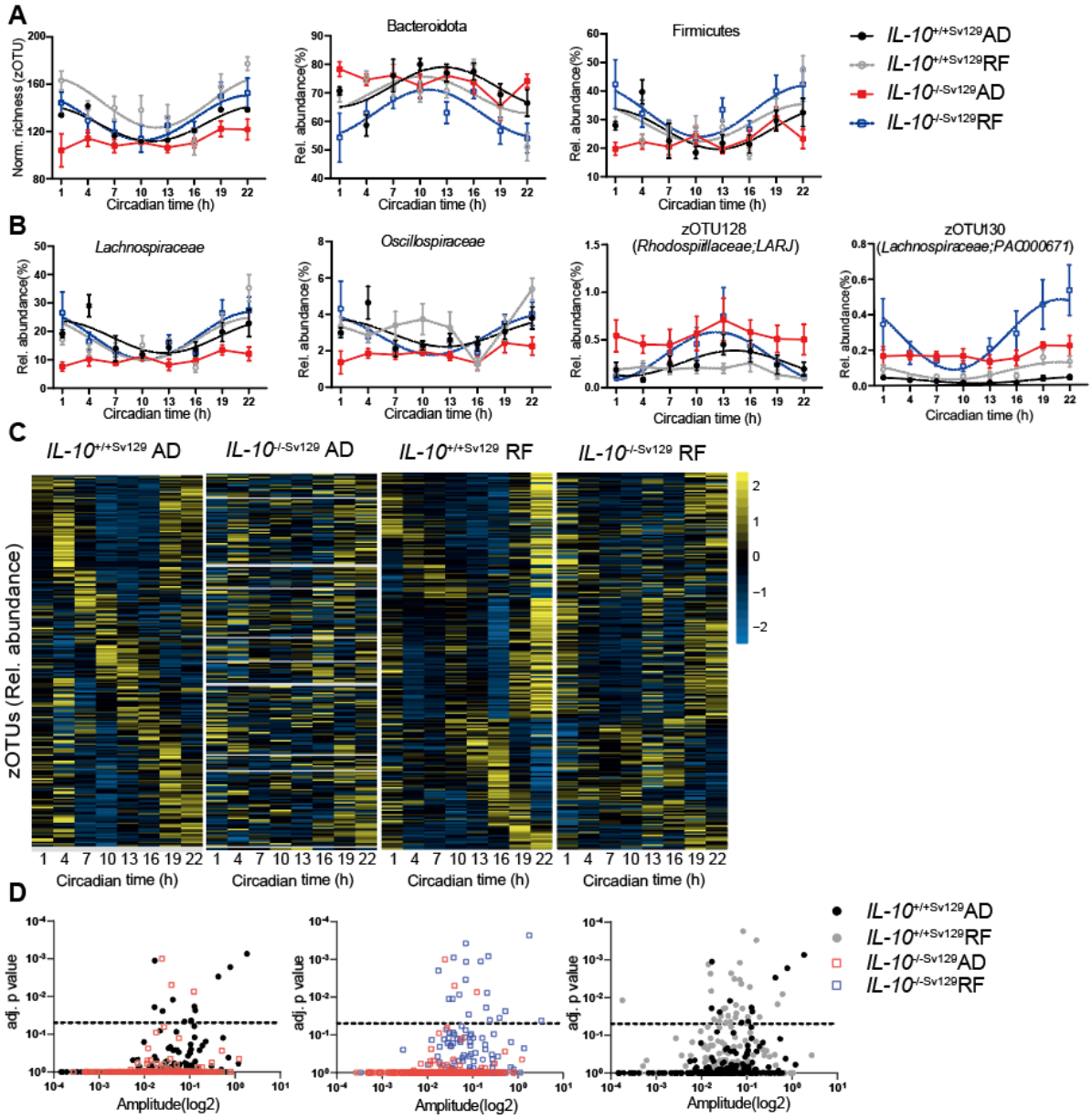

Figure 8 Microbial rhythmicity in *Il-10*$^{-/-Sv129}$ mice under different feeding conditions

(**A**) Circadian profile of normalized richness (left) and relative abundance of two major phyla (*Bacteroidota* and *Firmucutes*) in wild type and *Il-10*$^{-/-Sv129}$ mice under AD and RF conditions (right). (**B**) Relative abundance of highly abundant family *Lachnospiraceae* and *Oscillospiraceae* and relative abundance of two representative zOTUs from wild type and *Il-10*$^{-/-Sv129}$ mice under AD and RF conditions. (**C**) Heatmap depicting the relative abundance of 237 zOTUs (mean relative abundance>0.1%; prevalence > 10%). Data from *Il-10*$^{-/-Sv129}$ mice under AD or RF condition is normalized to the peak of each zOTU and ordered by the peak phase in wild type mice under AD or RF conditions respectively. Yellow and blue indicate high and low abundance respectively. (**D**) Manhattan plot of the amplitude and adj.p value of zOTUs identified in control and *Il-10*$^{-/-Sv129}$ mice under AD and RF conditions. Significant rhythms are illustrated with fitted cosine-wave regression using a line (significance: cos-fit p-value ≤ 0.05).

4.3 Characterization of microbiota-derived metabolites in *Il-10*$^{-/-Sv129}$ mice

To address the potential physiological relevance of disturbed microbial oscillations in *Il-10*$^{-/-Sv129}$ mice, fecal (un)targeted metabolite analysis was performed. Indeed, the identified metabolites clustered according to the genotype (**Fig. 7A**). Moreover, *Il-10*$^{-/-Sv129}$ mice showed loss of rhythmicity in 55 fully annotated metabolites, most of which belong to lipids and lipid-like metabolites, including fatty acids and BAs (**Fig. 7B**) For example, we found loss of rhythmicity and suppression of bile acid, including muricholic acid and 7-sulfocholic acid (**Fig. 7B)**. Targeted metabolomics for SCFAs, desaminotyrosine and bile-acids (BAs) further validated the differences in rhythmicity and overall concentrations between genotypes. For example, highly suppressed amplitude rhythms or loss of rhythmicity were observed for primary and secondary BAs in *Il-10*$^{-/-sv129}$ mice, such as deoxycholic acid (DCA) ($p<0.0001$), hyodeoxycholic acid ($p=0.0025$), 7-sulfocholic acid (7-sulfo-CA)($p<0.0001$) and α-muricholic acid ($p=0.0004$) (**Fig. 7C**). Most of these secondary BAs are key mediators involved in gut dysbiosis, especially in IBD[163]. Additionally, reduced SCFA levels, such as acetate ($p=0.0221$), butyrate ($p<0.0001$) and propionate ($p<0.0001$) were found in *Il-10*$^{-/-sv129}$ mice **(Fig. 7D)**, similar to observation on IBD-patients and related mouse models[164]. The concentration of valeric acid and desaminotyrosin were also suppressed in *Il-10*$^{-/-Sv129}$ mice (**Fig. 7D)**

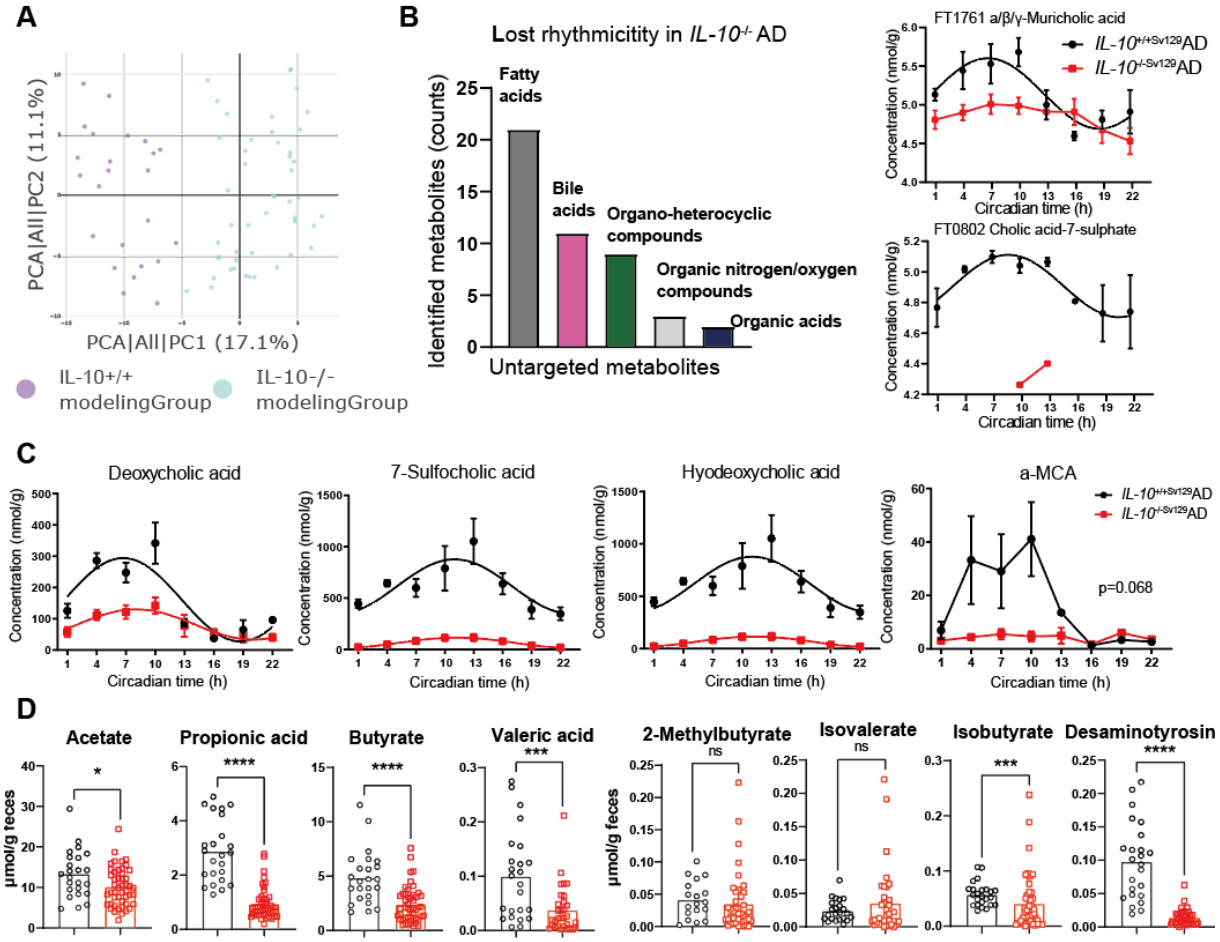

Figure 9 Disrupted microbiota composition resulted in altered fecal metabolites in *Il-10*$^{-/-Sv129}$ mice

(**A**) PCA-plot of fecal metabolites obtained from control and *Il-10*$^{-/-Sv129}$ mice through untargeted metabolomics. (**B**) Classification of the top 5 fully annotated super classes of metabolites measure by untargeted metabolomics and representative examples in wild type and *Il-10*$^{-/-Sv129}$ mice under AD condition. (**C**) Circadian profiles of bile acids (BAs) of wild type and *Il-10*$^{-/-Sv129}$ mice under AD condition. (**D**) Quantification of SCFA and desaminotyrosine measured by targeted metabolomics in fecal samples from control and *Il-10*$^{-/-Sv129}$ mice. Significant rhythms are illustrated with fitted cosine-regression; data points connected by straight lines indicate no significant cosine fit curves ($p > 0.05$) and thus no rhythmicity. Data are represented as mean ± SEM. Statistics were performed by Mann–Whitney U test. Asterisks indicate significant differences *$p<0.05$, **$p<0.01$, ***$p<0.001$.

Importantly, PICRUSt2 analysis[152] revealed that restoration of microbial rhythmicity in *Il-10*$^{-/-Sv129}$ mice under RF conditions was indeed reflected by restored rhythmicity of assigned pathways involved in fatty acid synthesis and SCFA fermentation (**Fig. 8**). Rhythmicity was identified by JTK_Cycle (Bonferroni adj. p-value ≤ 0.05). Altogether, these results indicate that

changes in microbial rhythmicity and composition observed in *Il-10*$^{-/-\text{Sv129}}$ mice can be restored by RF, and thus microbial rhythmicity might be involved in the beneficial effect of RF on colonic inflammation.

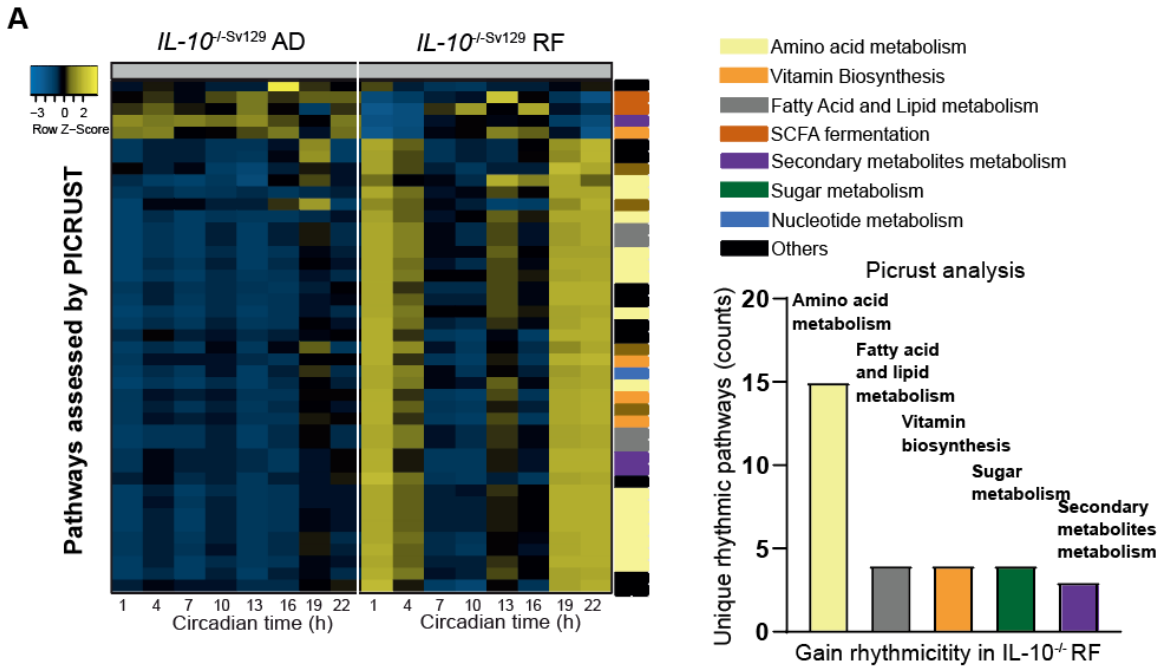

Figure 10 Heatmap of pathways (calculated by PICRUST 2.0) with restored rhythms *Il-10*$^{-/-\text{Sv129}}$ mice under RF

4.4 Colonization of arrhythmic microbiota did not alter the colitis development in germ free *Il-10*$^{-/-}$ mice

Recently we demonstrated that a functional intestinal clock is required to maintain GI homeostasis by driving the microbiome, including *Lachnospiraceae* and microbiota derived DCA and 7-sulfo-CA[27]. Notably, IL-10-deficient mice under germ free condition are free of colitis[165]. To differentiate whether a dysfunctional intestinal clock in *Il-10*$^{-/-\text{Sv129}}$ mice or arrhythmicity of the microbiome directly affect the severity of inflammation, we performed two distinct cecal microbiota transfer experiments. First colonialization of cecal content from intestine-specific clock deficient (*Bmal1*$^{\text{IEC-/-}}$) and littermates (*Bmal1*$^{\text{flox/flox}}$) donors was performed in order to transfer rhythmic and arrhythmic microbiota into Germ free (GF) *Il-10*$^{-/-}$

^{BL6} recipients (**Fig. 9A)**. Surprisingly, the weight of immune organs, such as spleen, MLN and colon did not differ between recipients, nor did the amount of immune cells that infiltrated into the colonic lamina propria ($CD4^+$ T-cells, macrophages and neutrophils) (**Fig. 9B**). Consistently, histological staining and scoring, as well as the expression of inflammatory marker gene *Tnf* reveal no pathological differences between both recipients (**Fig. 9C**). Similar levels of crypts loss and immune cell infiltration, as well as mucosal inflammation were identified between recipients. These results indicate that microbial rhythmicity might not directly induce intestinal inflammation.

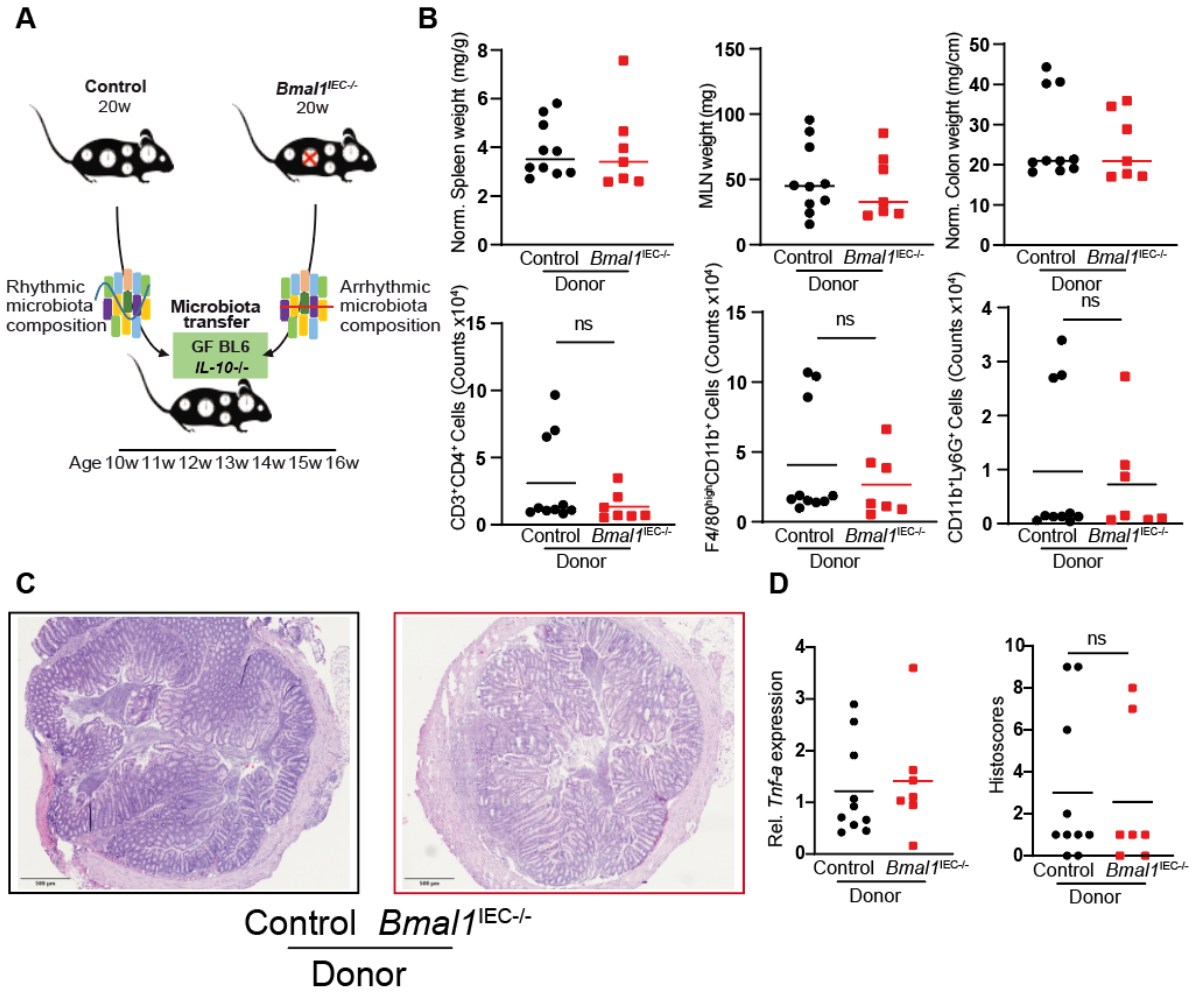

Figure 11 Characterization of colitis phenotype of *Il-10*$^{-/-}$ germ free mice colonized with rhythmic/arrhythmic microbiota

(**A**) Schematic illustration of experimental design. Cecal content from control (rhythmic) and *Bmal1*$^{IEC-/-}$ (arrhythmic) donors were transferred into germ-free *Il-10*$^{-/-BL6}$ mice. (**B**) Organ weights of spleen, MLN and colon (top) and amount of immune cells recruited into colonic

lamina propria (bottom) of recipients. (C) Representative H&E stainings of colonic cross section from the recipients. (**D**) *Tnf* gene expression, as well as histopathological scores. tatistics were performed by Mann–Whitney U test.

4.5 Disruption of the intestinal clock (*Bmal1*$^{IEC-/-}$) increase the inflammatory response in germ free mice colonized with diseased-associated microbiota

In order to investigate other factors which drives colitis development instead of microbial rhythmicity, we performed the second microbiota transfer experiment to demonstrate the importance of the host intestinal clock in IBD development. When GF *Bmal1*$^{IEC-/-}$ mice received disease-associated microbiota from inflamed *Il-10*$^{-/-BL6}$ mice, colon weights were significantly increased in comparison to control recipients (**Fig. 10A**). Similarly, immune cell recruitment into the colonic lamina propria, such as CD4+ cells including Th1 and Th17 cells, dendritic cells, macrophages, as well as neutrophils were severely elevated, and *Tnf* gene expression was increased (**Fig 10C-F**). However, the histological score obtained from a single colon cross section showed no clear difference between the recipients (**Fig. 10G**), which indicates the inflammation was not strong enough to induce tissue pathological changes.

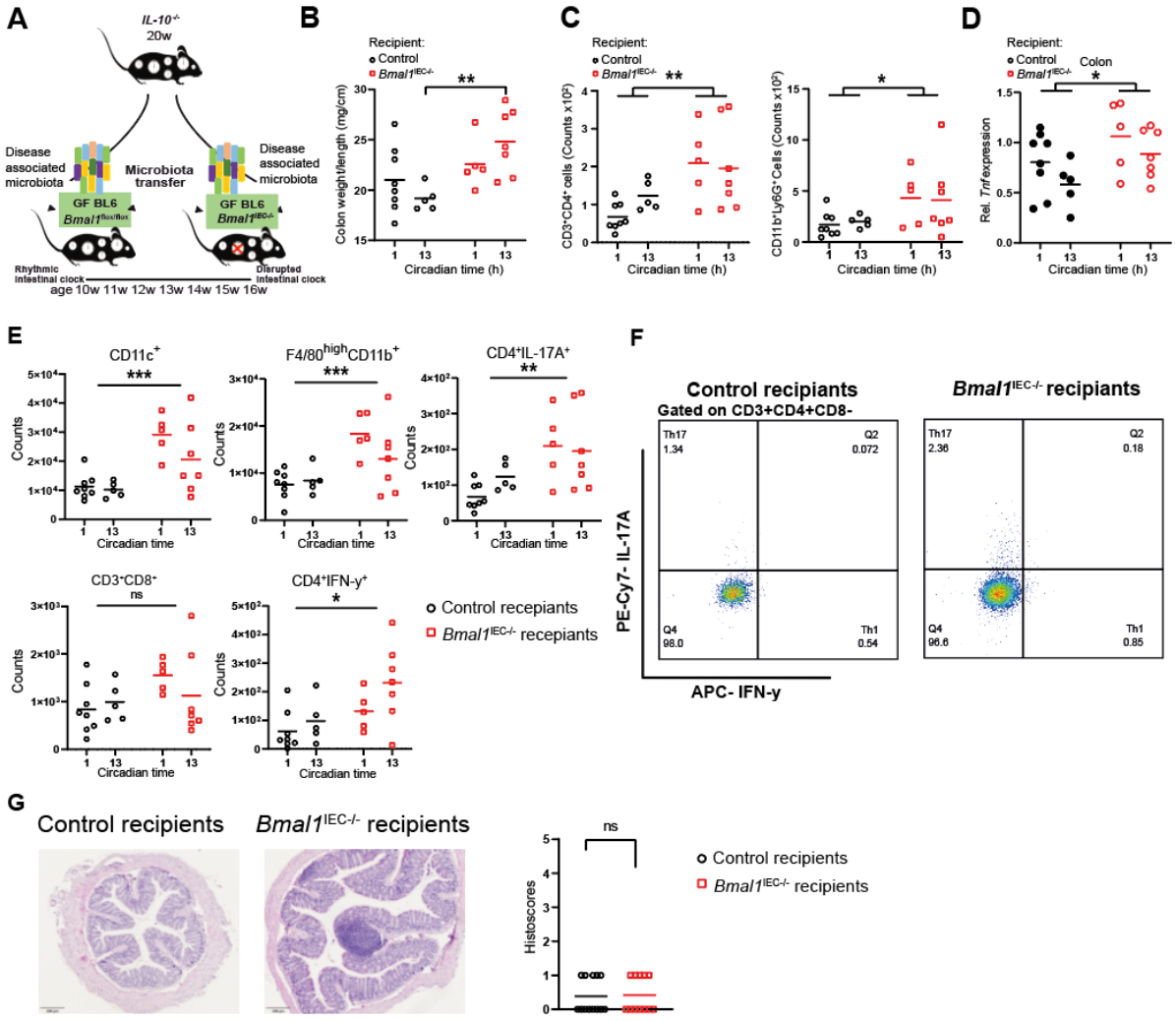

Figure 12 Germ free *Bmal1*$^{IEC-/-}$ mice colonized with disease-associated microbiota exhibited enhanced inflammatory response

(**A**) Schematic illustration of experiment design. Disease-associated microbiota from *Il-10*$^{-/-}$ donor was transferred to germ-free control (*Bmal1*$^{flox/flox}$) and *Bmal1*$^{IEC-/-}$ recipients. (**B**) Colon weight and (**C**) amount of CD4+ T cells and neutrophils recruited into colon lamina propria. (**D**) *Tnf* gene expression in colon tissues from recipients. (**E**) Other immune cells infiltrated into colon lamina propria. (**F**) Representative graph of gating strategy of Th1 and Th17 cells. (**G**) Representative H&E staining scans of colon sections from *Bmal1*$^{IEC-/-}$ mice received control and disease-associated microbiota (left) and histopathological scores (right). Statistics were performed by Mann–Whitney U test and two-way ANOVA followed with Benjamini-Hochberg correction. Asterisks indicate significant differences *p<0.05, **p<0.01, ***p<0.001.

4.6 Germ free *Bmal1*$^{IEC-/-}$ mice colonized with diseased-associated microbiota resulted in similar microbiome alteration in *Il-10*$^{-/-Sv129}$ mice

In addition to the changes identified in inflammatory response, we observed microbiota beta diversity clustering between circadian time points and recipients (**Fig. 10A**), as well as decreased abundance of *Lachnospiraceae* and increased *Erysipelotrichaceae* in cecal samples in *Bmal1*$^{IEC-/-}$ recipients, similar to results obtained from *Il-10*$^{-/-Sv129}$ mice (**Fig. 10B**). Accordingly, the concentrations of α-MCA, DCA, HDCA and MDCA in the cecal content were reduced in comparison to control recipients (**Fig. 10C**). Procrustes analysis (PA) revealed an association between zOTUs with BAs production, in particular the families *Lachnospiraceae* and *Oscillospiraceae* correlated with DCA and aMCA concentrations (p=0.0001) (**Fig. 10D, E**). Altogether, these results reflect an early stage of inflammation following colonialization with disease-associated microbiota when recipients lack a functional intestinal clock. Thus, the intestinal clock represents a functional link between the microbiome and GI inflammation.

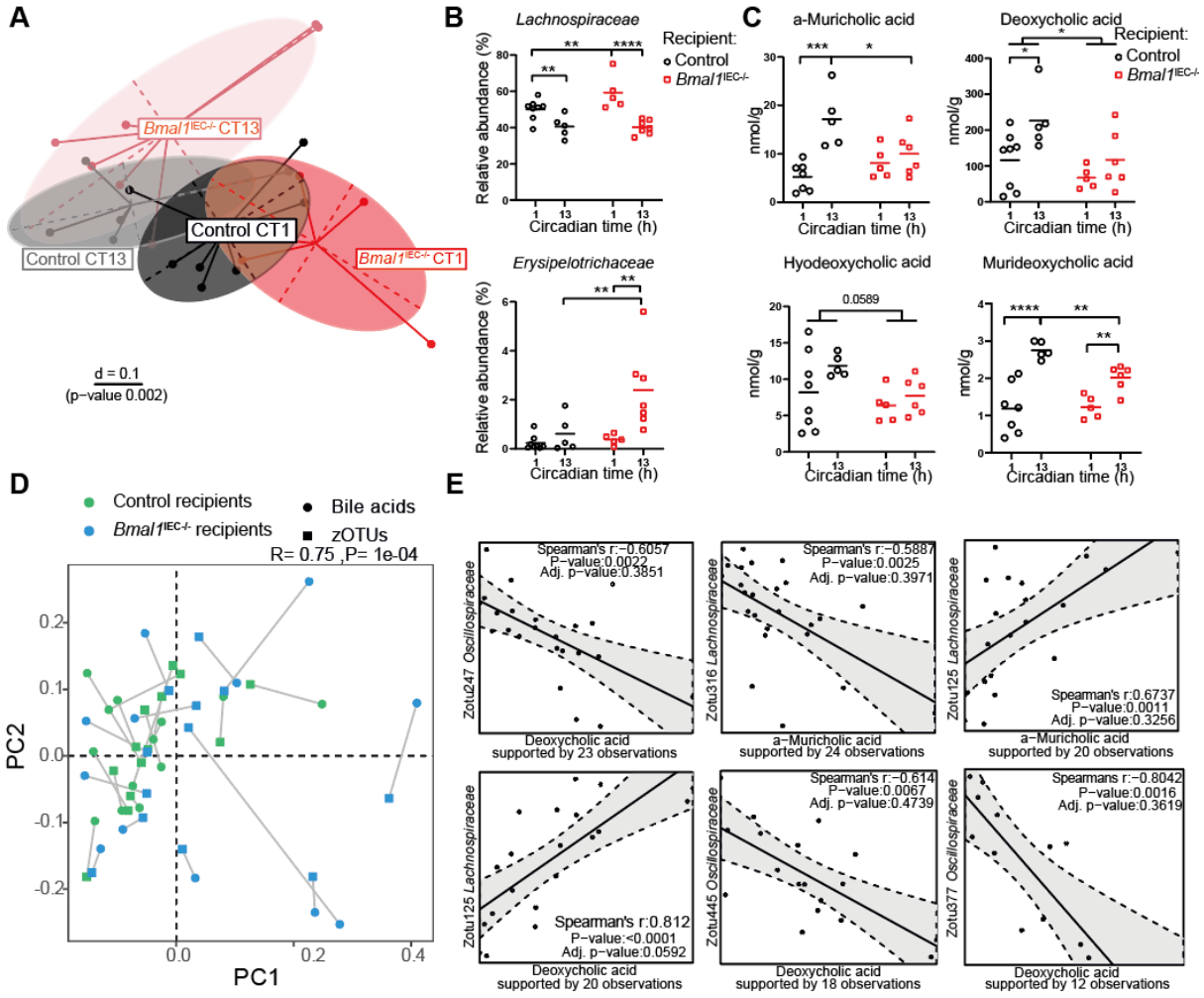

Figure 13 Germ free *Bmal1*$^{IEC-/-}$ mice colonized with disease-associated microbiota exhibited microbiome alteration observed in *Il-10*$^{-/-Sv129}$ mice

(**A**) Beta-diversity illustrated by MDS plots of cecal microbiota based on generalized UniFrac distances (GUniFrac) in control and *Bmal1*$^{IEC-/-}$ recipients at circadian time (CT) 1 and 13. (**B**) Relative abundance of families *Lachnosiraceae* and *Erysipelotrichaceae*. (**C**) Amount of α-muricholic acid (α-MCA), deoxycholic acid (DCA), hyodeoxycholic acid (HDCA) and murideoxycholic acid (MDCA) in cecal content of control and *Bmal1*$^{IEC-/-}$ recipients. (**D**) Procrustes analysis (PA) of cecal microbiota and bile acid levels. The length of the line is proportional to the divergence between the data from the same mouse. (**E**) Representative correlation plot between zOTUs and bile acids. Statistics were performed by Mann–Whitney U test and two-way ANOVA followed with Benjamini-Hochberg correction. Asterisks indicate significant differences *p<0.05, **p<0.01, ***p<0.001.

4.7 *Bmal1*$^{IEC-/-}$ mice do not develop IBD-like phenotype

To further investigate the functionality of the intestinal clock, we used a genetic mouse model lacking the essential clock gene *Bmal1* in intestinal epithelial cells (IECs) (*Bmal1*$^{IEC-/-}$). Colonic clock dysfunction in IECs was validated by arrhythmic *Bmal1* and *Rev-erba* (*Nr1d1)* expression and a highly reduced amplitude of *Per2* gene expression (**Fig. 12A**). Colon weight and the concentration of complement 3 in stools of *Bmal1*$^{IEC-/-}$ mice were significantly increased (**Fig. 12C**), although the body weight, jejunum and spleen weight as well as mesenteric lymph nodes weights remains identical (**Fig. 12B**). Importantly, the frequency of major immune cell populations in the colonic lamina propria, including $CD4^+$, $CD8^+$ T-cells and dendritic cells lost rhythmicity in *Bmal1*$^{IEC-/-}$ mice, whereas macrophage recruitment remained rhythmic (**Fig. 12D**). These results indicate that lacking of the intestinal clock induces immune alteration in the colon tract.

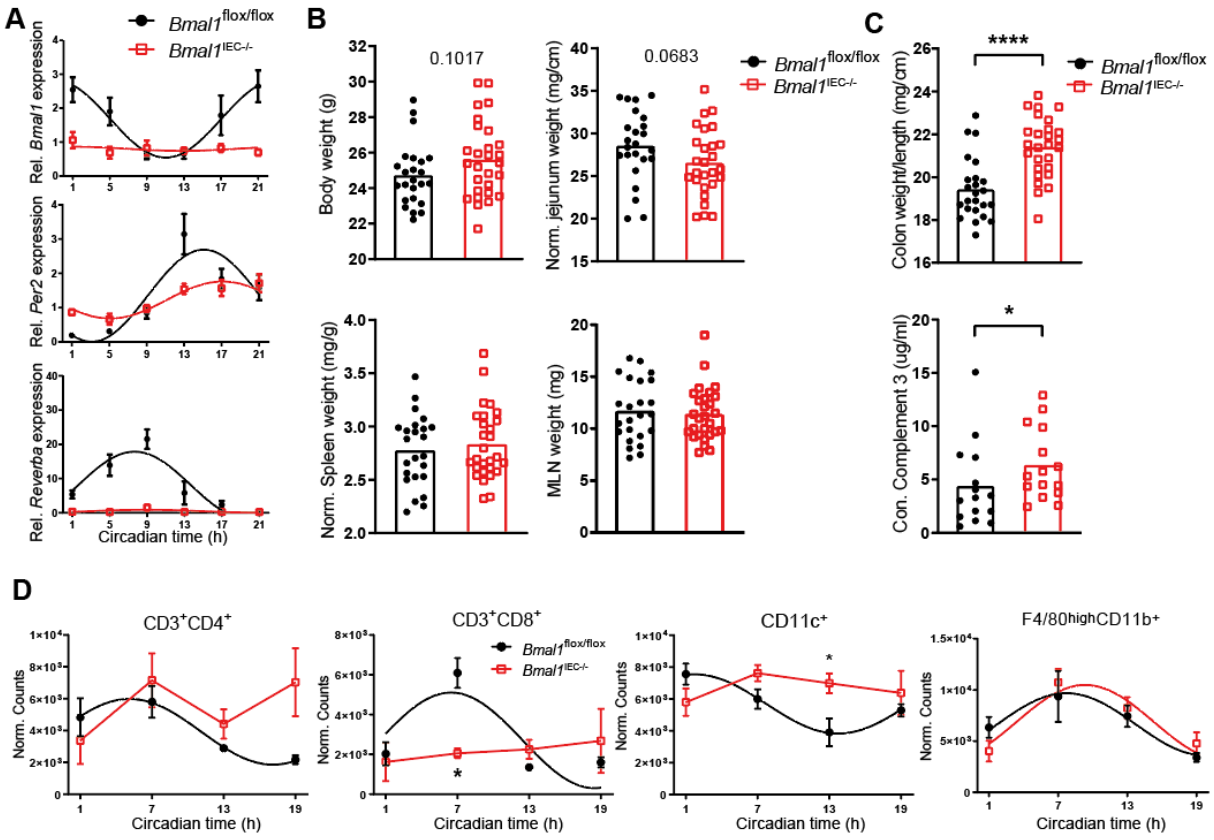

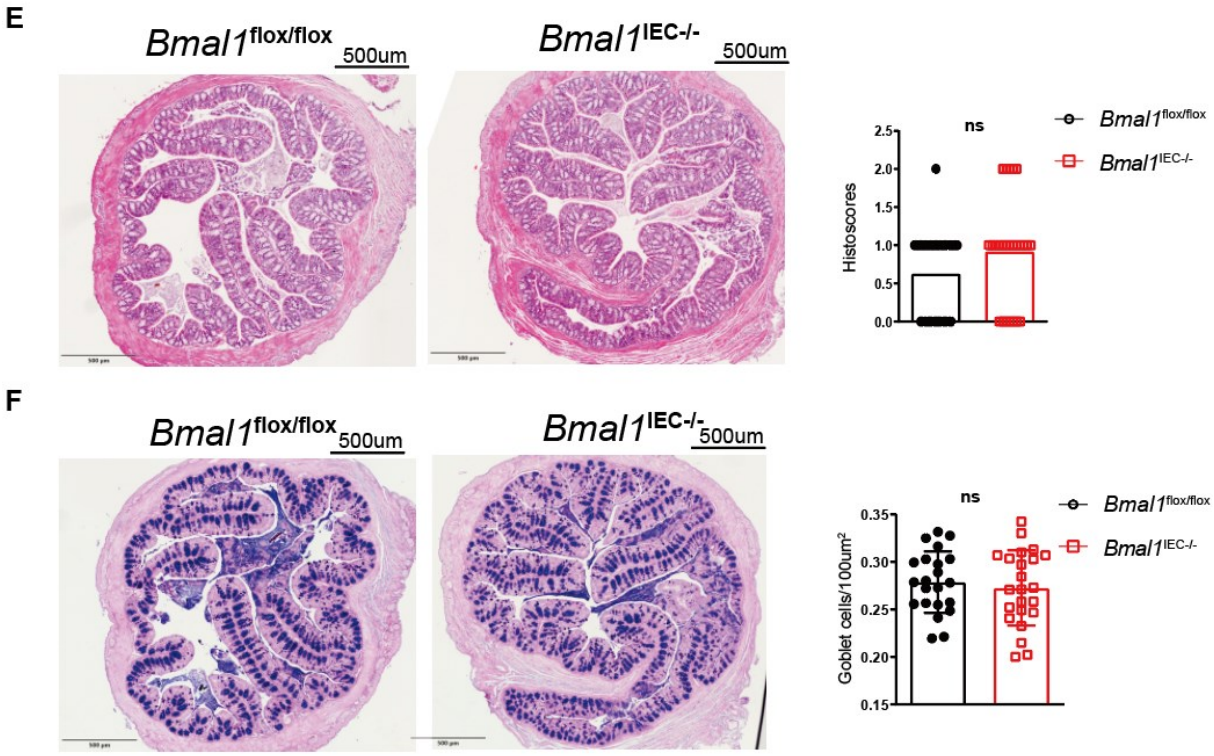

Figure 14 Phenotypic characterization of *Bmal1*$^{IEC-/-}$ mice

(**A**) Clock genes expression (*Bmal1*, *Per2*, *Reverba)* in colonic epithelial cells from control and *Bmal1*$^{IEC-/-}$ mice. (**B**) Body weight, organ weight of jejunum, spleen and MLN of control and *Bmal1*$^{IEC-/-}$ mice. (**C**) Colon weight (top) and complement 3 level in feces of control and *Bmal1*$^{IEC-/-}$ mice. (**D**) Amount of major subtypes of immune cells (CD4+, CD8+, Dendritic cells and macrophages) in the colon lamina propria of control and *Bmal1*$^{IEC-/-}$ mice. (**E**) Representative scans of H&E staining of colon cross sections from control and *Bmal1*$^{IEC-/-}$ mice (left) and histopathological scores (right). (**F**) Representative scans of PAS-AB staining of the same colon cross sections with (**E**) from control and *Bmal1*$^{IEC-/-}$ mice (left) and quantification of goblet cells (right). Significant rhythms are illustrated with fitted cosine-wave regression using a line (significance: cos-fit p-value ≤ 0.05). Statistics were performed by Mann–Whitney U test. Data are represented as mean ± SEM. Asterisks indicate significant differences *p<0.05, **p<0.01, ***p<0.001.

However, histopathology scores based on the colon cross section revealed that *Bmal1* deletion in epithelial cells did not induce direct tissue pathological changes (**Fig. 12E**). Moreover, results obtained from periodic acid-alcian blue (PAS-AB) staining indicate that the amount of goblet cells and mucus remained unchanged as well (**Fig. 12F**).

4.8 The intestinal clock regulates genes and pathways involved in immune response and metabolic processes

To systemically assess the importance of the intestinal clock under transcriptomic level, we performed bulk RNA-seq on colonic tissues from *Bmal1*$^{IEC-/-}$ and control littermates during a circadian day (24h with 4h interval, each time point n=4).

4.8.1 Genotype differences analysis between *Bmal1*$^{IEC-/-}$ and control mice

Interestingly, sample clustering according to the genotype was observed by principal component analysis (PCA). Of note, the variance distance according to time in control mice are wider than *Bmal1*$^{IEC-/-}$, indicating the difference under gene levels between samples obtained from day (CT1, 5, 9) and night (CT13, 17, 21) are less apparent in *Bmal1*$^{IEC-/-}$ mice (**Fig. 13A**). In addition, more than 200 genes were differentially expressed (Fold change>1.5, adj. $p<0.05$) between genotypes. For example, altered expression was found for genes, such as *Retnlb* (Resistin-like beta) and *Tff*2 (Trefoil factor 2) (**Fig. 13B**) involved in colitis development[166, 167].

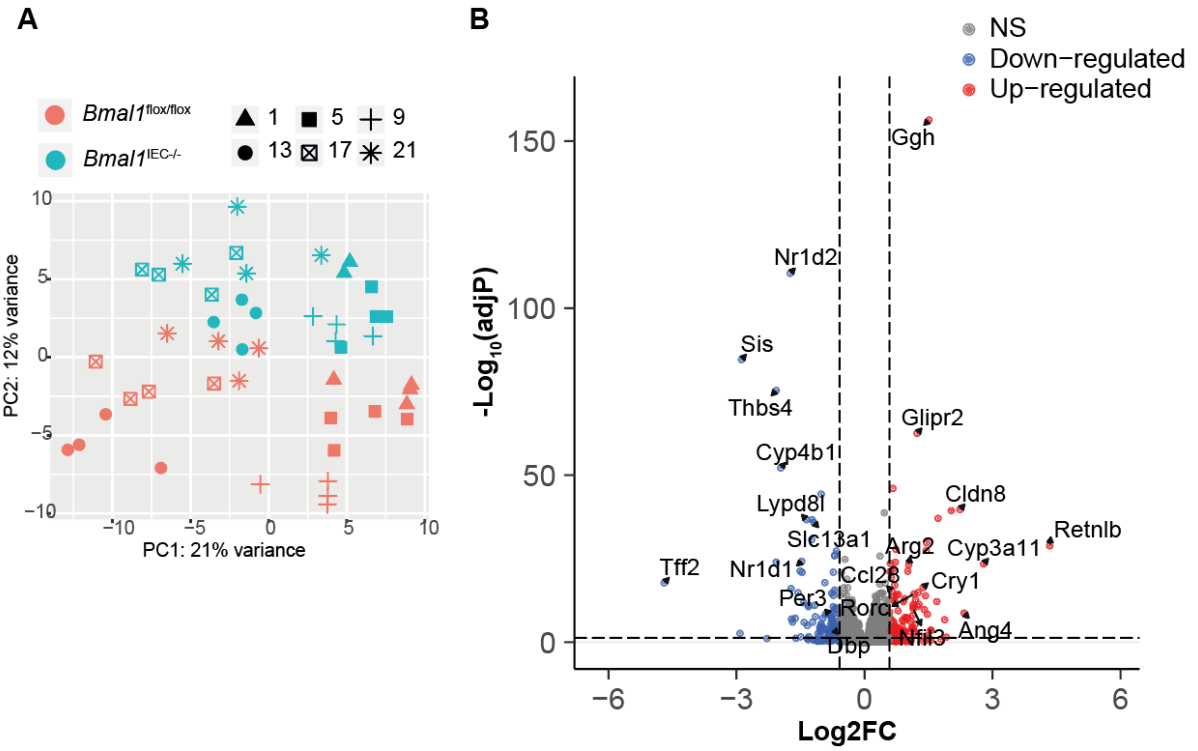

Figure 15 PCA plot of sample clustering and volcano plot for differentially expressed genes (DEGs)

(**A**) Principal Component Analysis of 46 colon samples obtained from control (red) and *Bmal1*$^{IEC-/-}$ (blue) mice every 4h throughout the circadian day in constant darkness. Different shapes indicate different circadian time (CT) points. (**B**) Volcano plot of transcriptional changes between colon tissues from control and *Bmal1*$^{IEC-/-}$ mice. Upregulated (adj $p < 0.05$, $FC > 1.5$) genes are indicated in red, while downregulated (adj $p < 0.05$, $FC > 1.5$) genes are marked in blue.

4.8.2 The intestinal clock regulates different set of genes during day and night

Consistently, gene ontology enrichment analysis highlighted pathways relevant for 'humoral immune response', 'defense response to bacterium' and 'T-cell apoptotic process' , indicating the involvement of the intestinal clock in regulating intestinal immune homeostasis (**Fig. 14A**). Additionally, we analysed the genotype difference between day and night respectively to investigate the time-dependent manner of the intestinal clock in regulating different genes. While taking time of the day into the model (CT1,5,9 as day, CT13,17,21 as night), 114 genes

are identified as differentially expressed genes(DEGs) during the day comparing to 196 genes at night, indicates that Bmal1 has more impact on transcription levels during night period, which is also the active phase of mice. DEGs are then allocated separately into different pathways for day and night. Indeed, in total 65 genes were differentially expressed between genotypes in both day and night. The intestinal clock dominantly controls the expression of unique genes involved in 'leukocyte apoptotic processes', 'response to insulin' and 'circadian rhythm' during the day, and metabolic processes, 'bile acid secretion', as well as 'defence response to bacterium' at night (**Fig. 14B**). These results highlighted the importance of considering timing of the treatment as another crucial factor in study design.

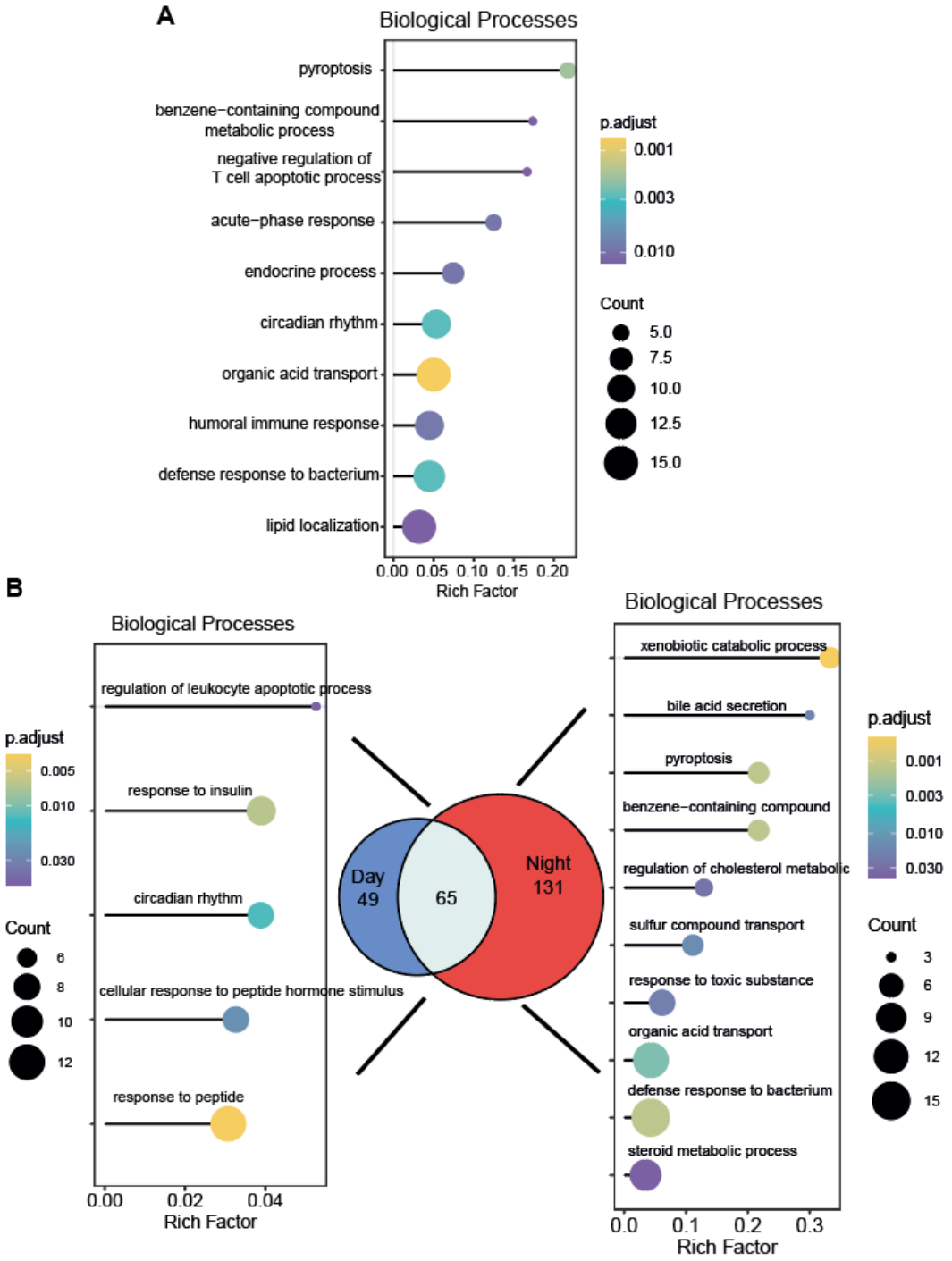

Figure 16 Gene ontology enrichment analysis of differentially expressed genes in colon tissue of *Bmal1*$^{IEC-/-}$ mice

(**A**) Gene Ontology enrichment analysis of DEGs between genotypes. (**B**) Gene Ontology enrichment analysis of DEGs between genotypes during day (left) and night (right). Venn diagram of DEGs during the day and at night.

4.8.3 Circadian characterization and profiling of intestinal clock controlled transcripts

In order to investigate the transcription alteration due to lack of the intestinal clock from circadian perspective, we analysed the rhythmic expression of annotated transcripts. Importantly, 7803 transcripts underwent circadian rhythmicity in controls, whereas more than 55% of these transcripts were arrhythmic in *Bmal1*$^{IEC-/-}$ mice (**Fig. 15A**). Additionally, the majority of the transcripts which maintained rhythmicity (3460 transcripts) in *Bmal1*$^{IEC-/-}$ mice showed a highly suppressed amplitude (**Fig. 15A, right**). DODR analysis[138] further confirmed that more than 200 genes either lost or changed rhythmicity (114/104 respectively) in *Bmal1*$^{IEC-/-}$ mice and are enriched in pathways including cell cycle, circadian rhythm, inflammatory response and cholesterol homeostasis, similar to results observed between genotype comparison (**Fig. 15B**). Particularly, genes such as *Ffar2* (free fatty acid receptor 2), *Abcc2* (ATP-binding cassette, sub-family C (CFTR/MRP), member 2), *Rorc* (RAR-related orphan receptor gamma) and *Hc* (hemolytic complement) which are involved in the inflammatory and immune response[168-171] lost rhythmicity and in addition significantly differed in their baseline expression between genotypes (**Fig. 15C**). Moreover, genes involved in goblet cells function, including *Muc3* (mucin 3), *Tff3* (trefoil factor 3), *Pigr* (polymeric immunoglobulin receptor) and *Fcgbp* (Fc fragment of IgG binding protein), lost rhythmicity in *Bmal1*$^{IEC-/-}$ mice (**Fig. 15D**)[172]. Genes relevant for cell development and migration, especially immune cells, such as *Casp4* (caspase 4), *Pdk1* (pyruvate dehydrogenase kinase, isoenzyme 1), *Cxcr4* (chemokine (C-X-C motif) receptor 4) and *Vcam-1* (vascular cell adhesion molecule 1)[173-176] showed an abnormal circadian phase or loss of rhythmicity upon intestinal-clock disruption (**Fig. 15E**).

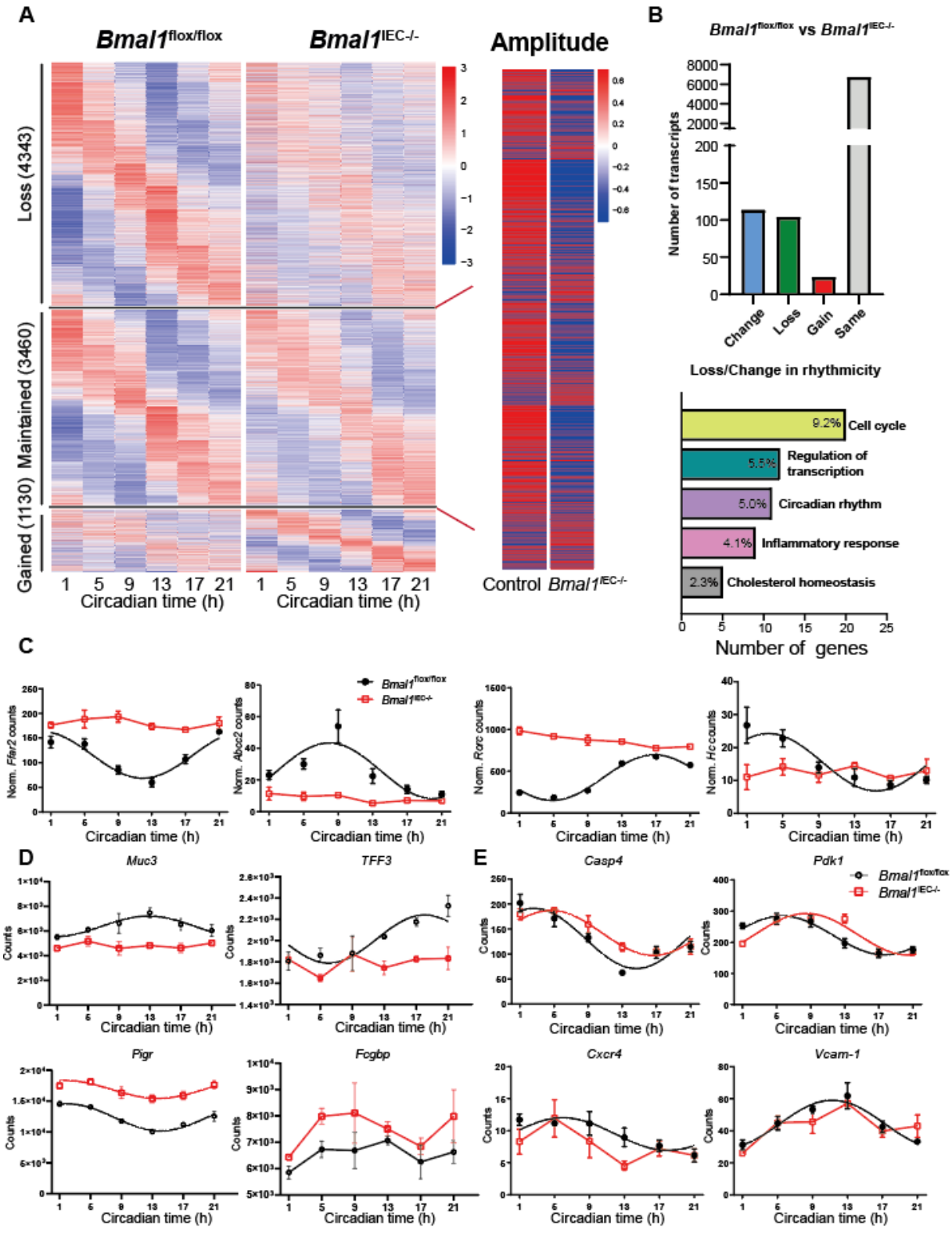

Figure 17 Intestinal clock regulates rhythms of various genes involved in IBD development

(**A**) Heatmap of transcripts which lost, maintained and gained rhythmicity in colon tissues from *Bmal1*$^{IEC-/-}$ mice (left) and amplitude comparison of the transcripts which maintained rhythmicity (right) (JTK_cycle adj.p <0.05 as rhythmic). Transcripts are ordered by the peak

phase of control groups. (**B**) Amount of transcripts calculated by compareRhythms (top) and GO enrichment analysis (top 5, bottom) which loss and change rhythmicity. (**C**) Circadian profile of *Ffar2*, *Abcc2*, *Rorc* and *Hc* gene expression. (**D**) Circadian profile of transcripts *Muc3, Tff3, Pig*r and *Fcgbp* and (**E**) Circadian profile of *Casp4, Pdk1, Cxcr4* and *Vcam-1* counts in control and *Bmal1*$^{IEC-/-}$ mice. Significant rhythms are illustrated with fitted cosine-wave regression using a line (significance: cos-fit p-value ≤ 0.05).

4.9 *Bmal1*$^{IEC-/-}$ mice are more susceptible to DSS-induced acute colonic inflammation

4.9.1 *Bmal1*$^{IEC-/-}$ mice exhibited enhanced inflammatory response after DSS treatment

In order to further confirm our findings from RNA-seq analysis, such as the crucial role of the intestinal clock in regulating immune and inflammatory response, *Bmal1*$^{IEC-/-}$mice and controls were released into DD and received drinking water supplemented with 2% dextran sulfate sodium (DSS) (**Fig. 16A**), a well-studied chemical to induce tissue damage followed by colitis[177]. By performing the experiment under DD, we excluded the external time cues and focus on the intestinal specific clock. 5 days of DSS treatment caused a significant reduction in body weight and an increased disease activity index (DAI) [128] (**Fig. 16B,C**), as well as shortened colon length (**Fig. 16D**) compared to DSS-treated controls. Accordingly, the expression of inflammatory markers, such as *Tnf* as well as neutrophil and macrophage recruitment to the colonic lamina propria was severely enhanced following DSS treatment in *Bmal1*$^{IEC-/-}$ mice (**Fig. 16E-F**), suggesting an increased inflammatory response.

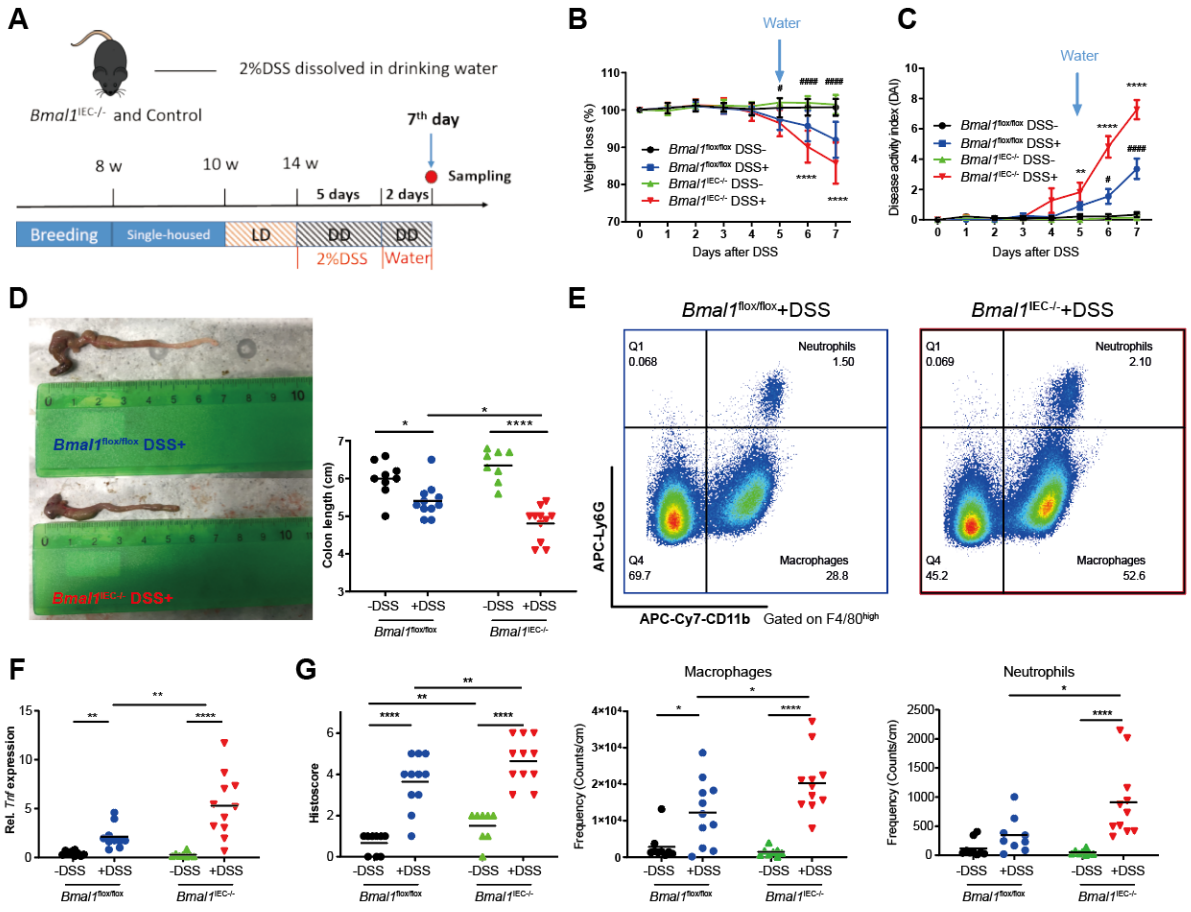

Figure 18 *Bmal1*$^{IEC-/-}$ mice developed severer colitis phenotype after DSS treatment

(**A**) Schematic illustration of the DSS treatment procedure. (**B**) Body weight change and (**C**) disease activity index of control and *Bmal1*$^{IEC-/-}$ during DSS/water administration. (**D**) Representative picture of colon (left) and colon length measurement (right). (**E**) Gating strategy for macrophages and neutrophils in colon lamina propria (top) and quantification (bottom). (**F**) *Tnf* expression of colon tissues. Statistics were performed by two-way ANOVA followed with Benjamini-Hochberg correction. Asterisks indicate significant differences between *Bmal1*$^{flox/flox}$ and *Bmal1*$^{IEC-/-}$ mice after DSS treatment *p<0.05, **p<0.01, ***p<0.001. Octothorpes indicate significant differences between *Bmal1*$^{flox/flox}$ mice with and without DSS treatment #p<0.05, ##p<0.01, ###p<0.001.

4.9.2 *Bmal1*$^{IEC-/-}$ mice developed severer colitis based on tissue histopathology evaluation

Consistently, the histopathological evaluation in colon tissues significantly differed between genotypes after DSS treatment, which was reflected by an increased histological scores in

Bmal1$^{IEC-/-}$mice. Crypt architectural distortion, crypt atrophy, diffuse mixed lamina propria inflammation, basal plasmacytosis, as well as basally located lymphoid aggregates were more apparent in colon cross section from *Bmal1*$^{IEC-/-}$ mice treated with DSS. Additionally, intestinal clock dysfunction caused loss of goblet cells following DSS treatment (**Fig. 5I**), which was previously identified as a critical factor during DSS-induced colitis[128]. These results demonstrate a higher sensitivity to DSS-induced colitis in mice lacking a functional intestinal clock.

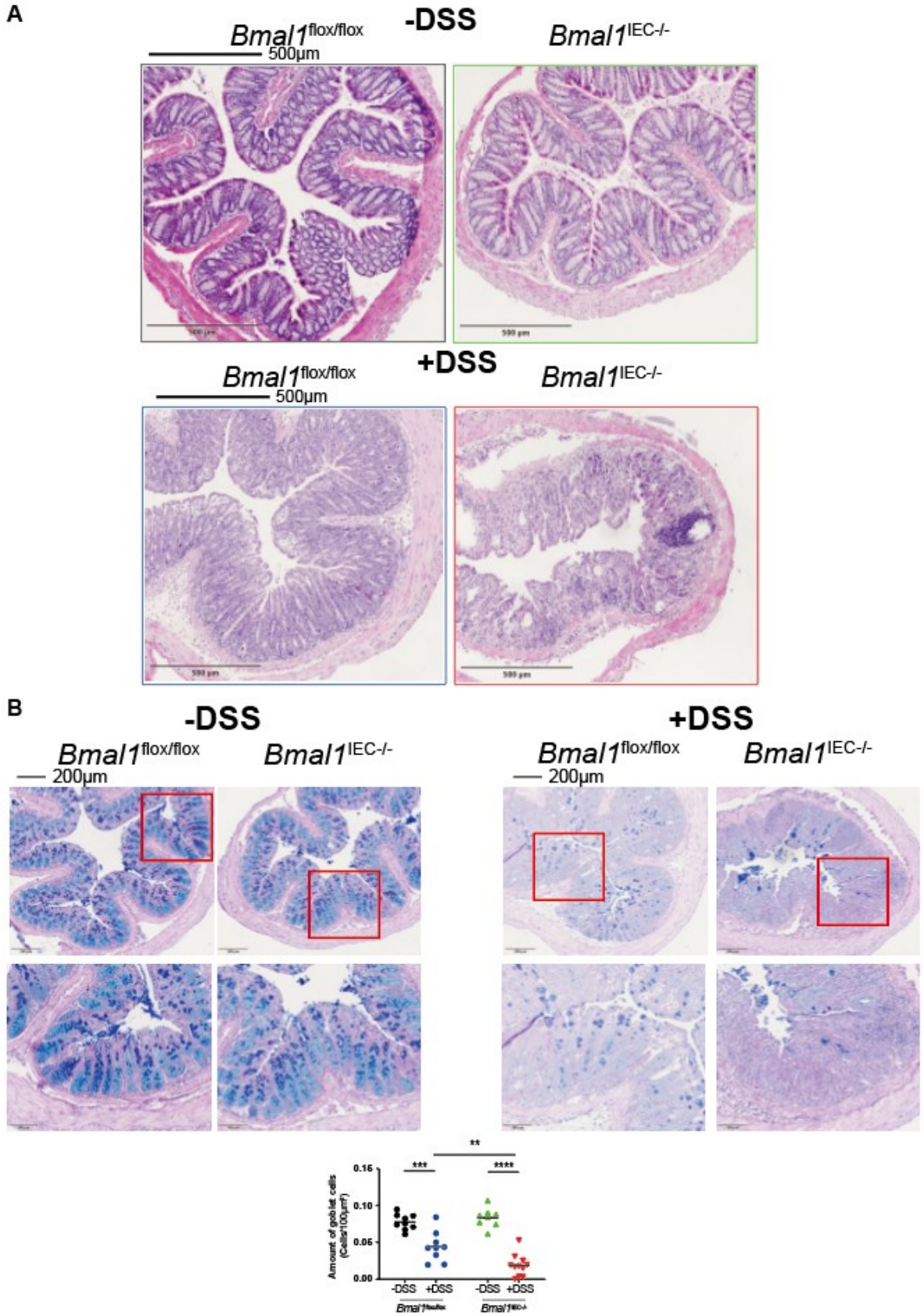

Figure 19 H&E and PAS-AB staining of colon tissues from *Bmal1*$^{IEC-/-}$ and control mice

(**A**) Representative H&E staining (**B**) and PAS-AB staining of colon sections from control and *Bmal1*$^{IEC-/-}$ with/without DSS treatment and quantification of amount of goblet cells. Quantification was based on a minimum of 20 crypts for each section. Statistics were performed by two-way ANOVA followed with Benjamini-Hochberg correction. Asterisks indicate significant differences between *Bmal1*$^{flox/flox}$ and *Bmal1*$^{IEC-/-}$ mice after DSS treatment *p<0.05, **p<0.01, ***p<0.001.

4.10 *Bmal1*$^{IEC-/-}$x*Il-10*$^{-/-BL6}$ mice developed more aggressive colitis phenotype

In order to genetically assess the impact of the intestinal clock on IBD development, we determined IBD pathology in a newly generated genetic mouse model prone to develop chronic colitis combined with a dysfunctional intestinal clock (*Bmal1*$^{IEC-/-}$ and *Il-10*$^{-/-BL6}$). IL-10-deficiency on BL6 background causes less severe colitis symptoms than on SV129 background [155], which is likely a results of less severe alterations in clock gene expression. Due to additionally lacking the intestinal clock, major clock genes expression in *Bmal1*$^{IEC-/-}$x*Il-10*$^{-/-BL6}$ mice were significantly suppressed or altered comparing to *IlL-10*$^{-/-BL6}$ and wild-type mice (**Fig.18B**). Accordingly, the additional loss of the intestinal clock dramatically reduced the survival of *Bmal1*$^{IEC-/-}$x*Il-10*$^{-/-BL6}$ mice compared to *Il-10*$^{-/-BL6}$ mice (**Fig. 18C**). In particular, all *Bmal1*$^{IEC-/-}$ x *IL-10*$^{-/-BL6}$ mice needed to be euthanized before the end of the experiment due to their dramatic disease burden, while around 30% of *Il-10*$^{-/-BL6}$ mice survived till the end of the experiment (**Fig. 18C**). Consequently, severer tissue inflammation was observed in *Bmal1*$^{IEC-/-}$x*Il-10*$^{-/-BL6}$ mice, which was reflected by an increased disease scores, as well as spleen, colon and MLNs weight (**Fig. 18D, E**). More importantly, H&E staining of the colon swiss roll reveals an overall enhanced tissue inflammation in *Bmal1*$^{IEC-/-}$x*Il-10*$^{-/-BL6}$ mice comparing to *Il-10*$^{-/-BL6}$ mice. Instead of the patchy inflammation phenotype along the colon, *Bmal1*$^{IEC-/-}$x*Il-10*$^{-/-BL6}$ mice exhibited complete pathological tissue changes from the proximal part till the distal part.

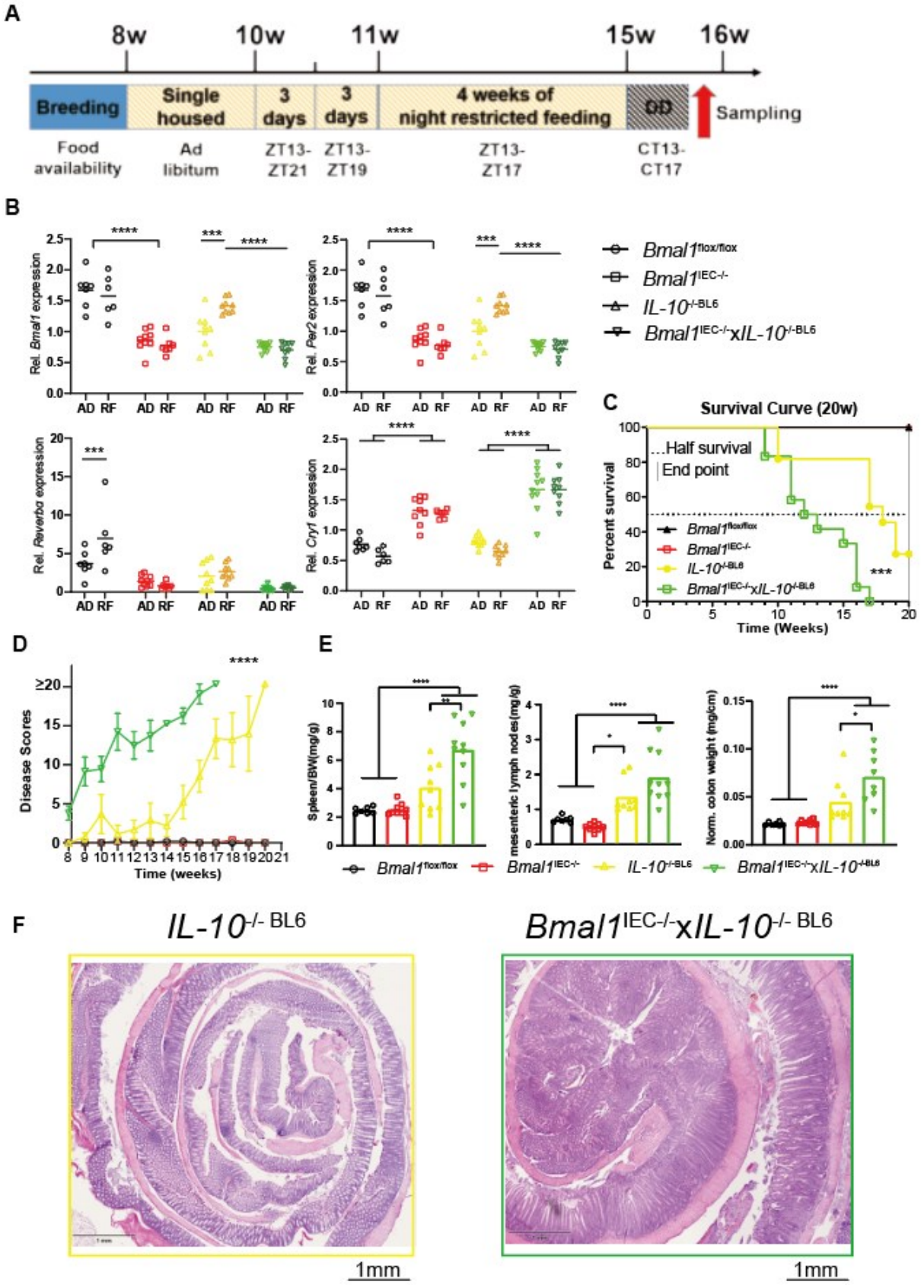

Figure 20 Additional lack of the intestinal clock accelerate the colitis progression in *Il-10*$^{-/-BL6}$ mice

(**A**) Schematic illustration of experimental RF design. (**B**) Colon clock genes expression and of control, *Bmal1*$^{IEC-/-}$, *Il-10*$^{-/-BL6}$ and *Bmal1*$^{IEC-/-}$x*Il-10*$^{-/-BL6}$ mice under AD and RF conditions. (**C**) Survival analysis of control, *Bmal1*$^{IEC-/-}$, *Il-10*$^{-/-BL6}$ and *Bmal1*$^{IEC-/-}$x*Il-10*$^{-/-BL6}$ mice under AD condition. (**D**) Disease scores and (**E**) organ weights of spleen, MLN and colon. (**F**) Representative H&E stainings of colon swiss rolls from *Il-10*$^{-/-BL6}$ and *Bmal1*$^{IEC-/-}$x*Il-10*$^{-/-BL6}$ mice under AD condition. Significances were calculated by one-way ANOVA, two-way ANOVA following Benjamini-Hochberg correction, and three-way ANOVA following Benjamini, Krieger and Yekutieli correction. * $p \leq 0.05$, ** $p \leq 0.01$, *** $p \leq 0.001$, **** $p \leq 0.0001$. Data are represented as mean ± SEM.

4.11 Circadian characterization of microbiota composition in *Bmal1*$^{IEC-/-}$x*Il-10*$^{-/-BL6}$ mice

Previous results revealed the microbial alteration under inflammatory condition in IL-10-deficient mice, which makes us curious in investigating the microbial diversity in *Bmal1*$^{IEC-/-}$x*Il-10*$^{-/-BL6}$ mice. Similar to our previous results obtained from *Bmal1*$^{IEC-/-}$ mice[27], circadian rhythmicity in community diversity (species richness) and on the level of the major phyla was dramatically disrupted in *Bmal1*$^{IEC-/-}$x*Il-10*$^{-/-BL6}$ mice, whereas *Il-10*$^{-/-BL6}$ mice showed slightly altered circadian oscillations of richness and the major phyla (**Fig. 19A-C**). This genotype effect was even more pronounced at the level of bacterial taxa. A heatmap showing peak relative abundances of zOTUs and its quantification confirmed the disruption of microbial rhythmicity in *Bmal1*$^{IEC-/-}$x*Il-10*$^{-/-BL6}$ mice, whereas intermediate phenotypes were noted in *Il-10*$^{-/-BL6}$ mice (**Fig. 19D, E**). Altogether, these data demonstrate that lack of the intestinal clock further promotes the microbial dysbiosis in IL-10-deficient mice and thus might accelerate the development and progression of colitis.

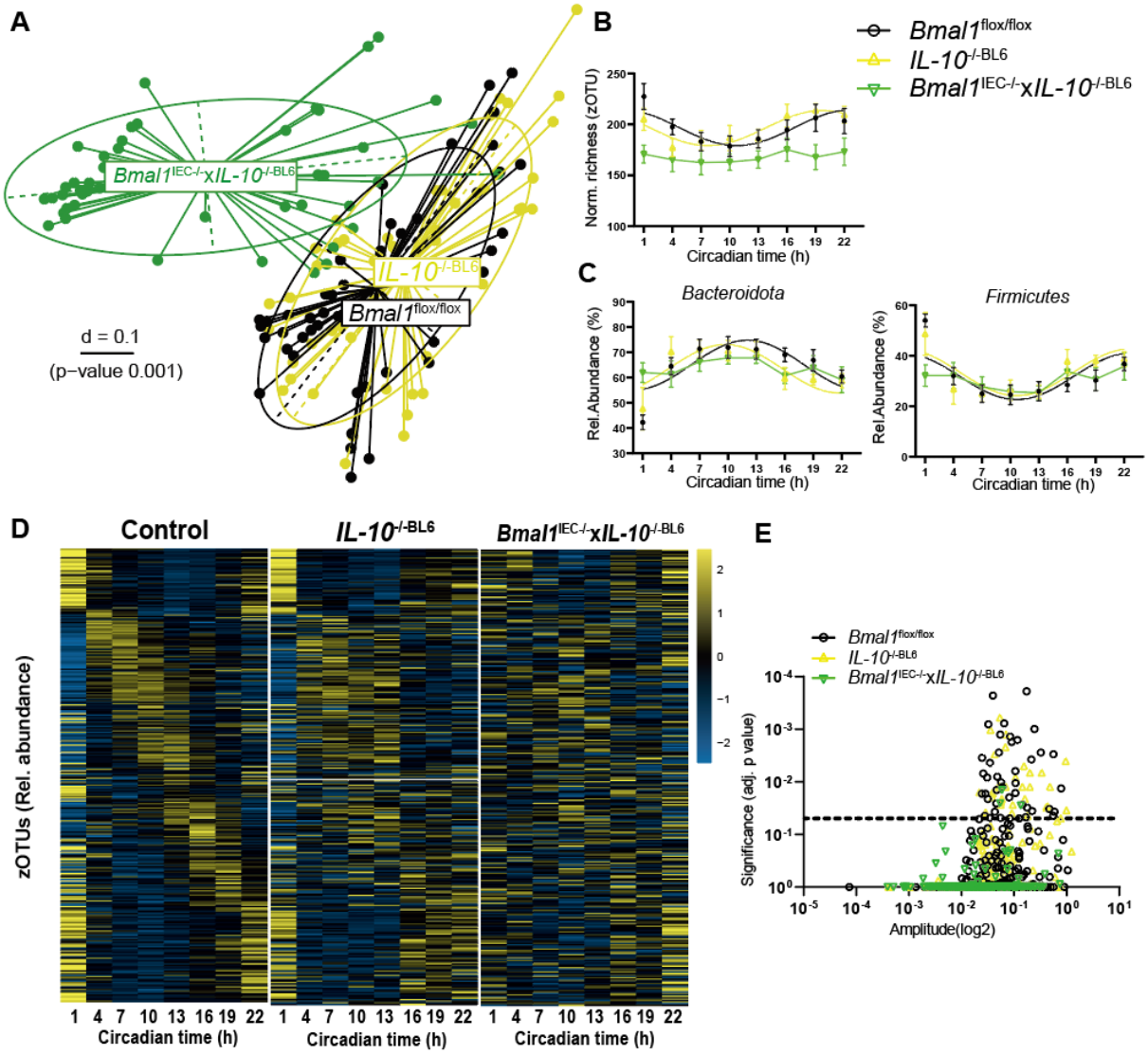

Figure 21 Considerable alteration of microbiota composition in *Bmal1*$^{IEC-/-}$x*Il-10*$^{-/-BL6}$ mice

(**A**) Beta-diversity illustrated by MDS plots of fecal microbiota based on generalized UniFrac distances (GUniFrac) in control, *Il-10*$^{-/-Sv129}$ and *Bmal1*$^{IEC-/-}$x*Il-10*$^{-/-}$ mice under AD condition. (**B**) Normalized richness and (**C**) abundance of major phyla (*Bacteroidota* and *Firmicutes*) in control, *Il-10*$^{-/-BL6}$ and *Bmal1*$^{IEC-/-}$x*Il-10*$^{-/-}$ mice under AD condition. (**D**) Heatmap depicting the relative abundance of identified zOTUs (mean relative abundance>0.1%; prevalence > 10%). Data from control, *Il-10*$^{-/-BL6}$ and *Bmal1*$^{IEC-/-}$x*Il-10*$^{-/-}$ mice are normalized to the peak of each zOTU and ordered by the peak phase in control group. Yellow means high abundance and blue low abundance. (**E**) Manhattan plot of the amplitude and adj.p value of zOTUs identified in control, *Il-10*$^{-/-BL6}$ and *Bmal1*$^{IEC-/-}$x*Il-10*$^{-/-}$ mice. Significant rhythms are illustrated with fitted cosine-regression; data points connected by straight lines indicate no significant cosine fit curves ($p > 0.05$) and thus no rhythmicity. Data are represented as mean ± SEM.

4.12 Restricted feeding requires a functional intestinal clock to ameliorate colitis symptoms

To evaluate whether the beneficial effect of RF on the severity of GI inflammation observed in *Il-10*$^{-/-Sv129}$ mice is caused directly by restoration of gut clock function, *Bmal1*$^{IEC-/-}$x*Il-10*$^{-/-BL6}$ mice, *Il-10*$^{-/-BL6}$ and controls were exposed to RF conditions (**Fig. 18A**). We validated that following exposure to RF, clock gene expression at CT13 was recovered similar to control levels in *Il-10*$^{-/-BL6}$ mice, whereas the expression was not restored in *Bmal1*$^{IEC-/-}$ mice and *Bmal1*$^{IEC-/-}$x*Il-10*$^{-/-BL6}$ mice, due to lack of the intestinal *Bmal1* (**Fig. 18B**). In line with our hypothesis, RF failed to improve the survival of *Il-10*$^{-/-BL6}$ mice when the intestinal clock was genetically dysfunctional (60%), whereas survival was significantly improved by RF in *Il-10*$^{-/-BL6}$ mice (100%) (**Fig. 20A**). Consistently, CD4+ immune cell recruitment to the colon lamina propria in *Bmal1*$^{IEC-/-}$x*Il-10*$^{-/-BL6}$ mice under RF condition was comparable to the AD condition. Furthermore, pathohistological evaluation by H&E staining (**Fig. 20C, D**), and colonic *Tnf* expression (**Fig. 20E**) were indistinguishable between AD and RF conditions in *Bmal1*$^{IEC-/-}$x*Il-10*$^{-/-BL6}$ mice. These results indicated that the beneficial effect of RF in rescuing colitis was dampened with the absent of the intestinal clock, which in turn highlighted the dominant role of the host intestinal clock in regulating colitis development and progression.

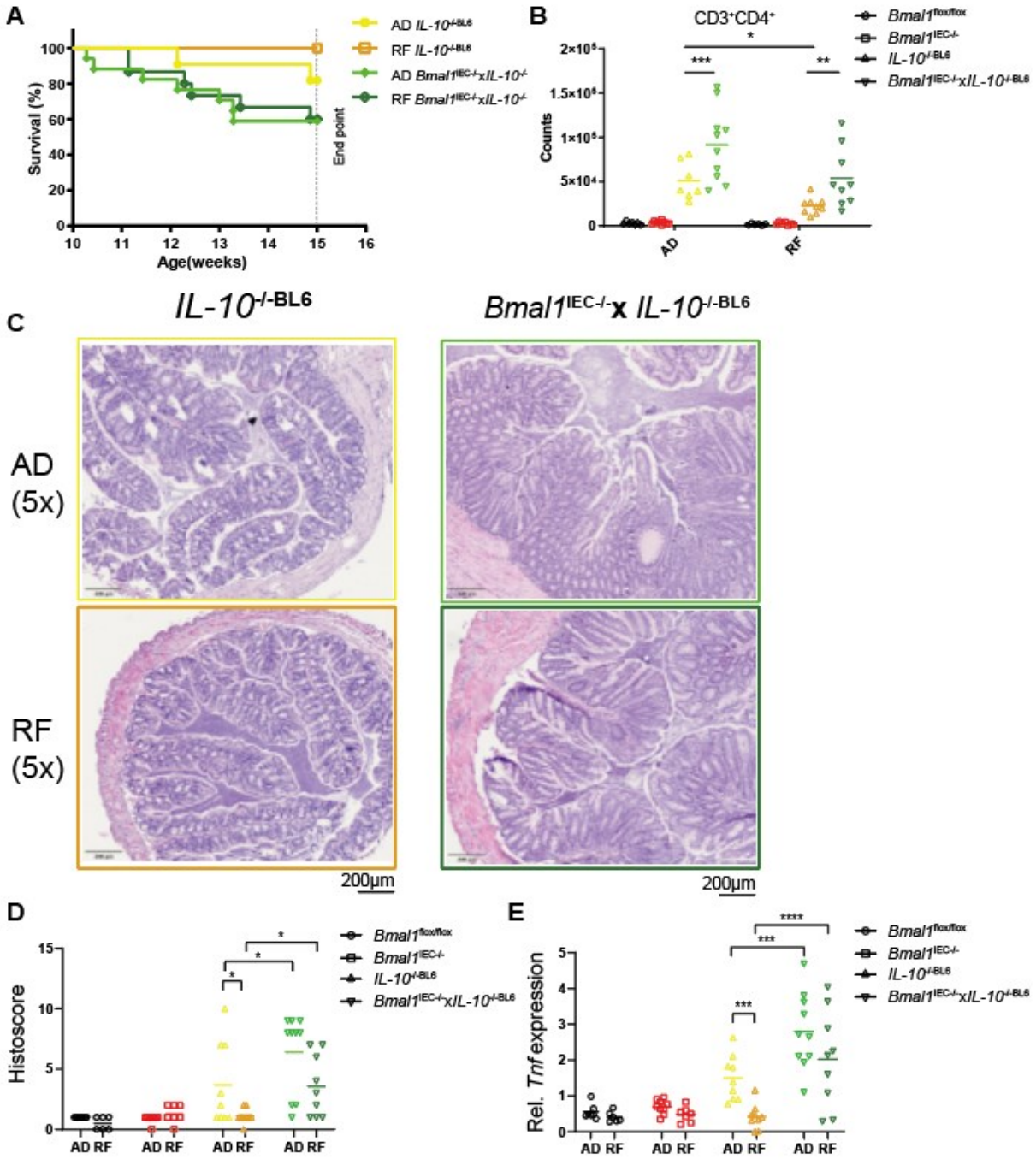

Figure 22 Restricted feeding did not ameliorate the colitis phenotype in *Bmal1*$^{IEC-/-}$x*Il-10*$^{-/-BL6}$ mice

(**A**) Survival analysis of *Il-10*$^{-/-BL6}$ and *Bmal1*$^{IEC-/-}$x*Il-10*$^{-/-BL6}$ mice under AD and RF condition. (**B**) Frequency of CD3+CD4+ cells in colon lamina propria measured by flow cytometry. (**C**) Representative H&E staining of colon cross section from *Il-10*$^{-/-BL6}$ and *Bmal1*$^{IEC-/-}$x*Il-10*$^{-/-BL6}$ mice under AD and RF conditions. (**D**) Histoscores and (**E**) inflammatory marker gene Tnf expression in controls, *Il-10*$^{-/-BL6}$ and *Bmal1*$^{IEC-/-}$x*Il-10*$^{-/-BL6}$ mice under AD and RF conditions. Significances were calculated by three-way ANOVA following Benjamini, Krieger and Yekutieli correction. * $p \leq 0.05$, ** $p \leq 0.01$, *** $p \leq 0.001$, **** $p \leq 0.0001$. Data are represented as individual dot.

4.13 Intestinal clock-controlled microbiota might play an important role in colitis development in IL-10-deficient mice

In addition to the intestinal clock, food presence is also one of the most important factor which drives microbiota composition and rhythmicity[99]. Although RF did not improve the colitis phenotype in *Bmal1*$^{IEC-/-}$ x *Il-10*$^{-/-BL6}$ mice, we investigate the microbial composition in control, *Il-10*$^{-/-BL6}$ and *Bmal1*$^{IEC-/-}$ x *Il-10*$^{-/-BL6}$ mice under RF condition as well. Indeed, similar to the observation under AD condition, microbial beta-diversity in *Bmal1*$^{IEC-/-}$ x *Il-10*$^{-/-BL6}$ mice was significantly different among the other groups under RF condition (**Fig. 21A**). Interestingly, RF in *Bmal1*$^{IEC-/-}$ x *Il-10*$^{-/-BL6}$ mice enhanced species richness to control levels, whereas microbiota rhythmicity remained arrhythmic (**Fig. 21B**), indicating that loss of microbial rhythms might be involved in the disease phenotype rather than the overall amount of species. Indeed, we identified 40 zOTUs which gained rhythmicity during RF in *Il-10*$^{-/-BL6}$ mice, but remained arrhythmic in *Bmal1*$^{IEC-/-}$ x *Il-10*$^{-/-BL6}$ mice. The majority of these zOTUs belong to the family *Lachnospiraceae, Muribaculaceae* and *Oscillospiraceae* (**Fig. 21C**), which were previously identified as intestinal clock-controlled[27]. Thus these intestinal clock-controlled microbiota might be highly involved in IBD development and contribute to the disease progression.

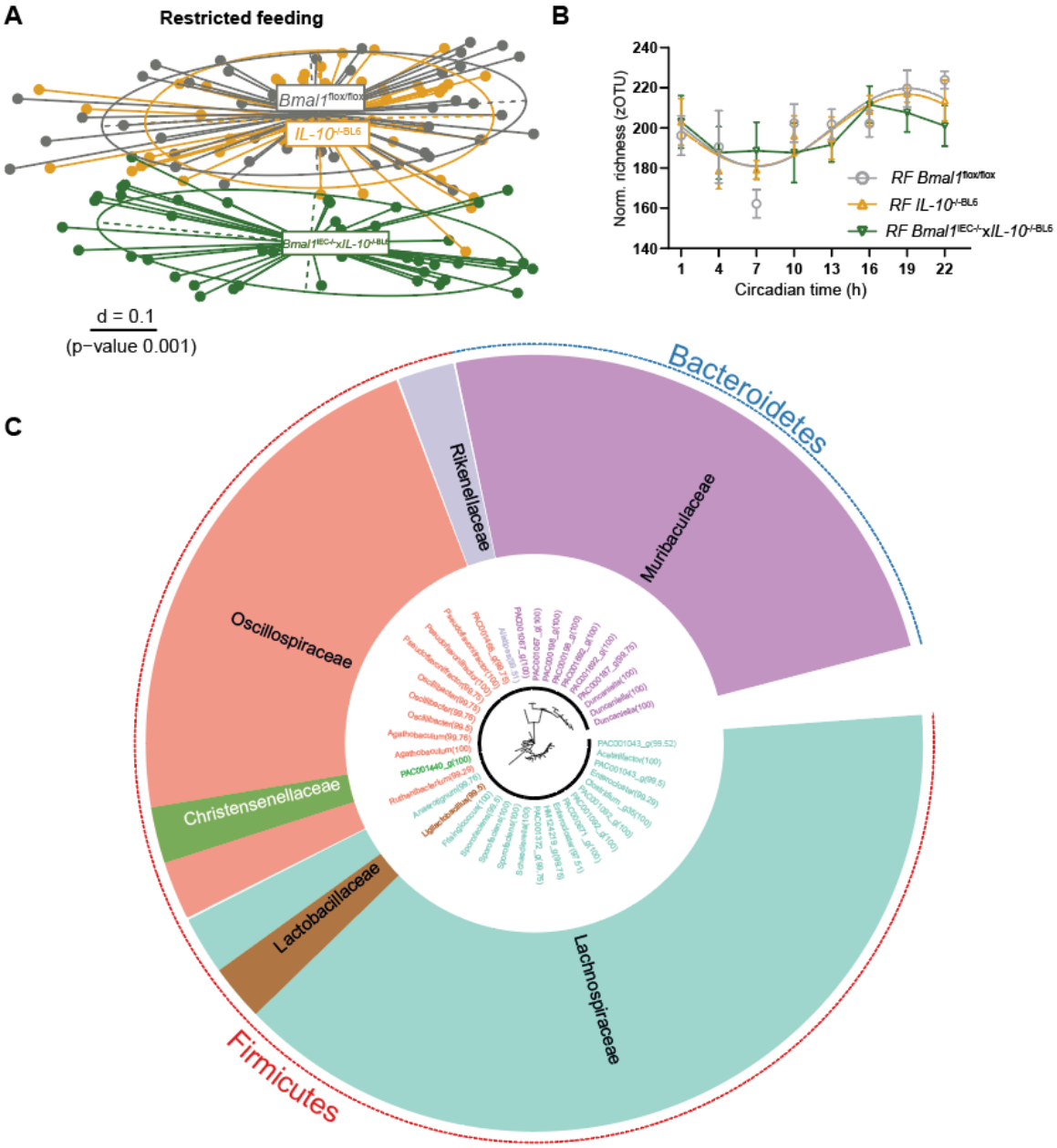

Figure 23 Comparison of microbiota composition in *Il-10*$^{-/-BL6}$ and *Bmal1*$^{IEC-/-}$ x*Il-10*$^{-/-BL6}$ mice under RF condition

(**A**) Beta-diversity illustrated by MDS plots of fecal microbiota based on generalized UniFrac distances (GUniFrac) in control, *Il-10*$^{-/-Sv129}$ and *Bmal1*$^{IEC-/-}$x*Il-10*$^{-/-}$ mice. (**B**) Normalized richness under RF condition. (**C**) Taxonomic tree of fecal microbiota which have restored rhythms in *Il-10*$^{-/-}$ mice after RF but not in *Bmal1*$^{IEC-/-}$x*Il-10*$^{-/-}$ mice after RF. Taxonomic ranks are from phylum (outer dashed ring), family (inner ring highlighted) to genera (middle, color coded according to family) which are indicated by the individual branches. Significant rhythms are illustrated with fitted cosine-regression; data points connected by straight lines indicate no significant cosine fit curves ($p > 0.05$) and thus no rhythmicity. Data are represented as mean ± SEM.

5 Discussion

Alterations in clock genes were found in colonic biopsy samples from IBD patients, especially patients with ulcerative colitis[33, 34]. In this study on *Il-10*$^{-/-}$ mice, a previously-described IBD-relevant mouse model for colitis[155], we provide evidence that a disrupted colonic circadian clock is a cause rather than the consequence of GI inflammation in IBD. DSS treatment severely enhanced chemically induced colitis in mice lacking a functional intestinal circadian clock. This is in accordance with previous literature which showed that environmental circadian disruption in form of shift work as well as system-wide genetic clock dysfunction, e.g. in *Per1/2*$^{-/-}$, *Rev-erbα*$^{-/-}$ and *Bmal1*$^{-/-}$ mice promotes the severity of DSS-induced colitis[111-113].

However, it is extremely complicated to clarify the role of specific peripheral clocks, especially the intestinal clock, under global clock disruption condition (chronic jet lag or whole body clock gene knock-out model), since central clock in SCN synchronize peripheral clocks through neural signals and hormones[2]. When the central pacemaker is impaired, it is unlikely that peripheral clocks would stay unaffected, which further leads people using intestinal-specific clock knockout model to better understand the role of intestinal clock in regulating intestinal homeostasis. We previously addressed the intestinal clock as the key regulator for maintaining microbiome rhythmicity, which is vital for intestinal metabolism and immune response[27] via using *Bmal1*$^{IEC-/-}$ mice. Moreover, on the same model, scientists identified intestinal clock as an accelerator in dietary fat absorption, therefore *Bmal1* deletion prevents high-fat diet induced obesity[178]. Researchers also revealed intestinal clock disruption accelerated the colorectal cancer[179], which is consistent with our findings that impaired intestinal clock enhances the susceptibility of intestinal diseases. Indeed, recent literature indicated disruption of diurnal

intestinal rhythmicity contributes to the DSS-induced colitis under normal light-dark condition[180]. However, we demonstrate for the first time that specifically loss of the circadian intestinal clock promotes the severity and prevalence of DSS-induced colitis symptoms in mice under constant darkness which exclude the intervention of light. The cause-effect relationship was further validated in a novel genetic mouse model for colitis which additionally lack a functional intestinal clock. These *Bmal1*$^{IEC-/-}$x*Il-10*$^{-/-BL6}$ mice develop a severely enhanced immune phenotype and dramatically reduced survival.

5.1 RNA-seq analysis revealed intestinal clock is a key mediator in regulating intestinal immune homeostasis

Unlike the central clock in SCN which regulates basic physiology such as activity/rest and body temperature, and synchronize peripheral clocks through neural signals and hormones[2], peripheral clocks dominantly controls the rhythms of tissue specific functions. Thus it is extremely important to investigate tissue specific clocks and functions when assessing tissue-relevant diseases.

In our study, understanding the function of the intestinal clock becomes critical since we focused on inflammatory bowel disease. In order to get a first glance on how the intestinal clock works on transcriptomic levels, bulk-RNAseq analysis was performed on mice with genetic dysfunction of the intestinal clock (*Bmal1*$^{IEC-/-}$), which helped us to understand potential mechanisms how a disrupted colon clock in e.g. *Il-10*$^{-/-}$ mice might affect GI inflammation. Indeed, a majority of intestinal-clock controlled genes were found to be involved in local immune functions and epithelial-microbe interactions. The intestinal clock regulates important inflammatory marker genes, such as *Tnf*, which are arrhythmic and enhanced in *Il-10*$^{-/-}$ mice

and have previously been linked to the development of IBD[181]. Intestinal clock-controlled genes are also involved in immune cell recruitment, such as *Ffar2,* which plays an important role in intestinal homeostasis by regulating immune cell abundance in colonic lymphoid tissues and the secretion of mucus-associated proteins and antimicrobial peptides[168] as well as *Abcc2,* which actively regulates mucosal inflammation[169]. Both genes are differentially expressed and lost rhythmicity in mice lacking an intestinal clock. Moreover, *Rorc* which encodes the IBD risk factor RORγ[170], was elevated and arrhythmic in mice lacking intestinal clock. These results further suggest the importance of the intestinal clock in modulating IBD-like phenotype.

In addition, the expression of the pro-migratory genes *Vcam-1* and *Cxcr4* undergoes diurnal oscillation in multiple lymphoid and non-lymphoid tissues[109, 182]. Here we further extended these observations to the colon, that the circadian expression of these two genes require a functional intestinal clock. Furthermore, *Cxcr4* mediates the diurnal oscillations in T cell distribution and responses[109] and *Vcam-1* is involved in the rhythmic pattern of leukocytes migration[182]. Therefore, arrhythmicity of these genes likely contributes to the immune cell recruitment to colon lamina propria and thus impact the local immune response and contribute to the IBD development and progression. Indeed, here we provide the first evidence for a functional role of the intestinal clock in regulating rhythmic immune and inflammatory processes including immune cell recruitment and microbiota composition, which are both key elements in IBD development or progression[181]. For example, a dysfunctional colon clock in *Il-10*$^{-/-}$ and *Bmal1*$^{IEC-/-}$ mice caused loss of rhythmicity in the recruitment of T cells into the colonic lamina propria. Similarly, rhythmic leukocyte trafficking into the bloodstream and tissue infiltration to lymph nodes, spleen and bone marrow has previously been described for T cells and monocytes and depends on cell- and tissue-specific circadian clocks [183]. The physiological importance of diurnal immune cell recruitment was demonstrated for T-cells recruitment in lymphoid organs which improved the immune response to antigens and bacterial

infection at night[109]. Moreover, clustering specifically of CD4+ cells in the intestine induced colitis in an adoptive transfer mouse model[184]. Consequently, arrhythmic leukocyte recruitment to the colon might have augmented the inflammatory response in mice with a disrupted colon circadian clock.

Interestingly, the intestinal clock tends to regulate different sets of genes during rest and active phase. DEGs are enriched mainly in leukocyte apoptotic process, insulin response, peptide hormone response and circadian rhythm during the day, while at night, more metabolic pathways are affected (e.g. xenobiotic catabolic process, bile acid secretion, cholesterol metabolic process, sulfur compound transport). These findings further support the potential therapy strategy that the timing of medicine treatment should be taken into account in clinical application[185].

However, although *Bmal1* deletion in IECs results in a wide range of alteration in immune response and metabolism related pathways, disruption of intestinal clock alone is not the decisive factor to induce tissue pathological changes. Unlike *Bmal1*$^{IEC-/-}$ mice, *Il-10*$^{-/-}$ mice are prone to get IBD-like intestinal inflammation spontaneously, whose intestinal clock is altered but still exists. Thus we generated the *Bmal1*$^{IEC-/-}$x*Il-10*$^{-/-BL6}$ mice, namely a mouse model that develops colitis via aging and does not harbour a functional intestinal clock at the same time. Indeed, lack of intestinal clock accelerates and exacerbates the colitis phenotype in *Il-10*$^{-/-BL6}$ mice, which results in shortened lifespan and increased disease activity. Similarly, mucin 2-interleukin 10-deficient double knocked-out mice were used to identify mucus layer as a key regulator in colitis[186]. Moreover, VDR-IL-10 double knocked-out mice were generated to validate that Vitamin D receptor (VDR) is essential to regulate gastrointestinal immunity[187]. Here in this study we first address the intestinal clock as a key regulator in colitis development.

5.2 Microbiome alteration caused by intestinal clock dysfunction might contribute to the GI diseases

Microbiota composition and function has frequently been associated to the development of GI inflammation[188] and loss of rhythmicity of the microbiome was linked to the development of obesity and Type 2 diabetes[94]. Germ-free mice are free of DSS induced colitis although they are more susceptible at higher DSS concentrations due to damage to the barrier[80], and absence of colitis as well as immune activation was characterized in germ free *Il-10*$^{-/-}$ mice[165]. Thus we also characterize the microbiota composition and its derived metabolites in our genetic modified mouse models.

Interestingly, microbiome rhythmicity was disrupted in *Il-10*$^{-/-\text{Sv129}}$ mice. This was likely caused by intestinal clock dysfunction in these mice, because the intestinal clock was recently identified as a major driver of microbiota rhythmicity[27]. Similar to previous results obtained from *Bmal1*$^{\text{IEC-/-}}$ mice[27], intestinal clock-controlled taxa involved in SCFA fermentation and secondary bile acid formation, such as *Lachnospiraceae* and *Oscillospiraceae*, were arrhythmic in *Il-10*$^{-/-\text{Sv129}}$ mice. Arrhythmicity of these specific taxa in *Il-10*$^{-/-\text{Sv129}}$ mice likely caused the reduced amplitudes or loss of rhythmicity in the levels of specific BAs, such as DCA, 7-sulfo CA, HDCA and α-MCA, which have frequently been linked to intestinal inflammation[189, 190]. Notably, reduced levels of secondary BAs, e.g. DCAs and HDCAs identified in *Bmal1*$^{IEC-/-}$ mice receiving disease-associated microbiota, were also found in in patients with UC and supplementation particularly with DCA ameliorates experimental colitis in mice[191]. Thus arrhythmic microbial metabolite production due to loss of rhythmic microbiota composition in *Il-10*$^{-/-}$ mice might promote their inflammatory immune response. Indeed, our recent transfer

experiments provided evidence that arrhythmic microbiota and derived products can alter GI immune homeostasis[27].

However, transfer of arrhythmic microbiota from *Bmal1*$^{IEC-/-}$ mice did not increase the severity of inflammation in germ-free *Il-10*$^{-/-}$ recipients, suggesting that intestinal clock dysfunction rather than loss of microbial rhythmicity predominantly induce colonic inflammation. Indeed, transfer of IBD-associated microbiota provide direct evidence for the physiological relevance of the intestinal circadian clock for the inflammatory response. Depending on the recipient genotype, disease-associated microbiota caused an inflammatory response, which reflects the one observed in *Il-10*$^{-/-Sv129}$ mice. Enhanced $CD4^+$ T-cells infiltration and elevated *Tnf* expression was only found in colonic tissues of *Bmal1*$^{IEC-/-}$ recipients. Moreover, similar to *Il-10*$^{-/-Sv129}$ mice, we found altered abundance of zOTUs belonging to *Lachnospiraceae* and *Erysipelotrichaceae*, and IBD-associated microbiota-derived products, such as α-MCA and DCA, were suppressed and their time difference was lost in *Bmal1*$^{IEC-/-}$ recipients. These results reflect the immune response observed in the *Il-10*$^{-/-}$ donors and thus indicate an activated, early inflammatory response although in colon cross sections no pathohistological tissue changes could be observed between genotypes. This might be due to the patchy colonic inflammation associated with the Crohn's disease-like phenotype reported in *Il-10*$^{-/-}$ mice[192]. Altogether, these results highlight the relevance of intestinal clock function for GI inflammatory processes involved in microbiota-induced IBD development. Interestingly, a functional intestinal clock in control recipients was capable of restoring the circadian time differences of zOTUs. These rhythmic hosts showed reduced immune cell recruitment into lamina propria and inflammatory marker gene expression and thus indicates that restoration of the intestinal clock might reduce GI inflammation.

5.3 Targeting the intestinal clock by RF is capable to ameliorate IBD symptoms

It is important to not only focus on the cause, but the cure, hence, we switched our focus to methods which are capable to restore the disrupted intestinal clock in *Il-10*$^{-/-}$ mice and thus, ameliorate the colitis severity and progression.

Time-restricted feeding is a widely applied approach to re-synchronize peripheral clocks and uncouple them from the SCN as day-restricted feeding in mice completely reversed the circadian clocks in various peripheral organs including liver, stomach, as well as intestine without influencing the central clock in SCN[13]. However, considerable amount of studies link the beneficial effect of RF with caloric restriction and body weight loss[120], while in our case, mice had comparable food intake between ad libitum and restricted feeding conditions. Moreover, it is extremely difficult to accurately measure the body weight of mice under RF condition. For example, at the end stage of RF protocol mice only have 4h to get food access, resulting in huge body weight changes before and after food intake. Thus it is not convincing to compare the body weight before eating (RF condition) with AD mice which have free access to food.

At the molecular level, the mechanisms how RF influence the circadian system can be mainly divided into two parts, the fasting state and feeding state. In details, the AMP/ATP ratio increases without the food intake, which activates AMP-activated protein kinase (AMPK) and AMPK in turn reduces the stability of serine71 of CRY1[193]. Fasting also activates the rate-limiting enzyme nicotinamide phosphoribosyltransferase (NAMPT) and thus increase the cellular availability of NAD+ and activates SIRT1. Importantly, SIRT1 is capable to bind CLOCK:BMAL1 and supress the transcription of *Per2*[119]. Thus fasting plays an important

role in regulating both transcription and stability of Per and Cry, which de-represses CLOCK:BMAL1 and increases their amplitude[194]. On the other hand, food intake directly activates the nutrient-activated serine/threonine protein kinase, rapamycin (mTOR) which induces CRY1[195]. Food presentation also suppressed NAMPT function and reduces cellular NAD^+, as well as inactivating SIRT1. In the scope of the cycle, fasting enhances the positive limb of the clock system (BMAL1) while feeding contributes to the negative limb (CRY and PER).

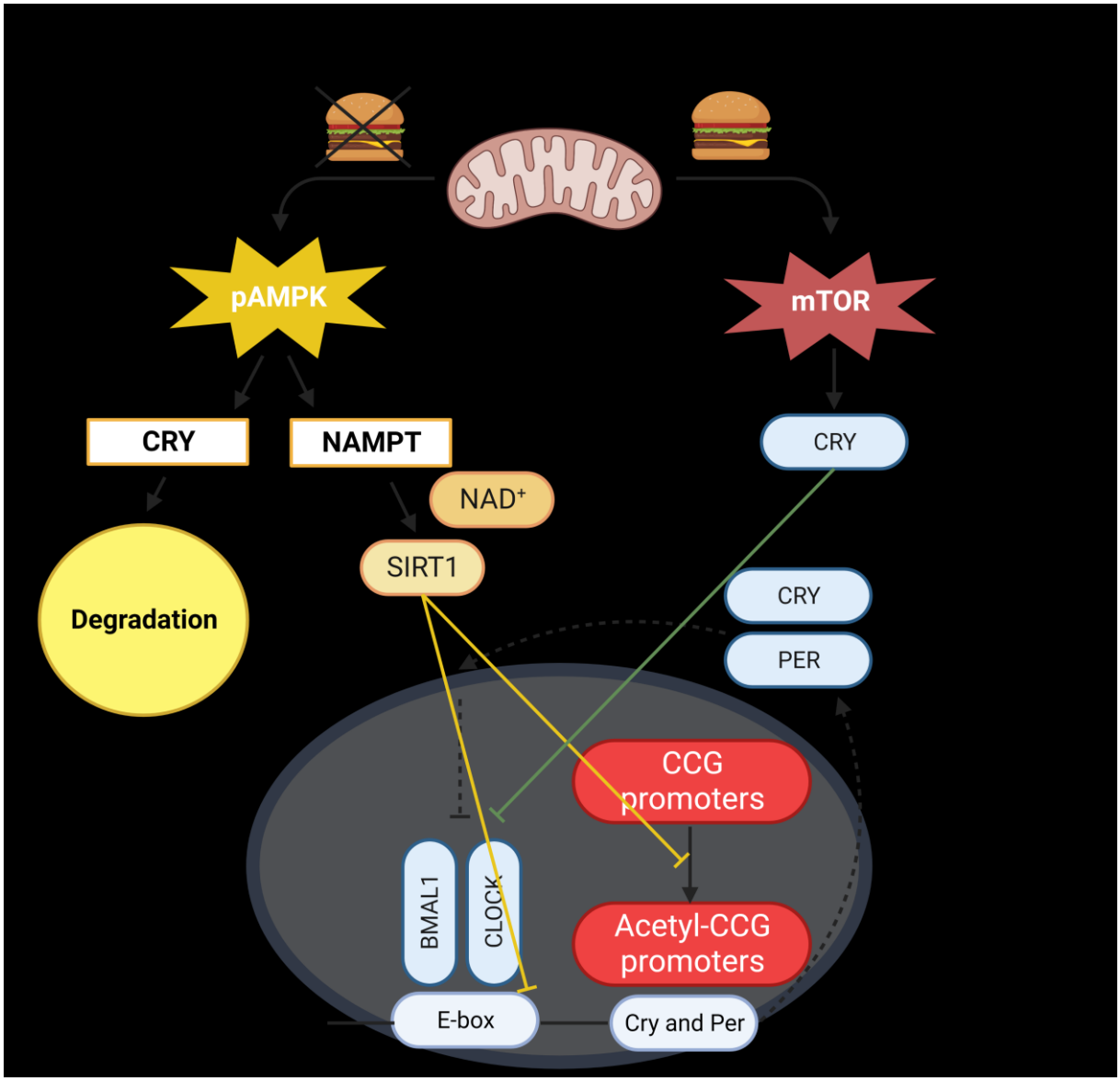

Figure 24 Molecular mechanisms of time restricted feeding in regulating circadian clock

In the fasting state, nutrient depletion activates AMPK and then induces the degradation of CRY by phosphorylation. Next, AMPK activates SIRT1 activity via NAMPT and SIRT1 binds with CLOCK:BMAL1 and represses the transcription of *Per2*. The acetyltransferase activity of clock is counteracted by SIRT1. In the feeding state, nutrient availability activates mTOR which induces CRY and thus represses CLOCK:BMAL1. AMPK:,AMP activated protein kinase; Bmal1, brain and muscle arnt like 1; CCG, clock-controlled genes; Clock, circadian locomotor output cycle kaput; cry, cryptochrome; mTOR, mechanistic target of rapamycin; NAD, nicotinamide adenine dinucleotide; NAMPT, nicotinamide phosphoribosyl transferase; Per, period; SIRT1, sirtuin1.

In order to determine whether intestinal clock function can be targeted to influence the immune response to GI inflammation, *Il-10*$^{-/-}$ mice were exposed to night time restricted feeding (RF). RF in mice kept in different light conditions was capable to influence the rhythmicity of major clock genes in intestinal tissues independent of the central clock [125, 126]. Here we demonstrate that the colonic circadian clock can indeed be restored by RF in a diseased-mouse model (*Il-10*$^{-/-}$) with disrupted colonic clock function. Targeting the colon clock by RF further led to restoration of rhythmic colon clock functions, such as $CD4^+$ T-cell recruitment into the colonic lamina propria and microbiome oscillations. In confirmation with our hypothesis RF ameliorated the IBD-like colitis phenotype in *Il-10*$^{-/-}$ mice and substantially enhanced their survival. This is in accordance with results obtained in mice showing that RF protects from DSS-induced colitis by affecting intestinal functions[196, 197]. Similarly, RF in a mouse model for arthritis influences leukocytes responsiveness and improves systemic inflammation[123]. In humans, meal timing was tested as treatment for a variety of diseases including diabetes, cancer and tissue injuries[198]. Although inconsistent meal times could be correlated to IBD symptoms[118], to our knowledge no clear evidence has been generated regarding the beneficial effect of RF on IBD patients.

5.4 The beneficial effects of RF require the presence of intestinal clock

However, the mechanism of RF on disease outcome remains unclear. Although our results indicate that RF might prevent or reduce inflammation by activating the intestinal clock, this is particularly difficult to prove due to the circadian system-wide effects of RF. Namely, RF was found to induce phase shifts in clock gene expression in the liver, kidney, pancreas, WAT and intestinal tissue[13, 124] and to affect gene expression involved in inflammatory signalling such as NF-kB, TLR or IL-17 in many tissues including the intestine[199]. Here, we provide the first direct mechanistic evidence that the effect of RF on the severity of IBD is gated by the intestinal clock, because RF failed to reduce the inflammatory phenotype (immune cells infiltration, inflammatory marker gene expression, histopathological scores) due to genetic dysfunction of the intestinal clock in *Bmal1*$^{IEC-/-}$x*Il-10*$^{-/-}$ mice. Our results are in accordance with a report indicating *Bmal1* gene expression in colonic/jejunal IECs could not be restored by RF[200].

Notably, we observed an improved richness following RF in *Bmal1*$^{IEC-/-}$x*Il-10*$^{-/-}$ mice, which has been associated with improved IBD conditions[201]. Thus, we cannot exclude that other factors, such as the microbiome[98, 99] and hormones[202], known to respond to RF independent of the intestinal clock, might additionally contribute to the improved disease outcome. Nevertheless, no significant improvements in tissue pathology or the inflammatory response nor enhanced overall survival following RF was observed in *Bmal1*$^{IEC-/-}$x*Il-10*$^{-/-}$ mice. Thus, these results demonstrate that the intestinal clock represents a target for treatment of gastrointestinal inflammation.

Taken together, our results demonstrate that a functional intestinal clock is essential to maintain GI homeostasis and represents a major player in IBD progression. In addition, our findings suggest that enhancing intestinal clock function by meal timing might become the next step to

develop novel strategies in circadian therapies of IBD and potentially other metabolic diseases in humans.

Conclusion

This work represents a novel approach identifying the host intestinal clock as the major driver in regulating intestinal inflammation and validate it as the target for the beneficial effects of time-restricted feeding. Our results demonstrate that a functional intestinal clock is essential to maintain gastrointestinal homeostasis and represents a major player in IBD progression. Taken together, our findings suggest that enhancing intestinal clock function by meal timing might become the next step to develop novel strategies in circadian therapies of IBD and potentially other metabolic diseases in humans.

List of Figures

References

1. Welsh, D.K., J.S. Takahashi, and S.A. Kay, Suprachiasmatic nucleus: cell autonomy and network properties. Annu Rev Physiol, 2010. **72**: p. 551-77.
2. Mohawk, J.A., C.B. Green, and J.S. Takahashi, Central and peripheral circadian clocks in mammals. Annu Rev Neurosci, 2012. **35**: p. 445-62.
3. Aschoff, J.r., Biological rhythms. Handbook of behavioral neurobiology. 1981, New York: Plenum Press. xix, 563 p.
4. Gekakis, N., et al., Role of the CLOCK protein in the mammalian circadian mechanism. Science, 1998. **280**(5369): p. 1564-9.
5. Reppert, S.M. and D.R. Weaver, Coordination of circadian timing in mammals. Nature, 2002. **418**(6901): p. 935-41.
6. Ueda, H.R., et al., System-level identification of transcriptional circuits underlying mammalian circadian clocks. Nat Genet, 2005. **37**(2): p. 187-92.
7. Berson, D.M., F.A. Dunn, and M. Takao, Phototransduction by retinal ganglion cells that set the circadian clock. Science, 2002. **295**(5557): p. 1070-3.
8. Moore, R.Y. and V.B. Eichler, Loss of a circadian adrenal corticosterone rhythm following suprachiasmatic lesions in the rat. Brain Res, 1972. **42**(1): p. 201-6.
9. Shigeyoshi, Y., et al., Light-induced resetting of a mammalian circadian clock is associated with rapid induction of the mPer1 transcript. Cell, 1997. **91**(7): p. 1043-53.
10. Shearman, L.P., et al., Two period homologs: circadian expression and photic regulation in the suprachiasmatic nuclei. Neuron, 1997. **19**(6): p. 1261-9.
11. Kiessling, S., P.J. Sollars, and G.E. Pickard, Light stimulates the mouse adrenal through a retinohypothalamic pathway independent of an effect on the clock in the suprachiasmatic nucleus. PLoS One, 2014. **9**(3): p. e92959.
12. Challet, E., et al., Synchronization of the molecular clockwork by light- and food-related cues in mammals. Biol Chem, 2003. **384**(5): p. 711-9.
13. Damiola, F., et al., Restricted feeding uncouples circadian oscillators in peripheral tissues from the central pacemaker in the suprachiasmatic nucleus. Genes Dev, 2000. **14**(23): p. 2950-61.
14. Tahara, Y., S. Aoyama, and S. Shibata, The mammalian circadian clock and its entrainment by stress and exercise. J Physiol Sci, 2017. **67**(1): p. 1-10.
15. Longo, V.D. and S. Panda, Fasting, Circadian Rhythms, and Time-Restricted Feeding in Healthy Lifespan. Cell Metab, 2016. **23**(6): p. 1048-1059.

16. Zhang, R., et al., A circadian gene expression atlas in mammals: implications for biology and medicine. Proc Natl Acad Sci U S A, 2014. **111**(45): p. 16219-24.
17. Panda, S., et al., Coordinated transcription of key pathways in the mouse by the circadian clock. Cell, 2002. **109**(3): p. 307-20.
18. Storch, K.F., et al., Extensive and divergent circadian gene expression in liver and heart. Nature, 2002. **417**(6884): p. 78-83.
19. Merrow, M., K. Spoelstra, and T. Roenneberg, The circadian cycle: daily rhythms from behaviour to genes. EMBO Rep, 2005. **6**(10): p. 930-5.
20. Kiessling, S., G. Eichele, and H. Oster, Adrenal glucocorticoids have a key role in circadian resynchronization in a mouse model of jet lag. J Clin Invest, 2010. **120**(7): p. 2600-9.
21. Kiessling, S., et al., Enhancing circadian clock function in cancer cells inhibits tumor growth. BMC Biol, 2017. **15**(1): p. 13.
22. Kiessling, S., et al., The circadian clock in immune cells controls the magnitude of Leishmania parasite infection. Sci Rep, 2017. **7**(1): p. 10892.
23. Karatsoreos, I.N., et al., Disruption of circadian clocks has ramifications for metabolism, brain, and behavior. Proc Natl Acad Sci U S A, 2011. **108**(4): p. 1657-62.
24. Panda, S., Circadian physiology of metabolism. Science, 2016. **354**(6315): p. 1008-1015.
25. Gombert, M., et al., The connection of circadian rhythm to inflammatory bowel disease. Transl Res, 2019. **206**: p. 107-118.
26. Segers, A. and I. Depoortere, Circadian clocks in the digestive system. Nat Rev Gastroenterol Hepatol, 2021. **18**(4): p. 239-251.
27. Heddes, M., et al., The intestinal clock drives the microbiome to maintain gastrointestinal homeostasis. Nat Commun, 2022. **13**(1): p. 6068.
28. Pan, X. and M.M. Hussain, Clock is important for food and circadian regulation of macronutrient absorption in mice. J Lipid Res, 2009. **50**(9): p. 1800-13.
29. Hoogerwerf, W.A., et al., Rhythmic changes in colonic motility are regulated by period genes. Am J Physiol Gastrointest Liver Physiol, 2010. **298**(2): p. G143-50.
30. Karpowicz, P., et al., The circadian clock gates the intestinal stem cell regenerative state. Cell Rep, 2013. **3**(4): p. 996-1004.
31. Mukherji, A., et al., Homeostasis in intestinal epithelium is orchestrated by the circadian clock and microbiota cues transduced by TLRs. Cell, 2013. **153**(4): p. 812-27.

32. Wang, Y., et al., The intestinal microbiota regulates body composition through NFIL3 and the circadian clock. Science, 2017. **357**(6354): p. 912-916.
33. Palmieri, O., et al., Systematic analysis of circadian genes using genome-wide cDNA microarrays in the inflammatory bowel disease transcriptome. Chronobiol Int, 2015. **32**(7): p. 903-16.
34. Liu, X., et al., Bidirectional Regulation of Circadian Disturbance and Inflammation in Inflammatory Bowel Disease. Inflamm Bowel Dis, 2017. **23**(10): p. 1741-1751.
35. Wang, D., et al., Influence of sleep disruption on inflammatory bowel disease and changes in circadian rhythm genes. Heliyon, 2022. **8**(10): p. e11229.
36. Helander, H.F. and L. Fandriks, Surface area of the digestive tract - revisited. Scand J Gastroenterol, 2014. **49**(6): p. 681-9.
37. Mowat, A.M. and W.W. Agace, Regional specialization within the intestinal immune system. Nat Rev Immunol, 2014. **14**(10): p. 667-85.
38. Kunisawa, J., I. Takahashi, and H. Kiyono, Intraepithelial lymphocytes: their shared and divergent immunological behaviors in the small and large intestine. Immunol Rev, 2007. **215**: p. 136-53.
39. Lee, E., L.R. Schiller, and J.S. Fordtran, Quantification of colonic lamina propria cells by means of a morphometric point-counting method. Gastroenterology, 1988. **94**(2): p. 409-18.
40. Furness, J.B., W.A. Kunze, and N. Clerc, Nutrient tasting and signaling mechanisms in the gut. II. The intestine as a sensory organ: neural, endocrine, and immune responses. Am J Physiol, 1999. **277**(5): p. G922-8.
41. Chang, S.Y., et al., Circulatory antigen processing by mucosal dendritic cells controls CD8(+) T cell activation. Immunity, 2013. **38**(1): p. 153-65.
42. Zeitz, M., et al., Phenotype and function of lamina propria T lymphocytes. Immunol Res, 1991. **10**(3-4): p. 199-206.
43. Ma, H., W. Tao, and S. Zhu, T lymphocytes in the intestinal mucosa: defense and tolerance. Cell Mol Immunol, 2019. **16**(3): p. 216-224.
44. Campbell, D.J. and E.C. Butcher, Rapid acquisition of tissue-specific homing phenotypes by CD4(+) T cells activated in cutaneous or mucosal lymphoid tissues. J Exp Med, 2002. **195**(1): p. 135-41.
45. Svensson, M., et al., CCL25 mediates the localization of recently activated CD8alphabeta(+) lymphocytes to the small-intestinal mucosa. J Clin Invest, 2002. **110**(8): p. 1113-21.

46. Shi, Y. and L. Mu, An expanding stage for commensal microbes in host immune regulation. Cell Mol Immunol, 2017. **14**(4): p. 339-348.
47. Smith, P.M. and W.S. Garrett, The gut microbiota and mucosal T cells. Front Microbiol, 2011. **2**: p. 111.
48. Ivanov, II, et al., The orphan nuclear receptor RORgammat directs the differentiation program of proinflammatory IL-17+ T helper cells. Cell, 2006. **126**(6): p. 1121-33.
49. Sathaliyawala, T., et al., Distribution and compartmentalization of human circulating and tissue-resident memory T cell subsets. Immunity, 2013. **38**(1): p. 187-97.
50. Luckheeram, R.V., et al., CD4(+)T cells: differentiation and functions. Clin Dev Immunol, 2012. **2012**: p. 925135.
51. Ishigame, H., et al., Differential roles of interleukin-17A and -17F in host defense against mucoepithelial bacterial infection and allergic responses. Immunity, 2009. **30**(1): p. 108-19.
52. Zenewicz, L.A., et al., Innate and adaptive interleukin-22 protects mice from inflammatory bowel disease. Immunity, 2008. **29**(6): p. 947-57.
53. Ivanov, II, et al., Induction of intestinal Th17 cells by segmented filamentous bacteria. Cell, 2009. **139**(3): p. 485-98.
54. Mayne, C.G. and C.B. Williams, Induced and natural regulatory T cells in the development of inflammatory bowel disease. Inflamm Bowel Dis, 2013. **19**(8): p. 1772-88.
55. Barnes, M.J. and F. Powrie, Regulatory T cells reinforce intestinal homeostasis. Immunity, 2009. **31**(3): p. 401-11.
56. Coombes, J.L. and F. Powrie, Dendritic cells in intestinal immune regulation. Nat Rev Immunol, 2008. **8**(6): p. 435-46.
57. Johansson, C. and B.L. Kelsall, Phenotype and function of intestinal dendritic cells. Semin Immunol, 2005. **17**(4): p. 284-94.
58. Kelsall, B., Recent progress in understanding the phenotype and function of intestinal dendritic cells and macrophages. Mucosal Immunol, 2008. **1**(6): p. 460-9.
59. Macpherson, A.J. and T. Uhr, Induction of protective IgA by intestinal dendritic cells carrying commensal bacteria. Science, 2004. **303**(5664): p. 1662-5.
60. Huang, F.P., et al., A discrete subpopulation of dendritic cells transports apoptotic intestinal epithelial cells to T cell areas of mesenteric lymph nodes. J Exp Med, 2000. **191**(3): p. 435-44.

61. Chieppa, M., et al., Dynamic imaging of dendritic cell extension into the small bowel lumen in response to epithelial cell TLR engagement. J Exp Med, 2006. **203**(13): p. 2841-52.
62. Platt, A.M. and A.M. Mowat, Mucosal macrophages and the regulation of immune responses in the intestine. Immunol Lett, 2008. **119**(1-2): p. 22-31.
63. Denning, T.L., et al., Lamina propria macrophages and dendritic cells differentially induce regulatory and interleukin 17-producing T cell responses. Nat Immunol, 2007. **8**(10): p. 1086-94.
64. Na, Y.R., et al., Macrophages in intestinal inflammation and resolution: a potential therapeutic target in IBD. Nat Rev Gastroenterol Hepatol, 2019. **16**(9): p. 531-543.
65. Sadik, C.D., N.D. Kim, and A.D. Luster, Neutrophils cascading their way to inflammation. Trends Immunol, 2011. **32**(10): p. 452-60.
66. Amulic, B., et al., Neutrophil function: from mechanisms to disease. Annu Rev Immunol, 2012. **30**: p. 459-89.
67. Fournier, B.M. and C.A. Parkos, The role of neutrophils during intestinal inflammation. Mucosal Immunol, 2012. **5**(4): p. 354-66.
68. Torres, J., et al., Crohn's disease. Lancet, 2017. **389**(10080): p. 1741-1755.
69. Kobayashi, T., et al., Ulcerative colitis. Nat Rev Dis Primers, 2020. **6**(1): p. 74.
70. Wilkins, T., K. Jarvis, and J. Patel, Diagnosis and management of Crohn's disease. Am Fam Physician, 2011. **84**(12): p. 1365-75.
71. Ng, S.C., et al., Worldwide incidence and prevalence of inflammatory bowel disease in the 21st century: a systematic review of population-based studies. Lancet, 2017. **390**(10114): p. 2769-2778.
72. Liu, J.Z., et al., Association analyses identify 38 susceptibility loci for inflammatory bowel disease and highlight shared genetic risk across populations. Nat Genet, 2015. **47**(9): p. 979-986.
73. de Lange, K.M., et al., Genome-wide association study implicates immune activation of multiple integrin genes in inflammatory bowel disease. Nat Genet, 2017. **49**(2): p. 256-261.
74. Xavier, R.J. and D.K. Podolsky, Unravelling the pathogenesis of inflammatory bowel disease. Nature, 2007. **448**(7152): p. 427-34.
75. Belkaid, Y. and T.W. Hand, Role of the microbiota in immunity and inflammation. Cell, 2014. **157**(1): p. 121-41.

76. Bunker, J.J. and A. Bendelac, IgA Responses to Microbiota. Immunity, 2018. **49**(2): p. 211-224.
77. Arabyan, N., et al., Salmonella Degrades the Host Glycocalyx Leading to Altered Infection and Glycan Remodeling. Sci Rep, 2016. **6**: p. 29525.
78. Thia, K.T., et al., Ciprofloxacin or metronidazole for the treatment of perianal fistulas in patients with Crohn's disease: a randomized, double-blind, placebo-controlled pilot study. Inflamm Bowel Dis, 2009. **15**(1): p. 17-24.
79. Schaubeck, M., et al., Dysbiotic gut microbiota causes transmissible Crohn's disease-like ileitis independent of failure in antimicrobial defence. Gut, 2016. **65**(2): p. 225-37.
80. Hernandez-Chirlaque, C., et al., Germ-free and Antibiotic-treated Mice are Highly Susceptible to Epithelial Injury in DSS Colitis. J Crohns Colitis, 2016. **10**(11): p. 1324-1335.
81. Spits, H., et al., Innate lymphoid cells--a proposal for uniform nomenclature. Nat Rev Immunol, 2013. **13**(2): p. 145-9.
82. Bernink, J.H., et al., Human type 1 innate lymphoid cells accumulate in inflamed mucosal tissues. Nat Immunol, 2013. **14**(3): p. 221-9.
83. Ermann, J., et al., Nod/Ripk2 signaling in dendritic cells activates IL-17A-secreting innate lymphoid cells and drives colitis in T-bet-/-.Rag2-/- (TRUC) mice. Proc Natl Acad Sci U S A, 2014. **111**(25): p. E2559-66.
84. te Velde, A.A., et al., Increased expression of DC-SIGN+IL-12+IL-18+ and CD83+IL-12-IL-18- dendritic cell populations in the colonic mucosa of patients with Crohn's disease. Eur J Immunol, 2003. **33**(1): p. 143-51.
85. Krajina, T., et al., Colonic lamina propria dendritic cells in mice with CD4+ T cell-induced colitis. Eur J Immunol, 2003. **33**(4): p. 1073-83.
86. Kamada, N., et al., Unique CD14 intestinal macrophages contribute to the pathogenesis of Crohn disease via IL-23/IFN-gamma axis. J Clin Invest, 2008. **118**(6): p. 2269-80.
87. Batista, F.D. and N.E. Harwood, The who, how and where of antigen presentation to B cells. Nat Rev Immunol, 2009. **9**(1): p. 15-27.
88. Polese, L., et al., B1a lymphocytes in the rectal mucosa of ulcerative colitis patients. World J Gastroenterol, 2012. **18**(2): p. 144-9.
89. Breese, E., et al., Interleukin-2- and interferon-gamma-secreting T cells in normal and diseased human intestinal mucosa. Immunology, 1993. **78**(1): p. 127-31.
90. Rovedatti, L., et al., Differential regulation of interleukin 17 and interferon gamma production in inflammatory bowel disease. Gut, 2009. **58**(12): p. 1629-36.

91. Zhang, Z., et al., Critical role of IL-17 receptor signaling in acute TNBS-induced colitis. Inflamm Bowel Dis, 2006. **12**(5): p. 382-8.
92. Awasthi, A. and V.K. Kuchroo, IL-17A directly inhibits TH1 cells and thereby suppresses development of intestinal inflammation. Nat Immunol, 2009. **10**(6): p. 568-70.
93. Fontenot, J.D., M.A. Gavin, and A.Y. Rudensky, Foxp3 programs the development and function of CD4+CD25+ regulatory T cells. Nat Immunol, 2003. **4**(4): p. 330-6.
94. Reitmeier, S., et al., Arrhythmic Gut Microbiome Signatures Predict Risk of Type 2 Diabetes. Cell Host Microbe, 2020. **28**(2): p. 258-272 e6.
95. Coleman, O.I., et al., Activated ATF6 Induces Intestinal Dysbiosis and Innate Immune Response to Promote Colorectal Tumorigenesis. Gastroenterology, 2018. **155**(5): p. 1539-1552 e12.
96. Lloyd-Price, J., et al., Multi-omics of the gut microbial ecosystem in inflammatory bowel diseases. Nature, 2019. **569**(7758): p. 655-662.
97. Gutierrez Lopez, D.E., et al., Circadian rhythms and the gut microbiome synchronize the host's metabolic response to diet. Cell Metab, 2021. **33**(5): p. 873-887.
98. Zarrinpar, A., et al., Diet and feeding pattern affect the diurnal dynamics of the gut microbiome. Cell Metab, 2014. **20**(6): p. 1006-17.
99. Thaiss, C.A., et al., Transkingdom control of microbiota diurnal oscillations promotes metabolic homeostasis. Cell, 2014. **159**(3): p. 514-29.
100. Bellet, M.M., et al., Circadian clock regulates the host response to Salmonella. Proc Natl Acad Sci U S A, 2013. **110**(24): p. 9897-902.
101. Edgar, R.S., et al., Cell autonomous regulation of herpes and influenza virus infection by the circadian clock. Proc Natl Acad Sci U S A, 2016. **113**(36): p. 10085-90.
102. Majumdar, T., et al., Circadian transcription factor BMAL1 regulates innate immunity against select RNA viruses. Innate Immun, 2017. **23**(2): p. 147-154.
103. Ehlers, A., et al., BMAL1 links the circadian clock to viral airway pathology and asthma phenotypes. Mucosal Immunol, 2018. **11**(1): p. 97-111.
104. Scheiermann, C., et al., Clocking in to immunity. Nature Reviews Immunology, 2018. **18**(7): p. 423-437.
105. Druzd, D., et al., Lymphocyte Circadian Clocks Control Lymph Node Trafficking and Adaptive Immune Responses. Immunity, 2017. **46**(1): p. 120-132.
106. Silver, A.C., et al., Circadian expression of clock genes in mouse macrophages, dendritic cells, and B cells. Brain Behav Immun, 2012. **26**(3): p. 407-13.

107. Besedovsky, L., J. Born, and T. Lange, Endogenous glucocorticoid receptor signaling drives rhythmic changes in human T-cell subset numbers and the expression of the chemokine receptor CXCR4. FASEB J, 2014. **28**(1): p. 67-75.
108. Abe, A., et al., An Enhancer of the IL-7 Receptor alpha-Chain Locus Controls IL-7 Receptor Expression and Maintenance of Peripheral T Cells. J Immunol, 2015. **195**(7): p. 3129-38.
109. Shimba, A., et al., Glucocorticoids Drive Diurnal Oscillations in T Cell Distribution and Responses by Inducing Interleukin-7 Receptor and CXCR4. Immunity, 2018. **48**(2): p. 286-298 e6.
110. Curtis, A.M., et al., Circadian clock proteins and immunity. Immunity, 2014. **40**(2): p. 178-86.
111. Preuss, F., et al., Adverse effects of chronic circadian desynchronization in animals in a "challenging" environment. Am J Physiol Regul Integr Comp Physiol, 2008. **295**(6): p. R2034-40.
112. Wang, S., et al., REV-ERBalpha integrates colon clock with experimental colitis through regulation of NF-kappaB/NLRP3 axis. Nat Commun, 2018. **9**(1): p. 4246.
113. Taleb, Z., et al., BMAL1 Regulates the Daily Timing of Colitis. Front Cell Infect Microbiol, 2022. **12**: p. 773413.
114. Ali, T., et al., Assessment of the relationship between quality of sleep and disease activity in inflammatory bowel disease patients. Inflamm Bowel Dis, 2013. **19**(11): p. 2440-3.
115. Ananthakrishnan, A.N., et al., Sleep duration affects risk for ulcerative colitis: a prospective cohort study. Clin Gastroenterol Hepatol, 2014. **12**(11): p. 1879-86.
116. Mazzoccoli, G., et al., Association study of a polymorphism in clock gene PERIOD3 and risk of inflammatory bowel disease. Chronobiol Int, 2012. **29**(8): p. 994-1003.
117. Liverani, E., et al., How to predict clinical relapse in inflammatory bowel disease patients. World J Gastroenterol, 2016. **22**(3): p. 1017-33.
118. Chakradeo, P.S., et al., Chronotype, social jet lag, sleep debt and food timing in inflammatory bowel disease. Sleep Med, 2018. **52**: p. 188-195.
119. Ramsey, K.M., et al., Circadian clock feedback cycle through NAMPT-mediated NAD+ biosynthesis. Science, 2009. **324**(5927): p. 651-4.
120. Chaix, A., et al., Time-restricted feeding is a preventative and therapeutic intervention against diverse nutritional challenges. Cell Metab, 2014. **20**(6): p. 991-1005.

121. Das, M., et al., Time-restricted feeding normalizes hyperinsulinemia to inhibit breast cancer in obese postmenopausal mouse models. Nat Commun, 2021. **12**(1): p. 565.
122. Mattson, M.P., V.D. Longo, and M. Harvie, Impact of intermittent fasting on health and disease processes. Ageing Res Rev, 2017. **39**: p. 46-58.
123. Ella, K., et al., Time restricted feeding modifies leukocyte responsiveness and improves inflammation outcome. Front Immunol, 2022. **13**: p. 924541.
124. Yamamuro, D., et al., Peripheral circadian rhythms in the liver and white adipose tissue of mice are attenuated by constant light and restored by time-restricted feeding. PLoS One, 2020. **15**(6): p. e0234439.
125. Polidarova, L., et al., Hepatic, duodenal, and colonic circadian clocks differ in their persistence under conditions of constant light and in their entrainment by restricted feeding. Chronobiol Int, 2011. **28**(3): p. 204-15.
126. Hoogerwerf, W.A., et al., Clock gene expression in the murine gastrointestinal tract: endogenous rhythmicity and effects of a feeding regimen. Gastroenterology, 2007. **133**(4): p. 1250-60.
127. Jud, C., et al., A guideline for analyzing circadian wheel-running behavior in rodents under different lighting conditions. Biol Proced Online, 2005. **7**: p. 101-16.
128. Kim, J.J., et al., Investigating intestinal inflammation in DSS-induced model of IBD. J Vis Exp, 2012(60).
129. Ellacott, K.L., et al., Assessment of feeding behavior in laboratory mice. Cell Metab, 2010. **12**(1): p. 10-7.
130. Bolger, A.M., M. Lohse, and B. Usadel, Trimmomatic: a flexible trimmer for Illumina sequence data. Bioinformatics, 2014. **30**(15): p. 2114-20.
131. Dobin, A., et al., STAR: ultrafast universal RNA-seq aligner. Bioinformatics, 2013. **29**(1): p. 15-21.
132. Li, H., et al., The Sequence Alignment/Map format and SAMtools. Bioinformatics, 2009. **25**(16): p. 2078-9.
133. Liao, Y., G.K. Smyth, and W. Shi, featureCounts: an efficient general purpose program for assigning sequence reads to genomic features. Bioinformatics, 2014. **30**(7): p. 923-30.
134. Love, M.I., W. Huber, and S. Anders, Moderated estimation of fold change and dispersion for RNA-seq data with DESeq2. Genome Biol, 2014. **15**(12): p. 550.
135. Durinck, S., et al., Mapping identifiers for the integration of genomic datasets with the R/Bioconductor package biomaRt. Nat Protoc, 2009. **4**(8): p. 1184-91.

136. Wu, T., et al., clusterProfiler 4.0: A universal enrichment tool for interpreting omics data. Innovation (Camb), 2021. **2**(3): p. 100141.
137. Wu, G., et al., MetaCycle: an integrated R package to evaluate periodicity in large scale data. Bioinformatics, 2016. **32**(21): p. 3351-3353.
138. Pelikan, A., et al., Venn diagram analysis overestimates the extent of circadian rhythm reprogramming. FEBS J, 2022. **289**(21): p. 6605-6621.
139. Godon, J.J., et al., Molecular microbial diversity of an anaerobic digestor as determined by small-subunit rDNA sequence analysis. Appl Environ Microbiol, 1997. **63**(7): p. 2802-13.
140. Edgar, R.C., Search and clustering orders of magnitude faster than BLAST. Bioinformatics, 2010. **26**(19): p. 2460-1.
141. Edgar, R.C., et al., UCHIME improves sensitivity and speed of chimera detection. Bioinformatics, 2011. **27**(16): p. 2194-200.
142. Edgar, R.C., UNOISE2: improved error-correction for Illumina 16S and ITS amplicon sequencing. bioRxiv, 2016: p. 081257.
143. Lagkouvardos, I., et al., Rhea: a transparent and modular R pipeline for microbial profiling based on 16S rRNA gene amplicons. PeerJ, 2017. **5**: p. e2836.
144. Kumar, S., et al., MEGA X: Molecular Evolutionary Genetics Analysis across Computing Platforms. Mol Biol Evol, 2018. **35**(6): p. 1547-1549.
145. Subramanian, B., et al., Evolview v3: a webserver for visualization, annotation, and management of phylogenetic trees. Nucleic Acids Res, 2019. **47**(W1): p. W270-W275.
146. Tourlousse, D.M., et al., Synthetic spike-in standards for high-throughput 16S rRNA gene amplicon sequencing. Nucleic Acids Res, 2017. **45**(4): p. e23.
147. Kessner, D., et al., ProteoWizard: open source software for rapid proteomics tools development. Bioinformatics, 2008. **24**(21): p. 2534-6.
148. Smith, C.A., et al., XCMS: processing mass spectrometry data for metabolite profiling using nonlinear peak alignment, matching, and identification. Anal Chem, 2006. **78**(3): p. 779-87.
149. Wishart, D.S., et al., HMDB 4.0: the human metabolome database for 2018. Nucleic Acids Res, 2018. **46**(D1): p. D608-D617.
150. Tsugawa, H., et al., MS-DIAL: data-independent MS/MS deconvolution for comprehensive metabolome analysis. Nat Methods, 2015. **12**(6): p. 523-6.
151. Reiter, S., et al., Development of a Highly Sensitive Ultra-High-Performance Liquid Chromatography Coupled to Electrospray Ionization Tandem Mass Spectrometry

Quantitation Method for Fecal Bile Acids and Application on Crohn's Disease Studies. J Agric Food Chem, 2021. **69**(17): p. 5238-5251.

152. Douglas, G.M., et al., PICRUSt2 for prediction of metagenome functions. Nat Biotechnol, 2020. **38**(6): p. 685-688.
153. Katakura, K., et al., Toll-like receptor 9-induced type I IFN protects mice from experimental colitis. J Clin Invest, 2005. **115**(3): p. 695-702.
154. Hughes, M.E., J.B. Hogenesch, and K. Kornacker, JTK_CYCLE: an efficient nonparametric algorithm for detecting rhythmic components in genome-scale data sets. J Biol Rhythms, 2010. **25**(5): p. 372-80.
155. Kuhn, R., et al., Interleukin-10-deficient mice develop chronic enterocolitis. Cell, 1993. **75**(2): p. 263-74.
156. Vollmers, C., et al., Time of feeding and the intrinsic circadian clock drive rhythms in hepatic gene expression. Proc Natl Acad Sci U S A, 2009. **106**(50): p. 21453-8.
157. Ott, S.J., et al., Reduction in diversity of the colonic mucosa associated bacterial microflora in patients with active inflammatory bowel disease. Gut, 2004. **53**(5): p. 685-93.
158. Gkouskou, K.K., et al., The gut microbiota in mouse models of inflammatory bowel disease. Front Cell Infect Microbiol, 2014. **4**: p. 28.
159. Halfvarson, J., et al., Dynamics of the human gut microbiome in inflammatory bowel disease. Nat Microbiol, 2017. **2**: p. 17004.
160. Labbe, A., et al., Bacterial bile metabolising gene abundance in Crohn's, ulcerative colitis and type 2 diabetes metagenomes. PLoS One, 2014. **9**(12): p. e115175.
161. Metwaly, A., et al., Integrated microbiota and metabolite profiles link Crohn's disease to sulfur metabolism. Nat Commun, 2020. **11**(1): p. 4322.
162. Vacca, M., et al., The Controversial Role of Human Gut Lachnospiraceae. Microorganisms, 2020. **8**(4).
163. Lavelle, A. and H. Sokol, Gut microbiota-derived metabolites as key actors in inflammatory bowel disease. Nat Rev Gastroenterol Hepatol, 2020. **17**(4): p. 223-237.
164. Parada Venegas, D., et al., Short Chain Fatty Acids (SCFAs)-Mediated Gut Epithelial and Immune Regulation and Its Relevance for Inflammatory Bowel Diseases. Front Immunol, 2019. **10**: p. 277.
165. Sellon, R.K., et al., Resident enteric bacteria are necessary for development of spontaneous colitis and immune system activation in interleukin-10-deficient mice. Infect Immun, 1998. **66**(11): p. 5224-31.

166. Morampudi, V., et al., The goblet cell-derived mediator RELM-beta drives spontaneous colitis in Muc2-deficient mice by promoting commensal microbial dysbiosis. Mucosal Immunol, 2016. **9**(5): p. 1218-33.
167. Aamann, L., E.M. Vestergaard, and H. Gronbaek, Trefoil factors in inflammatory bowel disease. World J Gastroenterol, 2014. **20**(12): p. 3223-30.
168. Chun, E., et al., Metabolite-Sensing Receptor Ffar2 Regulates Colonic Group 3 Innate Lymphoid Cells and Gut Immunity. Immunity, 2019. **51**(5): p. 871-884 e6.
169. Pazos, M., et al., Multidrug resistance-associated transporter 2 regulates mucosal inflammation by facilitating the synthesis of hepoxilin A3. J Immunol, 2008. **181**(11): p. 8044-52.
170. Leppkes, M., et al., RORgamma-expressing Th17 cells induce murine chronic intestinal inflammation via redundant effects of IL-17A and IL-17F. Gastroenterology, 2009. **136**(1): p. 257-67.
171. Kim, S.H., et al., Complement C5a promotes antigen cross-presentation by Peyer's patch monocyte-derived dendritic cells and drives a protective CD8(+) T cell response. Cell Rep, 2021. **35**(2): p. 108995.
172. Allaire, J.M., et al., Frontline defenders: goblet cell mediators dictate host-microbe interactions in the intestinal tract during health and disease. Am J Physiol Gastrointest Liver Physiol, 2018. **314**(3): p. G360-G377.
173. Papoff, G., et al., CASP4 gene silencing in epithelial cancer cells leads to impairment of cell migration, cell-matrix adhesion and tissue invasion. Sci Rep, 2018. **8**(1): p. 17705.
174. Lee, K.Y., et al., PDK1 nucleates T cell receptor-induced signaling complex for NF-kappaB activation. Science, 2005. **308**(5718): p. 114-8.
175. Contento, R.L., et al., CXCR4-CCR5: a couple modulating T cell functions. Proc Natl Acad Sci U S A, 2008. **105**(29): p. 10101-6.
176. Damle, N.K. and A. Aruffo, Vascular cell adhesion molecule 1 induces T-cell antigen receptor-dependent activation of CD4+T lymphocytes. Proc Natl Acad Sci U S A, 1991. **88**(15): p. 6403-7.
177. Chassaing, B., et al., Dextran sulfate sodium (DSS)-induced colitis in mice. Curr Protoc Immunol, 2014. **104**: p. 15 25 1-15 25 14.
178. Yu, F., et al., Deficiency of intestinal Bmal1 prevents obesity induced by high-fat feeding. Nat Commun, 2021. **12**(1): p. 5323.
179. Chun, S.K., et al., Disruption of the circadian clock drives Apc loss of heterozygosity to accelerate colorectal cancer. Sci Adv, 2022. **8**(32): p. eabo2389.

180. Jochum, S.B., et al., Colonic Epithelial Circadian Disruption Worsens Dextran Sulfate Sodium-Induced Colitis. Inflamm Bowel Dis, 2022.
181. Kaser, A., S. Zeissig, and R.S. Blumberg, Inflammatory bowel disease. Annu Rev Immunol, 2010. **28**: p. 573-621.
182. He, W., et al., Circadian Expression of Migratory Factors Establishes Lineage-Specific Signatures that Guide the Homing of Leukocyte Subsets to Tissues. Immunity, 2018. **49**(6): p. 1175-1190 e7.
183. Pick, R., et al., Time-of-Day-Dependent Trafficking and Function of Leukocyte Subsets. Trends Immunol, 2019. **40**(6): p. 524-537.
184. Leithauser, F., et al., Clustering of colonic lamina propria CD4(+) T cells to subepithelial dendritic cell aggregates precedes the development of colitis in a murine adoptive transfer model. Lab Invest, 2001. **81**(10): p. 1339-49.
185. Ruben, M.D., et al., Dosing time matters. Science, 2019. **365**(6453): p. 547-549.
186. van der Sluis, M., et al., Combined defects in epithelial and immunoregulatory factors exacerbate the pathogenesis of inflammation: mucin 2-interleukin 10-deficient mice. Lab Invest, 2008. **88**(6): p. 634-42.
187. Froicu, M., Y. Zhu, and M.T. Cantorna, Vitamin D receptor is required to control gastrointestinal immunity in IL-10 knockout mice. Immunology, 2006. **117**(3): p. 310-8.
188. de Vos, W.M., et al., Gut microbiome and health: mechanistic insights. Gut, 2022. **71**(5): p. 1020-1032.
189. Vantrappen, G., et al., Bile acid studies in uncomplicated Crohn's disease. Gut, 1977. **18**(9): p. 730-5.
190. Rutgeerts, P., Y. Ghoos, and G. Vantrappen, Bile acid studies in patients with Crohn's colitis. Gut, 1979. **20**(12): p. 1072-7.
191. Sinha, S.R., et al., Dysbiosis-Induced Secondary Bile Acid Deficiency Promotes Intestinal Inflammation. Cell Host Microbe, 2020. **27**(4): p. 659-670 e5.
192. Arrieta, M.C., et al., Reducing small intestinal permeability attenuates colitis in the IL10 gene-deficient mouse. Gut, 2009. **58**(1): p. 41-8.
193. Lamia, K.A., et al., AMPK regulates the circadian clock by cryptochrome phosphorylation and degradation. Science, 2009. **326**(5951): p. 437-40.
194. Regmi, P. and L.K. Heilbronn, Time-Restricted Eating: Benefits, Mechanisms, and Challenges in Translation. iScience, 2020. **23**(6): p. 101161.

195. Ramanathan, C., et al., mTOR signaling regulates central and peripheral circadian clock function. PLoS Genet, 2018. **14**(5): p. e1007369.
196. Zhang, X., et al., Effects of alternate-day fasting, time-restricted fasting and intermittent energy restriction DSS-induced on colitis and behavioral disorders. Redox Biol, 2020. **32**: p. 101535.
197. Song, S., et al., Time-restricted feeding ameliorates dextran sulfate sodium-induced colitis via reducing intestinal inflammation. Front Nutr, 2022. **9**: p. 1043783.
198. de Cabo, R. and M.P. Mattson, Effects of Intermittent Fasting on Health, Aging, and Disease. N Engl J Med, 2019. **381**(26): p. 2541-2551.
199. Deota, S., et al., Diurnal transcriptome landscape of a multi-tissue response to time-restricted feeding in mammals. Cell Metab, 2023. **35**(1): p. 150-165 e4.
200. Mukherji, A., A. Kobiita, and P. Chambon, Shifting the feeding of mice to the rest phase creates metabolic alterations, which, on their own, shift the peripheral circadian clocks by 12 hours. Proc Natl Acad Sci U S A, 2015. **112**(48): p. E6683-90.
201. Alam, M.T., et al., Microbial imbalance in inflammatory bowel disease patients at different taxonomic levels. Gut Pathog, 2020. **12**: p. 1.
202. Le Minh, N., et al., Glucocorticoid hormones inhibit food-induced phase-shifting of peripheral circadian oscillators. EMBO J, 2001. **20**(24): p. 7128-36.

Acknowledgement

First and foremost, I would like to take this opportunity to thank Prof. Dirk Haller for granting me as part of the Nutrition & Immunology team. Thanks for supporting me during the hard times, especially when the projects got stuck. Thanks for the scientific training and input, as well as giving suggestions promptly.

My great appreciation goes to Dr. Silke Kiessling for her 'full-time' support, I would not have the chance to study and doing research at TUM without her. Thanks for accepting me join the group and exploring the interesting and challenging chrono-world. Thanks for open discussions as friends, both science-wise and life-wise. Thanks for all communications and wonderful time we had together.

How lucky I am to have my friendly, helpful and nice chrono-colleagues, Baraa, Marjolein and Liza. The time we have spent together is a treasure which I will benefit for my whole life. Thanks for holding hands and sharing all the pressure during the happy and shitty times. I will remember all the tough nights when we were doing night shifts, and all the support I got from you.

Special thanks to Nico, my Lieber Freund. For the Feierabend and the talks. For being there discussing scientific and gossip topics. Thanks for always showing up asap, giving support whenever I needed. Thanks for being my colleague, my beer mentor, my language partner, my translator, and most importantly, my real friend.

Thanks to all members of the Nutrition & Immunology group. I really appreciate the time we spent together as friends or colleagues. Thanks to everyone who helped me and decorated my life in this small town in Germany.

Finally, most thanks as ever to my family. Thanks for supporting me, encouraging me, helping me and holding my hand. Thanks for being so close to me even though being so far, especially during the hard times.

Pursuing PhD in this lab is one of the most correct decisions I have ever made. I really appreciate the four and a half years we spend together. The memory of each one of you, will be carefully kept deep in my heart and support me to start the next journey.